Measurement of the top quark polarization and $t\bar{t}$ spin correlations using dilepton final states in proton-proton collisions at $\sqrt{s} = 13$ TeV

A. M. Sirunyan *et al.*[*]

(CMS Collaboration)

Measurements of the top quark polarization and top quark pair ($t\bar{t}$) spin correlations are presented using events containing two oppositely charged leptons (e^+e^-, $e^\pm\mu^\mp$, or $\mu^+\mu^-$) produced in proton-proton collisions at a center-of-mass energy of 13 TeV. The data were recorded by the CMS experiment at the LHC in 2016 and correspond to an integrated luminosity of 35.9 fb^{-1}. A set of parton-level normalized differential cross sections, sensitive to each of the independent coefficients of the spin-dependent parts of the $t\bar{t}$ production density matrix, is measured for the first time at 13 TeV. The measured distributions and extracted coefficients are compared with standard model predictions from simulations at next-to-leading-order (NLO) accuracy in quantum chromodynamics (QCD), and from NLO QCD calculations including electroweak corrections. All measurements are found to be consistent with the expectations of the standard model. The normalized differential cross sections are used in fits to constrain the anomalous chromo-magnetic and chromoelectric dipole moments of the top quark to $-0.24 < C_{\mathrm{tG}}/\Lambda^2 < 0.07$ TeV^{-2} and $-0.33 < C_{\mathrm{tG}}^l/\Lambda^2 < 0.20$ TeV^{-2}, respectively, at the 95% confidence level.

I. INTRODUCTION

The top quark is the heaviest known fundamental particle and has a lifetime on the order of 10^{-25} s [1]. This is shorter than the quantum chromodynamic (QCD) hadronization time scale $1/\Lambda_{\mathrm{QCD}} \approx 10^{-24}$ s, and much shorter than the spin decorrelation time scale $m_t/\Lambda_{\mathrm{QCD}}^2 \approx 10^{-21}$ s [2] (where m_t is the top quark mass). Thus, not only does the top quark decay before hadronization occurs, but also its spin information is preserved in the angular distribution of its decay products.

At the CERN LHC, top quarks are produced mostly in pairs via gluon fusion ($gg \to t\bar{t}$). The quarks are unpolarized at leading order (LO), owing to the parity-conserving nature (longitudinal polarization) and approximate time invariance (transverse polarization) of QCD interactions. In the standard model (SM), a small longitudinal polarization arises from electroweak (EW) corrections, while a small transverse polarization comes from absorptive terms at one loop (both <1% [3,4]). The spins of the top quarks and antiquarks are strongly correlated, and the configuration of spins depends on the invariant mass of the $t\bar{t}$ pair ($m_{t\bar{t}}$), with like (unlike) helicity pairs dominating at low (high) $m_{t\bar{t}}$.

This paper presents a measurement of all the independent coefficients of the top quark spin-dependent parts of the $t\bar{t}$ production density matrix, as described in Ref. [4], using events (labeled dileptonic) in which the decay of the $t\bar{t}$ pair leads to two oppositely charged leptons (e^+e^-, $e^\pm\mu^\mp$, or $\mu^+\mu^-$) in the final state. The analysis uses a data sample of proton-proton (pp) collision events collected by the CMS experiment at a center-of-mass (CM) energy of 13 TeV in 2016, corresponding to an integrated luminosity of 35.9 fb^{-1} [5]. Similar measurements have been made by the ATLAS Collaboration at $\sqrt{s} = 8$ TeV [6]. Differential $t\bar{t}$ cross sections corresponding to a subset of the coefficients, and other observables sensitive to the top quark polarization and $t\bar{t}$ spin correlations, have been measured by the ATLAS and CMS Collaborations at $\sqrt{s} = 7$, 8, and 13 TeV [7–11].

In this analysis, each coefficient is extracted from a measured normalized differential $t\bar{t}$ cross section, using the same event selection and reconstruction as described in Ref. [12]. The distributions are corrected to the parton level and extrapolated to the full phase space, using a refined unfolding procedure with no regularization bias. In addition to full statistical and systematic covariance matrices for each measured distribution, matrices are provided for the combined set of all measured bins, allowing constraints to be placed using several measured distributions simultaneously.

The absence of direct signals of beyond-the-SM (BSM) particles in the LHC data analyzed so far suggests that BSM phenomena might only be directly observed at an

[*]Full author list given at the end of the article.

energy scale larger than that probed at the LHC. However, BSM physics could still indirectly manifest itself in new vertices and modified couplings. Such effects can be accommodated by adding higher-dimensional operators to the SM Lagrangian in an effective field theory (EFT) approach. The coefficients measured in this analysis are sensitive to all but one of the operators of mass dimension six relevant for hadronic $t\bar{t}$ production [4]. We set limits on contributions from these operators using simultaneous fits to the measured normalized differential cross sections, including constraints on the chromomagnetic and chromoelectric dipole moments of the top quark.

II. FORMALISM AND OBSERVABLES

The square of the matrix element for $t\bar{t}$ production and decay to two leptons (with appropriate color and spin summation implied) [13] can be written as

$$|\mathcal{M}(q\bar{q}/gg \to t\bar{t} \to \ell^+\nu b\ell^-\bar{\nu}\,\bar{b})|^2 \propto \rho R\bar{\rho}. \quad (1)$$

Here, ℓ refers to an electron or muon, R is the spin density matrix related to on-shell $t\bar{t}$ production, and ρ and $\bar{\rho}$ are the decay spin density matrices for the top quark and antiquark, respectively. The narrow width of the top quark compared to its mass allows factorization of the production and decay processes.

The aim of this analysis is to study the properties of the R matrix, which is purely a function of the partonic initial state and production kinematic variables, and is therefore sensitive to BSM phenomena in $t\bar{t}$ production [13]. While the analysis is also sensitive to BSM effects in $t\bar{t}$ decays, these effects are heavily constrained [14,15], and therefore have a minimal effect on the measured distributions [4,13].

The production spin density matrix R can be decomposed in the t and $\bar{t}$ spin spaces using a Pauli matrix basis:

$$R \propto \tilde{A}\mathbb{1} \otimes \mathbb{1} + \tilde{B}_i^+\sigma^i \otimes \mathbb{1} + \tilde{B}_i^-\mathbb{1} \otimes \sigma^i + \tilde{C}_{ij}\sigma^i \otimes \sigma^j, \quad (2)$$

where $\mathbb{1}$ is the 2×2 unit matrix, σ^i are the Pauli matrices, and the first (second) matrix in each tensor product refers to the top quark (antiquark) spin space. The function $\tilde{A}$ determines the total $t\bar{t}$ production cross section and the top quark kinematic distributions, $\tilde{\mathbf{B}}^\pm$ are three-dimensional vectors of functions that characterize the degree of top quark or antiquark polarization in each direction, and $\tilde{C}$ is a 3×3 matrix of functions that characterize the correlation between the top quark and antiquark spins.

We choose an orthonormal basis to decompose the top quark spin, where these functions have definite properties with respect to discrete symmetries [4,16]. This basis is illustrated in Fig. 1. Working in the $t\bar{t}$ CM frame, we use the helicity axis $\hat{k}$ defined by the top quark direction and the direction $\hat{p}$ of the incoming parton to define the direction perpendicular to the scattering plane $\hat{n} = (\hat{p} \times \hat{k})/\sin\Theta$, where Θ is the top quark scattering angle. The direction in
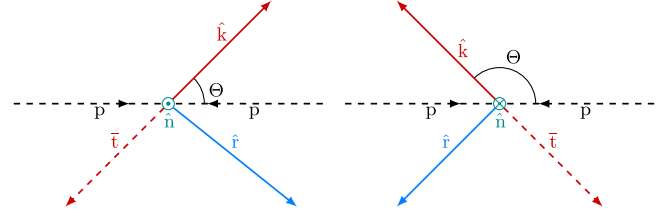

FIG. 1. Coordinate system used for the spin measurements, illustrated in the scattering plane for $\Theta < \pi/2$ (left) and $\Theta > \pi/2$ (right), where the signs of $\hat{r}$ and $\hat{n}$ are flipped at $\Theta = \pi/2$ as shown in Eq. (4). The $\hat{k}$ axis is defined by the top quark direction, measured in the $t\bar{t}$ CM frame. For the basis used to define the coefficient functions in Eq. (3), the incoming particles p represent the incoming partons, while for the basis used to measure the coefficients in Eqs. (8)–(10) they represent the incoming protons.

the scattering plane mutually perpendicular to $\hat{k}$ and the transverse axis $\hat{n}$ is given by $\hat{r} = (\hat{p} - \hat{k}\cos\Theta)/\sin\Theta$.

We expand $\tilde{B}_i^\pm$ and $\tilde{C}_{ij}$ in terms of the orthonormal basis $\{\hat{k}, \hat{r}, \hat{n}\}$:

$$
\begin{aligned}
\tilde{B}_i^\pm &= b_k^\pm\hat{k}_i + b_r^\pm\hat{r}_i + b_n^\pm\hat{n}_i, \\
\tilde{C}_{ij} &= c_{kk}\hat{k}_i\hat{k}_j + c_{rr}\hat{r}_i\hat{r}_j + c_{nn}\hat{n}_i\hat{n}_j \\
&\quad + c_{rk}(\hat{r}_i\hat{k}_j + \hat{k}_i\hat{r}_j) + c_{nr}(\hat{n}_i\hat{r}_j + \hat{r}_i\hat{n}_j) \\
&\quad + c_{kn}(\hat{k}_i\hat{n}_j + \hat{n}_i\hat{k}_j) + c_n(\hat{r}_i\hat{k}_j - \hat{k}_i\hat{r}_j) \\
&\quad + c_k(\hat{n}_i\hat{r}_j - \hat{r}_i\hat{n}_j) + c_r(\hat{k}_i\hat{n}_j - \hat{n}_i\hat{k}_j). \quad (3)
\end{aligned}
$$

The coefficient functions $b_i^\pm$, c_{ij}, and c_i are functions of the partonic CM energy squared s and $\cos\Theta$. They can each be classified with respect to P, CP, T, and Bose-Einstein symmetry, and their P and CP symmetry properties are summarized in Table I. The approximate CP invariance of the SM requires the $\tilde{C}$ matrix to be symmetric (i.e., the CP-odd coefficient functions vanish: $c_k = c_r = c_n = 0$) and the top quark and antiquark to have the same polarization coefficient functions (i.e., $b_i^+ = b_i^-$). The P invariance of QCD forces the P-odd coefficient functions to vanish in the absence of EW interactions, so large values are allowed only for the P- and CP-even spin correlations c_{kk}, c_{rr}, c_{nn}, and c_{rk} (and the transverse polarization coefficient functions $b_n^\pm$, but these are zero at tree level in QCD by T invariance). Any deviation from these expectations would be a sign of BSM phenomena.

The Bose-Einstein symmetry of the gg initial state requires a redefinition of the $\hat{r}$ and $\hat{n}$ axes (which are odd under Bose-Einstein symmetry) to allow nonzero values of the relevant coefficient functions [4]:

$$\{\hat{k}, \hat{r}, \hat{n}\} \to \{\hat{k}, \text{sign}(\cos\Theta)\hat{r}, \text{sign}(\cos\Theta)\hat{n}\}, \quad (4)$$

i.e., we have used the sign of the cosine of the top quark scattering angle, which is odd under Bose-Einstein symmetry, to define a "forward" direction for each event.

TABLE I.   Observables and their corresponding measured coefficients, production spin density matrix coefficient functions, and P and CP symmetry properties. For the laboratory-frame asymmetries shown in the last two rows, there is no direct correspondence with the coefficient functions.

Observable	Measured coefficient	Coefficient function	Symmetries
$\cos\theta_1^k$	B_1^k	b_k^+	P-odd, CP-even
$\cos\theta_2^k$	B_2^k	b_k^-	P-odd, CP-even
$\cos\theta_1^r$	B_1^r	b_r^+	P-odd, CP-even
$\cos\theta_2^r$	B_2^r	b_r^-	P-odd, CP-even
$\cos\theta_1^n$	B_1^n	b_n^+	P-even, CP-even
$\cos\theta_2^n$	B_2^n	b_n^-	P-even, CP-even
$\cos\theta_1^{k*}$	B_1^{k*}	b_k^+	P-odd, CP-even
$\cos\theta_2^{k*}$	B_2^{k*}	b_k^-	P-odd, CP-even
$\cos\theta_1^{r*}$	B_1^{r*}	b_r^+	P-odd, CP-even
$\cos\theta_2^{r*}$	B_2^{r*}	b_r^-	P-odd, CP-even
$\cos\theta_1^k\cos\theta_2^k$	C_{kk}	c_{kk}	P-even, CP-even
$\cos\theta_1^r\cos\theta_2^r$	C_{rr}	c_{rr}	P-even, CP-even
$\cos\theta_1^n\cos\theta_2^n$	C_{nn}	c_{nn}	P-even, CP-even
$\cos\theta_1^r\cos\theta_2^k + \cos\theta_1^k\cos\theta_2^r$	$C_{rk} + C_{kr}$	c_{rk}	P-even, CP-even
$\cos\theta_1^r\cos\theta_2^k - \cos\theta_1^k\cos\theta_2^r$	$C_{rk} - C_{kr}$	c_n	P-even, CP-odd
$\cos\theta_1^n\cos\theta_2^r + \cos\theta_1^r\cos\theta_2^n$	$C_{nr} + C_{rn}$	c_{nr}	P-odd, CP-even
$\cos\theta_1^n\cos\theta_2^r - \cos\theta_1^r\cos\theta_2^n$	$C_{nr} - C_{rn}$	c_k	P-odd, CP-odd
$\cos\theta_1^n\cos\theta_2^k + \cos\theta_1^k\cos\theta_2^n$	$C_{nk} + C_{kn}$	c_{kn}	P-odd, CP-even
$\cos\theta_1^n\cos\theta_2^k - \cos\theta_1^k\cos\theta_2^n$	$C_{nk} - C_{kn}$	$-c_r$	P-odd, CP-odd
$\cos\varphi$	D	$-(c_{kk} + c_{rr} + c_{nn})/3$	P-even, CP-even
$\cos\varphi_{\text{lab}}$	$A_{\cos\varphi}^{\text{lab}}$	$\cdots$	$\cdots$
$\lvert\Delta\phi_{\ell\ell}\rvert$	$A_{\lvert\Delta\phi_{\ell\ell}\rvert}$	$\cdots$	$\cdots$

The top quark spin cannot be measured directly, but the angular distribution of the decay products of a top quark is correlated with its spin axis [2]:

$$\frac{1}{\Gamma}\frac{d\Gamma}{d\cos\chi_a} = \frac{1}{2}(1 + \kappa_a\cos\chi_a), \qquad (5)$$

where Γ is the top quark decay width, χ_a is the angle between the direction of decay product a and the top quark spin axis in the top quark rest frame, and κ_a is the spin analyzing power. The charged lepton has maximal spin analyzing power, $\kappa_{\ell^+} \approx 1$ [17]. For top antiquark decay, the sign is reversed: $\kappa_{\ell^-} = -\kappa_{\ell^+}$.

Each of the 15 coefficient functions from Eq. (3) (six $b_i^\pm$ and nine $c_{ij/i'}$) is probed by a normalized differential cross section at the parton level, using the charged lepton directions measured in the rest frames of their parent top quark and antiquark as proxies for the top quark and antiquark spins. Since the measurements are made in pp collisions, the basis is adjusted from that of Eq. (4) by defining $\hat{p} = (0, 0, 1)$, the direction of the proton beam in the positive z direction in the laboratory frame, in the derivation of $\hat{r}$ and $\hat{n}$ [4]. This basis is illustrated in Fig. 1.

The fourfold angular distribution for the two leptons follows from Eqs. (1) and (2), and is given by

$$\frac{1}{\sigma}\frac{d^4\sigma}{d\Omega_1 d\Omega_2} = \frac{1}{(4\pi)^2}(1 + \mathbf{B_1}\cdot\hat{\ell}_1 + \mathbf{B_2}\cdot\hat{\ell}_2 - \hat{\ell}_1\cdot C\cdot\hat{\ell}_2), \qquad (6)$$

where σ is the $t\bar{t}$ production cross section, $\Omega_{1,2}$ are the solid angles of the leptons in their parent top quark and antiquark rest frames, and $\hat{\ell}_{1,2}$ are the corresponding unit vectors. The negative sign in front of the matrix C is chosen to define same-helicity top quarks as having positive spin correlation. The elements of the vectors $\mathbf{B_{1,2}}$ and the matrix C are the following coefficients [in whose definitions the factors of κ_{ℓ^+} and κ_{ℓ^-} from Eq. (5) are absorbed]:

(1) B_1^i and B_2^i, the top quark and antiquark polarization coefficients with respect to each reference axis i (sensitive to b_i^+ and b_i^-).

(2) C_{ii}, the "diagonal" spin correlation coefficient for each reference axis i (sensitive to c_{ii}).

(3) C_{ij}, the "cross" spin correlation coefficients for each pair of axes $i \neq j$, whose sums and differences $C_{ij} \pm C_{ji}$ are sensitive to c_{ij} and $c_{i'}$.

These measurable coefficients are closely related to the production spin density matrix coefficient functions from Eq. (3), but are not identical, owing to the different basis used for the spin measurement. We do not measure the coefficients differentially or attempt to separate the contributions from different initial states. The association

between the measured coefficients and the coefficient functions is given in Table I.

For each of the 15 coefficients that make up $\mathbf{B}_{1,2}$ and C, a change of variables can be made to obtain a single-differential cross section that depends only on that coefficient. After integrating out the azimuthal angles, Eq. (6) reduces to

$$\frac{1}{\sigma}\frac{d^2\sigma}{d\cos\theta_1^i\, d\cos\theta_2^j}$$
$$=\frac{1}{4}(1+B_1^i\cos\theta_1^i+B_2^j\cos\theta_2^j-C_{ij}\cos\theta_1^i\cos\theta_2^j), \quad (7)$$

where θ_1^i (θ_2^j) is the angle of the positively (negatively) charged lepton, measured with respect to axis i (j) in the rest frame of its parent top quark (antiquark). By changing variables (if necessary) and integrating out one of the angles, we can derive single-differential cross sections with respect to $\cos\theta_1^i$, $\cos\theta_2^i$, and $\cos\theta_1^i\cos\theta_2^j$:

$$\frac{1}{\sigma}\frac{d\sigma}{d\cos\theta_1^i}=\frac{1}{2}(1+B_1^i\cos\theta_1^i),$$
$$\frac{1}{\sigma}\frac{d\sigma}{d\cos\theta_2^i}=\frac{1}{2}(1+B_2^i\cos\theta_2^i),$$
$$\frac{1}{\sigma}\frac{d\sigma}{dx}=\frac{1}{2}(1-C_{ij}x)\ln\left(\frac{1}{|x|}\right),$$
$$x=\cos\theta_1^i\cos\theta_2^j. \quad (8)$$

Similarly, starting from Eq. (6), we obtain (for $i\neq j$)

$$\frac{1}{\sigma}\frac{d\sigma}{dx_\pm}=\frac{1}{2}\left(1-\frac{C_{ij}\pm C_{ji}}{2}x_\pm\right)\cos^{-1}|x_\pm|,$$
$$x_\pm=\cos\theta_1^i\cos\theta_2^j\pm\cos\theta_1^j\cos\theta_2^i. \quad (9)$$

Thus, in order to determine the 15 coefficients, the $t\bar{t}$ production cross section is measured as a function of each of the following 15 observables at the parton level:

(1) The three $\cos\theta_1^i$ terms and three $\cos\theta_2^i$ terms to measure B_1^i and B_2^i, the top quark and antiquark polarization coefficients with respect to each reference axis i.

(2) The three $\cos\theta_1^i\cos\theta_2^i$ terms to measure C_{ii}, the diagonal spin correlation coefficient for each axis i.

(3) The six sum and difference terms $\cos\theta_1^i\cos\theta_2^j\pm\cos\theta_1^j\cos\theta_2^i$ to measure $C_{ij}\pm C_{ji}$, the sums and differences of the cross spin correlation coefficients for each pair of axes $i\neq j$.

We do not measure the separate cross spin correlation $\cos\theta_1^i\cos\theta_2^j$ distributions, because it is the sums and differences that are sensitive to the c_{ij} and c_i coefficients of Eq. (3) (see Table I).

In addition, we measure four further $\cos\theta_{1,2}^i$ distributions based on modified axes $\hat{k}^*$ and $\hat{r}^*$, equal to $\pm\hat{k}$ or $\pm\hat{r}$, depending on the sign of $|y_t|-|y_{\bar{t}}|$, the difference of the moduli of the top quark and antiquark rapidities in the laboratory frame. The use of the modified axes probes the coefficient functions in different areas of phase space, providing sensitivity to different combinations of four-quark operators [4].

The spin correlation coefficient D is related to the diagonal C coefficients as $D=-\text{Tr}[C]/3=-(C_{kk}+C_{rr}+C_{nn})/3$. We make a direct measurement of the D coefficient using the distribution of the dot product of the two lepton directions measured in their parent top quark and antiquark rest frames [4], $\hat{\ell}_1\cdot\hat{\ell}_2=\cos\varphi$:

$$\frac{1}{\sigma}\frac{d\sigma}{d\cos\varphi}=\frac{1}{2}(1-D\cos\varphi). \quad (10)$$

We also measure two related laboratory-frame distributions, using the following observables:

(1) $\cos\varphi_{\text{lab}}=\hat{\ell}_1^{\text{lab}}\cdot\hat{\ell}_2^{\text{lab}}$, defined by analogy to $\cos\varphi$, but using the lepton directions measured in the laboratory frame, which have excellent experimental resolution.

(2) $|\Delta\phi_{\ell\ell}|$, the absolute value of the difference in azimuthal angle ϕ between the two leptons in the laboratory frame.

The association between the 22 measured observables and the coefficients and coefficient functions is given in Table I. Except for the laboratory-frame distributions, the distribution shapes are completely determined by the coefficients, following the functional forms of Eqs. (8)–(10). The laboratory-frame observables (given in the last two rows of Table I) do not directly relate to any of the coefficients, and we instead quantify the shapes of their distributions by calculating the asymmetry (A) in the number of events (N) about the center of the distribution:

$$A_{\cos\varphi}^{\text{lab}}=\frac{N(\cos\varphi_{\text{lab}}>0)-N(\cos\varphi_{\text{lab}}<0)}{N(\cos\varphi_{\text{lab}}>0)+N(\cos\varphi_{\text{lab}}<0)},$$
$$A_{|\Delta\phi_{\ell\ell}|}=\frac{N(|\Delta\phi_{\ell\ell}|>\pi/2)-N(|\Delta\phi_{\ell\ell}|<\pi/2)}{N(|\Delta\phi_{\ell\ell}|>\pi/2)+N(|\Delta\phi_{\ell\ell}|<\pi/2)}. \quad (11)$$

III. THE CMS DETECTOR

The central feature of the CMS apparatus is a super-conducting solenoid of 6 m internal diameter, providing a magnetic field of 3.8 T. Within the solenoid volume are a silicon pixel and strip tracker, a lead tungstate crystal electromagnetic calorimeter (ECAL), and a brass and scintillator hadron calorimeter, each composed of a barrel and two end cap sections. Forward calorimeters extend the pseudorapidity (η) coverage provided by the barrel and end cap detectors. Muons are measured in gas-ionization

detectors embedded in the steel flux-return yoke outside the solenoid. Events of interest are selected using a two-tiered trigger system [18]. The first level, composed of custom hardware processors, uses information from the calorimeters and muon detectors to select events at a rate of around 100 kHz within a time interval of less than 4 μs. The second level, known as the high-level trigger (HLT), consists of a farm of processors running a version of the full event reconstruction software optimized for fast processing, and reduces the event rate to around 1 kHz before data storage. A more detailed description of the CMS detector, together with a definition of the coordinate system used and the relevant kinematic variables, can be found in Ref. [19].

IV. EVENT SIMULATION

Simulated $t\bar{t}$ events with a top quark mass of $m_t = 172.5$ GeV are produced at next-to-leading order (NLO) in QCD at the matrix element (ME) level by the POWHEG v. 2 [20–23] generator (POWHEGv2). The h_{damp} parameter of POWHEGv2, which regulates the damping of real emissions in the NLO calculation when matching to the parton shower (PS), is set to 272.72 GeV [24]. The PS and hadronization are performed by PYTHIA 8.219 [25] (referred to as PYTHIA8 in the following) with the CUETP8M2T4 tune [24,26,27].

In order to assess the level of variation when using an alternative ME and matching procedure, an alternative $t\bar{t}$ sample is generated using the MADGRAPH5_aMC@NLO 2.3.3 [28] generator including up to two extra partons at the ME level with NLO precision. The decays of the top quarks are modeled using MADSPIN [29], and events are matched to PYTHIA8 for PS and hadronization using the FxFx jet merging prescription [30]. This sample is referred to as MG5_aMC@NLO + PYTHIA8 [FxFx].

Signal $t\bar{t}$ events are defined as those with two charged leptons (e^+e^-, $e^\pm\mu^\mp$, or $\mu^+\mu^-$), originating from W boson decays and not from τ lepton decays. All other $t\bar{t}$ events are regarded as a background. The largest background contributions originate from $t\bar{t}$ events with leptonically decaying τ leptons, single top quarks produced in association with a W boson (tW), and, in events with same-flavor leptons, Z/γ^* bosons produced with additional jets (Z + jets). Additional significant backgrounds include W boson production with additional jets (W + jets), diboson (WW, WZ, and ZZ) events, and the production of a $t\bar{t}$ pair in association with a W or a Z boson ($t\bar{t} + W/Z$). Other sources of background are negligible in comparison to the uncertainties in the main backgrounds, and are not included in this analysis.

The W + jets process is simulated at LO precision using MADGRAPH5_aMC@NLO with up to four additional partons at the ME level and matched to PYTHIA8 using the MLM jet merging prescription [31]. The Z + jets process is simulated at NLO precision using MADGRAPH5_aMC@NLO with up to two additional partons at the ME level and matched to PYTHIA8 using the FxFx prescription. The $t\bar{t} + W/Z$

processes are simulated with MADGRAPH5_aMC@NLO with NLO precision at the ME level and matched to PYTHIA8. In the case of $t\bar{t} + W$, one extra parton is simulated at the ME level and the calculation is matched to PYTHIA8 using the FxFx prescription. Single top quark production is simulated with POWHEG v. 1 [32,33] with the h_{damp} parameter set to 172.5 GeV and using the CUETP8M2T4 tune in PYTHIA8. Diboson events are simulated at LO with PYTHIA8. The NNPDF3.0_lo_as_0130 and NNPDF3.0_nlo_as_0118 [34,35] parton distribution function (PDF) sets are used for the LO and NLO simulations, respectively.

The cross sections used to normalize the simulated predictions are calculated at the highest orders of perturbative QCD currently available: next-to-next-to-leading order (NNLO) for W + jets and Z + jets [36]; approximate NNLO for single top quark production in the tW channel [37]; and NLO for diboson [38] and $t\bar{t} + W/Z$ [39]. The $t\bar{t}$ simulation is normalized to a cross section of $831.8^{+19.8}_{-29.2}(\mathrm{scale}) \pm 35.1(\mathrm{PDF} + \alpha_S)$ pb (where α_S is the strong coupling constant), calculated with the TOP++2.0 program [40] at NNLO, including resummation of next-to-next-to-leading-logarithmic soft-gluon terms and assuming $m_t = 172.5$ GeV.

Additional pp interactions within the same or nearby bunch crossings (pileup) are simulated for all samples, using a pileup multiplicity distribution that reflects the distribution of reconstructed vertices in data. The interactions of particles with the CMS detector are simulated using GEANT4 (v. 9.4) [41].

V. EVENT SELECTION

The event selection [12] targets the dileptonic decay $t\bar{t} \to b\ell^+\nu\bar{b}\ell^-\bar{\nu}$. To maximize the trigger efficiency, both single-lepton and dilepton trigger paths are used. For the single-electron (single-muon) trigger, a transverse momentum threshold of $p_T = 27(24)$ GeV is applied. The same-flavor dilepton triggers require either an electron pair with $p_T > 23(12)$ GeV for the leading (trailing) electron, or a muon pair with $p_T > 17(8)$ GeV for the leading (trailing) muon, where leading (trailing) refers to the electron or muon with the highest (second-highest) p_T in the event. The different-flavor dilepton triggers require either an electron with $p_T > 12$ GeV and a muon with $p_T > 23$ GeV, or an electron with $p_T > 23$ GeV and a muon with $p_T > 8$ GeV.

The events selected by the HLT are reconstructed offline using a particle-flow algorithm [42], which aims at reconstructing each individual particle in an event using an optimized combination of information from the various elements of the CMS detector. Electron candidates are reconstructed from a combination of the track momentum at the main interaction vertex and the corresponding clusters in the ECAL with a Gaussian sum filter algorithm [43]. Electron candidates with ECAL clusters in the region between the barrel and end cap ($1.44 < |\eta_{\mathrm{cluster}}| < 1.57$)

have a reduced reconstruction efficiency and are excluded. A relative isolation criterion $I_{rel} < 0.0588$ (0.0571) is applied for electron candidates in the barrel (end cap). The I_{rel} is defined as the p_T sum of all neutral hadron, charged hadron, and photon candidates within a distance of 0.3 from the electron candidate in η–ϕ space, divided by the p_T of the electron candidate, with a correction to suppress the residual effect of pileup. Additional electron identification requirements are applied to reject misidentified electron candidates and candidates originating from photon conversions [42,43]. Muon candidates are reconstructed using the track information from the tracker and the muon system [44]. A relative isolation requirement of $I_{rel} < 0.15$ within a distance of 0.4 in η–ϕ space from the muon candidate is applied. In addition, muon identification requirements are used to reject misidentified muon candidates and candidates originating from decay-in-flight processes [44]. Both electron and muon candidates are required to have $p_T > 25(20)$ GeV for the leading (trailing) candidate and $|\eta| < 2.4$.

Jets are reconstructed by clustering the particle-flow candidates using the anti-k_T clustering algorithm with a distance parameter of 0.4 [45,46]. The jet momentum is determined as the vector sum of all particle momenta in the jet, and is found from simulation to be within 5–10% of the true momentum over the whole p_T spectrum and detector acceptance. Pileup can contribute additional tracks and calorimetric energy depositions to the jet momentum. To mitigate this effect, tracks identified to originate from pileup vertices are discarded, and an offset correction is applied to correct for remaining contributions from neutral particles from pileup [42]. Jet energy corrections are derived from simulation to bring the measured response of jets to that of particle-level jets on average. *In situ* measurements of the momentum imbalance in dijet, photon + jet, Z + jet, and multijet events are used to account for any residual differences in the jet energy scale (JES) between data and simulation. Additional selection criteria are applied to remove badly reconstructed jets [42,47]. Jets are selected if they have $p_T > 30$ GeV and $|\eta| < 2.4$. Jets are rejected if the distance in η–ϕ space between the jet and the closest lepton is less than 0.4. Jets originating from the hadronization of b quarks (b jets) are identified (b tagged) by combining information related to secondary decay vertices reconstructed within the jets and track-based lifetime information in an algorithm (CSVv2) that provides a b jet identification efficiency of 79–87% and a probability to misidentify light- and charm-flavor jets as b jets of approximately 10 and 40%, respectively [48].

The missing transverse momentum vector $\vec{p}_T^{miss}$ is defined as the projection on the plane perpendicular to the beam axis of the negative vector sum of the momenta of all reconstructed particles in an event. Its magnitude is referred to as p_T^{miss}.

The selected events are required to have exactly two isolated electrons or muons of opposite electric charge and at least two jets. At least one of the jets is required to be b tagged. Events with a lepton-pair invariant mass $m_{\ell\bar{\ell}} < 20$ GeV are removed in order to suppress contributions from heavy-flavor resonance decays and low-mass Drell-Yan processes. In the e^+e^- and $\mu^+\mu^-$ channels, backgrounds from Z + jets processes are further suppressed by requiring $p_T^{miss} > 40$ GeV and vetoing events with $76 < m_{\ell\bar{\ell}} < 106$ GeV. The remaining background yield from Z + jets events, which is large in the e^+e^- and $\mu^+\mu^-$ channels, is determined by applying a factor derived from simulation to the number of Z + jets events observed in data in a control region where $m_{\ell\bar{\ell}}$ is close to the Z boson mass [49,50]. A correction to account for non-Z + jets backgrounds in the control region is derived from the $e^\pm\mu^\mp$ channel. The simulated Z + jets yield is corrected by up to 5% in each channel to match the determination from data.

The four-momenta of the top quark and antiquark in each event are estimated using a kinematic reconstruction algorithm [12,49]. The algorithm considers all possible assignments of reconstructed jets and leptons to the b quarks and leptons from top quark decay, and solves for the unknown neutrino momenta using the following assumptions and constraints: p_T^{miss} is assumed to originate solely from the two neutrinos; the invariant mass of each reconstructed W boson (m_W) must equal 80.4 GeV [1]; and the invariant mass of each reconstructed top quark must equal 172.5 GeV. Effects of detector resolution are accounted for by randomly smearing the measured energies and directions of the reconstructed jets and leptons according to their simulated resolutions. The assumed value of m_W is varied according to a simulated Breit-Wigner distribution, with a width of 2.1 GeV [1]. For a given application of the smearing, the solution of the equations for the neutrino momenta yielding the smallest reconstructed $m_{t\bar{t}}$ is chosen. For each solution, a weight is calculated based on the spectrum of the true invariant mass of the lepton and b jet system from top quark decay at the particle level [12]. The weights are summed over 100 applications of the smearing, and the top quark and antiquark four-momenta are calculated as a weighted average. Considering only the combinations with the most b-tagged jets, the assignment of jets and leptons that yields the maximum sum of weights is chosen. The efficiency of the kinematic reconstruction, defined as the fraction of the selected $t\bar{t}$ events where a solution is found, is about 90% in both data and simulation. Events with no real solution for the neutrino momenta are excluded from further analysis.

After applying the full event selection, 34 890 events in the e^+e^- channel, 70 346 events in the $\mu^+\mu^-$ channel, and 150 410 events in the $e^\pm\mu^\mp$ channel are observed. The difference in the e^+e^- and $\mu^+\mu^-$ channel yields is attributable to the lower efficiencies of the electron identification and isolation requirements. The differential cross section

measurements are made using the combination of events from the three channels, where the fraction of signal events in the data sample, estimated from simulation, is 79%.

In Figs. 2 and 3, distributions of all the reconstructed angular observables (defined in Sec. II) are shown. There is reasonable agreement between the data and the sum of the expected signal and background contributions given the systematic uncertainties. In addition to the systematic uncertainties discussed in Sec. VII, two uncertainties that affect only the normalization of the measured differential cross section are considered: the 2.5% uncertainty in the integrated luminosity of the data sample [5] is applied to the normalization of all simulated predictions, and a 1.5% normalization uncertainty is applied to the $t\bar{t}$ prediction to account for the uncertainty in the dileptonic branching fraction (BF) [1]. The shapes of the reconstructed distributions differ substantially from the expected parton-level functional forms of Eqs. (8)–(10) owing to the effects of bin migration, detector acceptance and efficiency, and background events, which are described in Sec. VI.

VI. UNFOLDING THE DIFFERENTIAL CROSS SECTIONS

The effects of detector acceptance and efficiency sculpt the reconstructed distributions, and the smearing introduced by the detector response, kinematic reconstruction algorithm, PS, and hadronization leads to the migration of events across bins. In order to measure the differential cross sections at the parton level in the full phase space, these effects are accounted for by using the TUnfold regularized unfolding method [51]. The response matrix used in the unfolding is calculated for each measured distribution using the default $t\bar{t}$ simulation, where the momenta of the parton-level top quarks are defined after QCD radiation has been simulated but before the top quark decays.

To keep the bin-to-bin migrations small (to avoid strong bin-to-bin correlations in the unfolded distributions), the widths of the measurement bins are chosen according to the reconstruction resolution of the observable. This is quantified both directly by comparing the generator level and detector level observables in simulation, and by measuring the purity and stability. Purity is defined as the fraction of events in a given bin at the detector level that originate from the same bin at the generator level, and stability is defined as the fraction of events in a given bin at the generator level that are reconstructed in the same bin at the detector level. For all observables measured in the top quark rest frame, the use of six bins of uniform width is found to be well matched to the reconstruction resolution. The purities and stabilities are typically 40%. For the observables measured in the laboratory frame ($\cos\varphi_{\mathrm{lab}}$ and $|\Delta\phi_{\ell\ell}|$), six uniform-width bins are also used. These observables have excellent experimental resolution, and the purities and stabilities are $>99\%$.

The presence of background events is accounted for prior to performing the unfolding. After subtracting all other background components, the background from dileptonic $t\bar{t}$ events with leptonically decaying τ leptons is subtracted as a fraction of the total remaining events. The fraction is evaluated per bin as the ratio of the background to the total dileptonic $t\bar{t}$ events in simulation. Thus, the shapes of the distributions for dileptonic $t\bar{t}$ events are taken from data, and any dependence on the total cross section used in the normalization of the simulated $t\bar{t}$ sample is avoided.

In TUnfold, a procedure based on matrix inversion is used to obtain an unfolded distribution from the measured distribution by applying a χ^2 minimization technique. The potential large statistical fluctuations and strong anticorrelations between adjacent bins arising from the matrix inversion are suppressed by introducing a term in the χ^2 expression that smooths (regularizes) the shape of the unfolded distribution [51]. The regularization term penalizes the curvature of a vector constructed from the product of the difference between the unfolded and simulated bin values and a factor calculated using the expected functional form [Eqs. (8)–(10)] such that a deviation in the coefficient corresponds to a linear change in the vector. Since linear changes are unconstrained by regularization of the curvature, and the functional forms at the parton level (which are unaffected by BSM phenomena in $t\bar{t}$ production) depend only on the coefficient, this ensures that the regularization cannot introduce a bias in the unfolded distribution. For the laboratory-frame distributions there are no such simple functional forms, and no factor is applied to the difference vector. However, this choice is of little consequence because the regularization is very weak owing to the low level of bin migration.

The use of wide bins for the response matrix loses information about its dependence inside each bin, meaning the unfolding can be biased if the physical process density differs from the simulation. Since the curvature regularization is unbiased, we make use of narrower bins in the TUnfold χ^2 minimization; a factor 4 narrower is found to be sufficient to reduce the bias from binning to a negligible level. We have thus replaced the biased implicit regularization from binning with an unbiased regularization of the curvature within each of the original bins.

The regularization level is determined for each distribution by minimizing the average global correlation coefficient (ρ_{avg}) [51], where ρ_{avg} is determined after rebinning to the original six bins.

For each measured bin, we perform tests using pseudo-data to confirm a linear response of the method to variations in the coefficient, and confirm that the distribution of the difference between the nominal bin value and that measured in pseudodata, normalized to the measured uncertainty, is consistent with having zero mean and unit width.

The data in the three channels are combined before unfolding in order to model correlations between channels
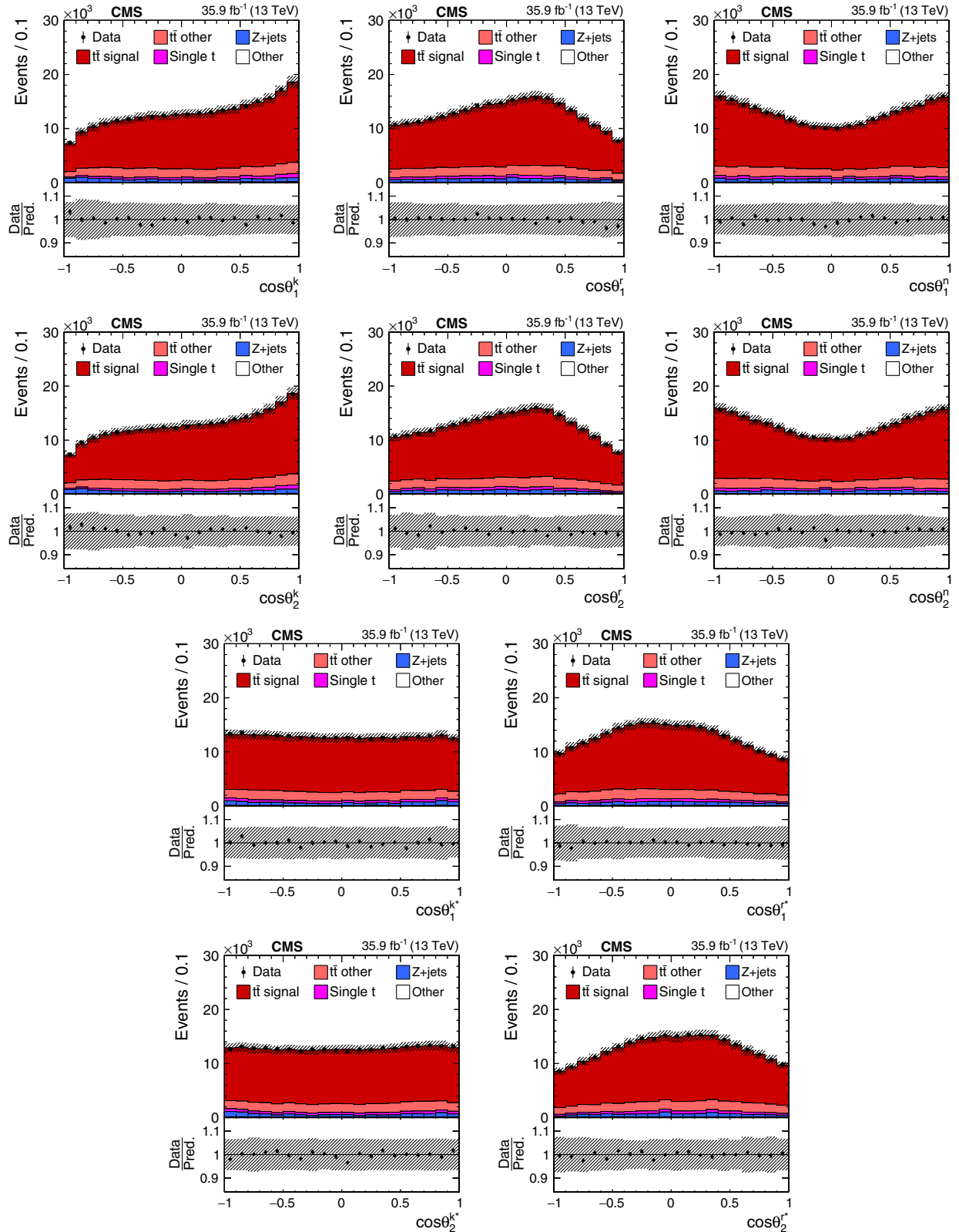
FIG. 2. Reconstructed distributions of $\cos\theta^i$ for top quarks (antiquarks) in the first and third (second and fourth) rows, where i refers to the reference axis with which the angle θ^i is measured. From left to right, $i = \hat{k}, \hat{r}, \hat{n}$ (upper two rows), and $i = \hat{k}^*, \hat{r}^*$ (lower two rows). The data (points) are compared to the simulated predictions (histograms). The vertical bars on the points represent statistical uncertainties, and the estimated systematic uncertainties in the simulated histograms are indicated by hatched bands. The ratio of the data to the sum of the predicted signal and background is shown in the lower panels.

FIG. 3. Reconstructed angular distributions used in the measurement of the $t\bar{t}$ spin correlation observables. The data (points) are compared to the simulated predictions (histograms). The vertical bars on the points represent statistical uncertainties, and the estimated systematic uncertainties in the simulated histograms are indicated by hatched bands. The ratio of the data to the sum of the predicted signal and background is shown in the lower panels.
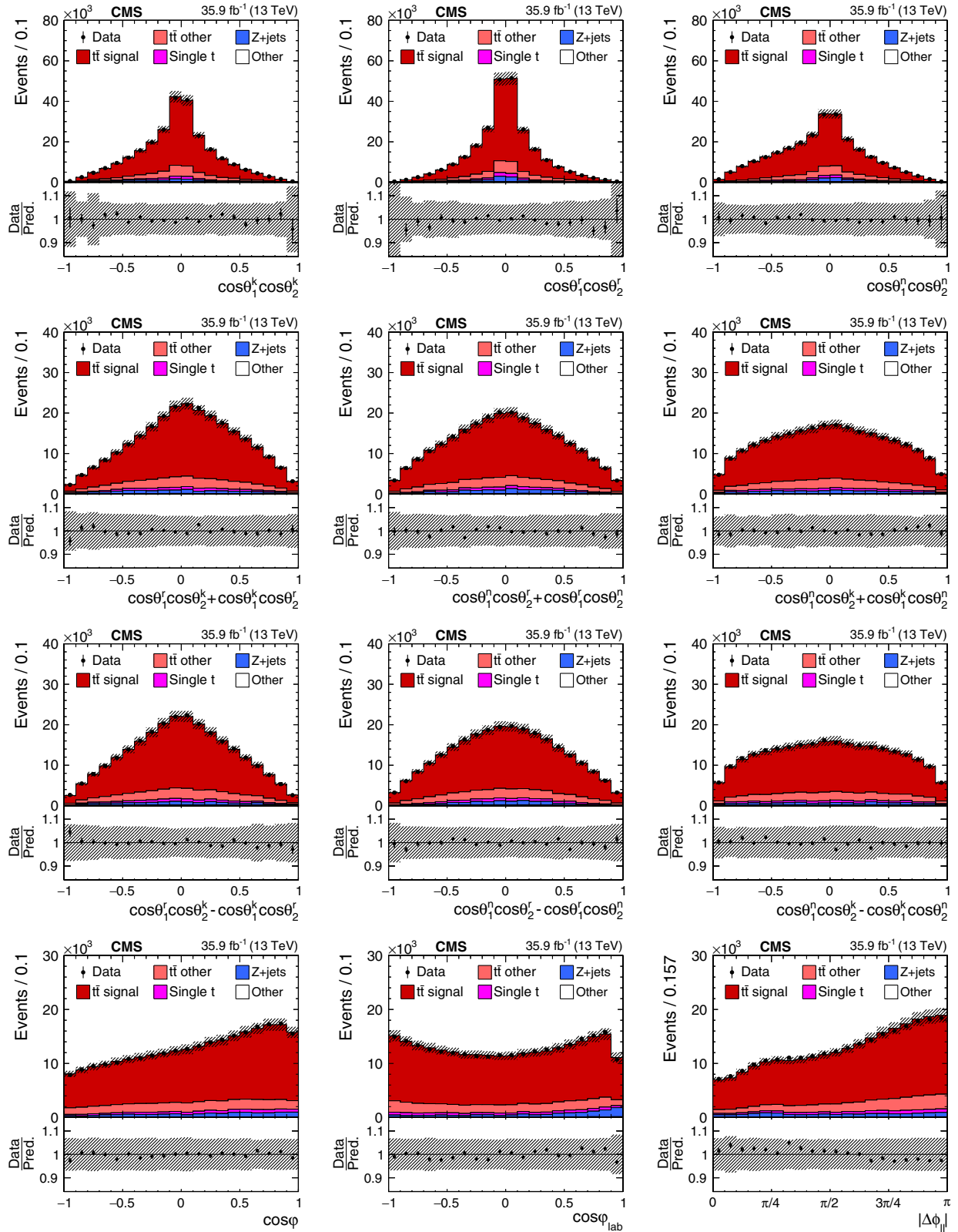
in situ and reduce statistical uncertainties in poorly populated regions of the response matrix. After unfolding, each distribution is normalized to unit area to measure the normalized differential cross section.

VII. SYSTEMATIC UNCERTAINTIES

The systematic uncertainties arising from the detector performance and the modeling of the signal and background processes are evaluated from the difference between the nominal measurement and that obtained by repeating the unfolding procedure using simulated events with the appropriate systematic variation. Each source of systematic uncertainty is represented by a covariance matrix for the bins of the measured normalized differential cross sections. The total systematic uncertainty is derived from the sum of these covariance matrices. In this section, each of the applied variations is detailed and categorized into experimental and theoretical sources of uncertainty.

A. Experimental sources of uncertainty

Many of the experimental sources of uncertainty relate to the scale factors (SFs), defined as the ratio of the efficiencies in data and simulation, that are applied to the simulation in order to accurately model the data.

The efficiencies of the triggers in data are measured as the fraction of events passing alternative triggers based on a p_T^{miss} requirement that also satisfy the criteria of the trigger of interest [12,52]. As the efficiency of the p_T^{miss} requirement is only weakly correlated with the dilepton trigger efficiencies, the bias introduced by the p_T^{miss} requirement is negligible. The efficiencies are close to unity in both data and simulation, as are the corresponding SFs. To estimate the uncertainty from the modeling of the trigger efficiency, the SFs are varied within their uncertainties, both globally for all bins and depending on the η of the leptons. The total trigger uncertainty is derived by taking the maximum deviation produced by the two variations in each unfolded bin.

The SFs for the lepton identification and isolation efficiencies are determined with a tag-and-probe method using Z + jets event samples [50,53]. Measured in bins of η and p_T, the SFs are generally within 10% of unity for electrons, and consistent with unity for muons. The lepton identification and isolation uncertainty is estimated by varying the SFs within their uncertainties. The efficiency of the kinematic reconstruction of the top quarks is found to be consistent between data and simulation within around 0.2%. An associated uncertainty is derived by varying the corresponding SFs by $\pm 0.2\%$.

The uncertainty from the modeling of the number of pileup events is obtained by changing the inelastic pp cross section assumed in simulation by $\pm 4.6\%$, consistent with the cross section uncertainty presented in Ref. [54].

The uncertainty arising from the imperfect modeling of the b tagging efficiency is determined by varying the measured SFs within their uncertainties, both globally and depending on the p_T and η of the b jets. The total uncertainty is derived by taking the maximum observed deviation in each unfolded bin. The b tagging uncertainties for heavy-flavor (b and c) and light-flavor (u, d, s, and gluon) jets are calculated separately, and combined in quadrature to give the total b tagging uncertainty. To avoid double counting of the uncertainty related to the b tagging efficiency, when necessary, the SFs for b tagging efficiency are recalculated in the evaluation of the remaining sources of experimental and theoretical uncertainty described in this section, using the procedure given in Ref. [12].

The uncertainty arising from the JES is determined by varying the individual sources of uncertainty in the JES in bins of the jet p_T and η, and taking the quadrature sum of the differences [55]. The JES variations are propagated to the uncertainties in p_T^{miss}. An additional uncertainty in the calculation of p_T^{miss} is estimated by varying the energies of reconstructed particles not clustered into jets (unclustered energy). The uncertainty from the jet energy resolution (JER) is determined by the variation of the JER in simulation within its uncertainty in different η regions [55].

B. Theoretical sources of uncertainty

The uncertainty arising from the missing higher-order terms in the simulation of the signal process at the ME level is assessed by varying the renormalization and factorization scales (μ_R and μ_F) in the POWHEGv2 simulation up and down by a factor of 2 with respect to their nominal values, both individually and simultaneously (six variations in total). The nominal choice for the scales is $m_T^t = \sqrt{m_t^2 + p_{T,t}^2}$, where $p_{T,t}$ denotes the p_T of the top quark in the $t\bar{t}$ rest frame. In the PS simulation, the corresponding uncertainty is estimated by four additional variations: changing the scale of initial- and final-state radiation individually up and down by factors of 2 and $\sqrt{2}$, respectively, as suggested in Ref. [27]. The total scale uncertainty is taken as the maximum deviation from the nominal prediction from all ten variations.

The uncertainty originating from the scheme used to match the ME-level calculation to the PS simulation is derived by varying the h_{damp} parameter in POWHEGv2 by factors of 1.42 and 0.63, according to the results of tuning this parameter from Ref. [24].

The default setup in PYTHIA8 includes a multiple parton interaction (MPI) based model of color reconnection (CR) with early resonance decays switched off. To estimate the uncertainty from this choice of model, the analysis is repeated with three other CR models within PYTHIA8: the MPI-based scheme with early resonance decays switched on, a gluon-move scheme [56], and a QCD-inspired scheme [57]. The total uncertainty from CR modeling is

estimated by taking the maximum deviation from the nominal result. The uncertainty related to modeling of the underlying event is estimated by varying the parameters used to derive the CUETP8M2T4 tune in the default setup.

The uncertainty from the b quark fragmentation function is assessed from the largest deviation when varying the Bowler-Lund function within its uncertainties [58] and repeating the analysis with the Peterson model for b quark fragmentation [59]. An uncertainty from the semileptonic BF of b hadrons is estimated by correcting the $t\bar{t}$ simulation to match the BF in Ref. [1].

The uncertainty from the PDFs is assessed from the standard deviation of the result when using the replicas of the NNPDF3.0 PDF set in the signal simulation [34,60]. An additional uncertainty is derived by varying the α_S value within its uncertainty in the PDF set [60]. The dependence of the measurement on the assumed m_t value is estimated by varying the chosen m_t in the default setup by ± 1 GeV with respect to the default value of 172.5 GeV.

Previous CMS studies have shown that the p_T distribution of the top quark measured from data is softer than that in the NLO simulation of $t\bar{t}$ production [12,49,61–63]. This is understood to arise at least partly from the missing higher-order QCD terms [64–67]. The change in the measurement when reweighting the simulated $t\bar{t}$ event sample to match the top quark p_T spectrum in data is taken as a two-sided systematic uncertainty associated with the signal modeling.

Since $t\bar{t}$ events producing electrons or muons originating from the decay of τ leptons are considered a background, the measured differential cross sections are sensitive to the relative BFs of W bosons decaying to τ leptons and electrons or muons, and the τ semileptonic BFs assumed in the simulation. An uncertainty of 2.5% is assigned to the relative normalization of this background process. The shape and absolute normalization of this process is taken from data, as described in Sec. VI. The normalizations of all other backgrounds are varied by $\pm 30\%$ [12,50].

VIII. RESULTS

A. Normalized differential cross sections

Normalized differential cross sections at the parton level are measured for the 22 observables introduced in Sec. II. For the top quark polarization observables measured using the nominal ($\hat{k}$, $\hat{r}$ and $\hat{n}$) and modified ($\hat{k}^*$ and $\hat{r}^*$) reference axes, the results are shown in Figs. 4 and 5, respectively. The results for the observables that probe the diagonal $t\bar{t}$ spin correlation coefficients and for the laboratory-frame spin correlation observables are shown in Fig. 6. For the cross spin correlation observables, the results are shown in Fig. 7. The measured distributions are compared with predictions from the POWHEGv2 and MADGRAPH5_aMC@NLO simulations and with calculations for $t\bar{t}$ production at NLO in QCD with

EW corrections [3,4], as well as similar calculations in the absence of top quark polarization or spin correlations. For the observables measured in the top quark rest frame, the latter are equivalent to the predictions of Eqs. (8)–(10), with the coefficients set to zero. For the laboratory-frame observables, dedicated calculations were made using the computational setup described in Refs. [3,68]. In addition, the only NNLO QCD prediction [69] is shown for the $|\Delta\phi_{\ell\ell}|$ distribution in Fig. 6.

The effect of spin correlations is most clearly visible in the $\cos\varphi$ distribution in Fig. 6, where the data strongly favor the predictions with spin correlations compared to the uncorrelated prediction. The presence of spin correlations can also be seen in the other distributions sensitive to P- and CP-even spin correlations: the three $\cos\theta_1^i \cos\theta_2^i$ distributions and the two laboratory-frame distributions ($\cos\varphi_{lab}$ and $|\Delta\phi_{\ell\ell}|$) in Fig. 6, and the $\cos\theta_1^r \cos\theta_2^k + \cos\theta_1^k \cos\theta_2^r$ distribution in Fig. 7. However, the measurements are not sensitive to the small level of top quark polarization predicted in the SM, and do not significantly disfavor the unpolarized predictions in Figs. 4 and 5.

The statistical and systematic correlation matrices for the normalized differential cross sections are determined simultaneously for all 132 measured bins to allow the fitting of multiple distributions, and are shown in Fig. 8. The statistical correlations are estimated using a bootstrap resampling of the data [70], and the systematic correlations are estimated by simultaneously evaluating the systematic variations described in Sec. VII for all measured bins. The statistical correlations among bins from the same distribution exhibit a typical pattern of correlation and anticorrelation arising from the unfolding. The statistical correlations between bins from different distributions are typically small, but the relationships between some of the distributions result in stronger correlations (for example, $\cos\theta_{1,2}^{i*}$ and $\cos\theta_{1,2}^i$ are the same up to a sign). The systematic correlations are in general much stronger, and the pattern of positive and negative correlations reflects the relative changes in shape of the different distributions in response to the systematic variations.

The agreement between the measured distributions and the four theoretical predictions shown in Figs. 4–7 is quantified by evaluating the χ^2, taking the uncertainties from the sum of the measured statistical and systematic covariance matrices (and not including any uncertainties in the prediction). The results are shown in Table II. For the observables measured in the top quark rest frame, there is generally good agreement between the measured distributions and all the predictions in the presence of spin correlations. For the two observables measured in the laboratory frame, there is greater variation between the predictions. The POWHEGv2 prediction best describes the data for $\cos\varphi_{lab}$, while for $|\Delta\phi_{\ell\ell}|$ the MADGRAPH5_aMC@NLO prediction provides the best agreement. The NNLO QCD prediction shown in Fig. 6 also describes the observed $|\Delta\phi_{\ell\ell}|$ distribution well, with a

FIG. 4.   Unfolded data (points) and predicted (horizontal lines) normalized differential cross sections with respect to $\cos\theta^i$ for top quarks (antiquarks) in the first (second) column, probing polarization coefficients B_1^i (B_2^i). From top to bottom, the reference axis $i = \hat{k}$, $\hat{r}$, $\hat{n}$. The vertical lines on the points represent the total uncertainties, with the statistical components indicated by horizontal bars. The ratios of various predictions to the data are shown in the lower panels.
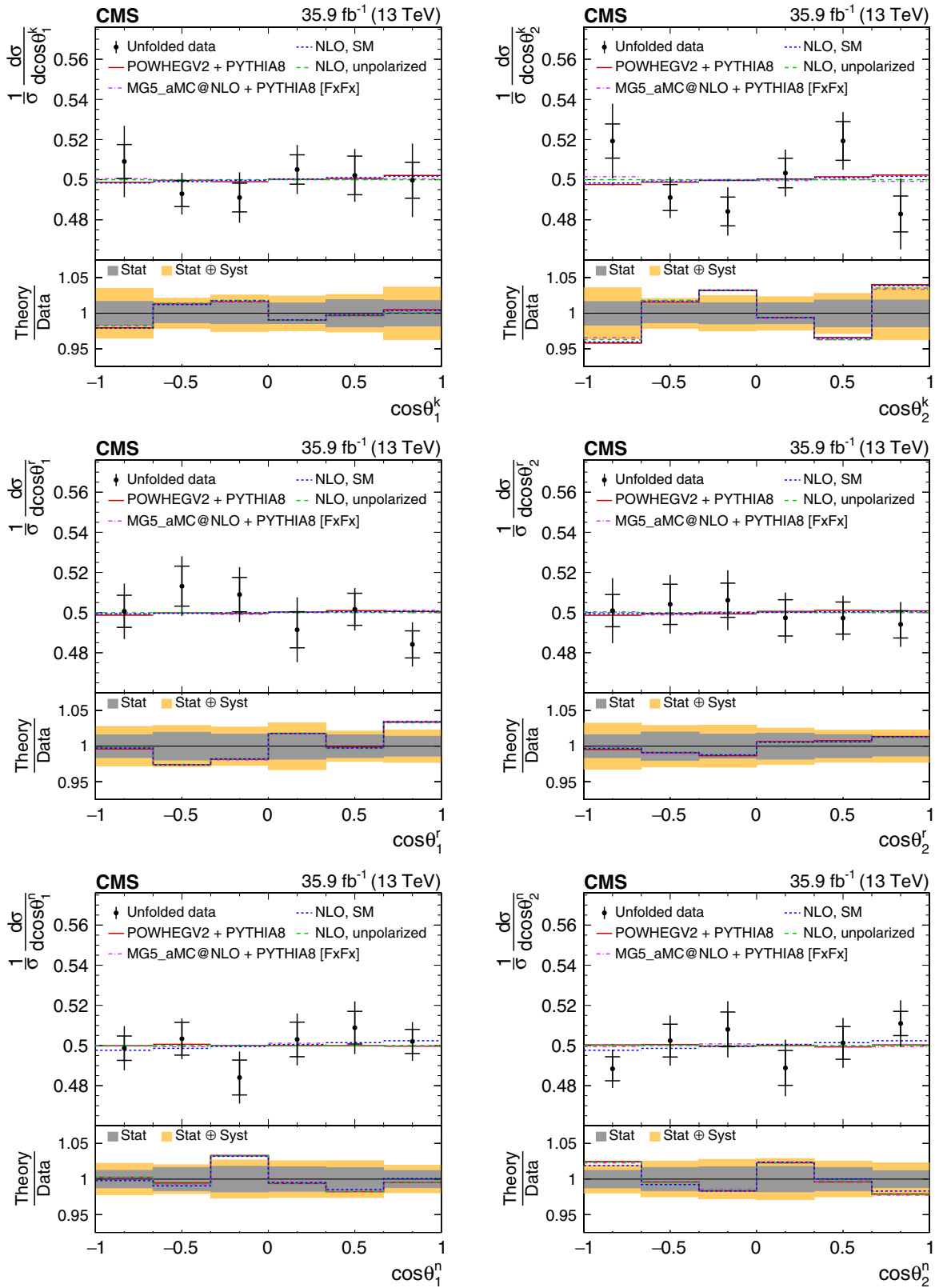
FIG. 5.   Unfolded data (points) and predicted (horizontal lines) normalized differential cross sections with respect to $\cos\theta^{i*}$ for top quarks (antiquarks) in the first (second) column, probing polarization coefficients B_1^{i*} (B_2^{i*}). The reference axis $i* = \hat{k}*$ (top row) and $\hat{r}*$ (bottom row). The vertical lines on the points represent the total uncertainties, with the statistical components indicated by horizontal bars. The ratios of various predictions to the data are shown in the lower panels.
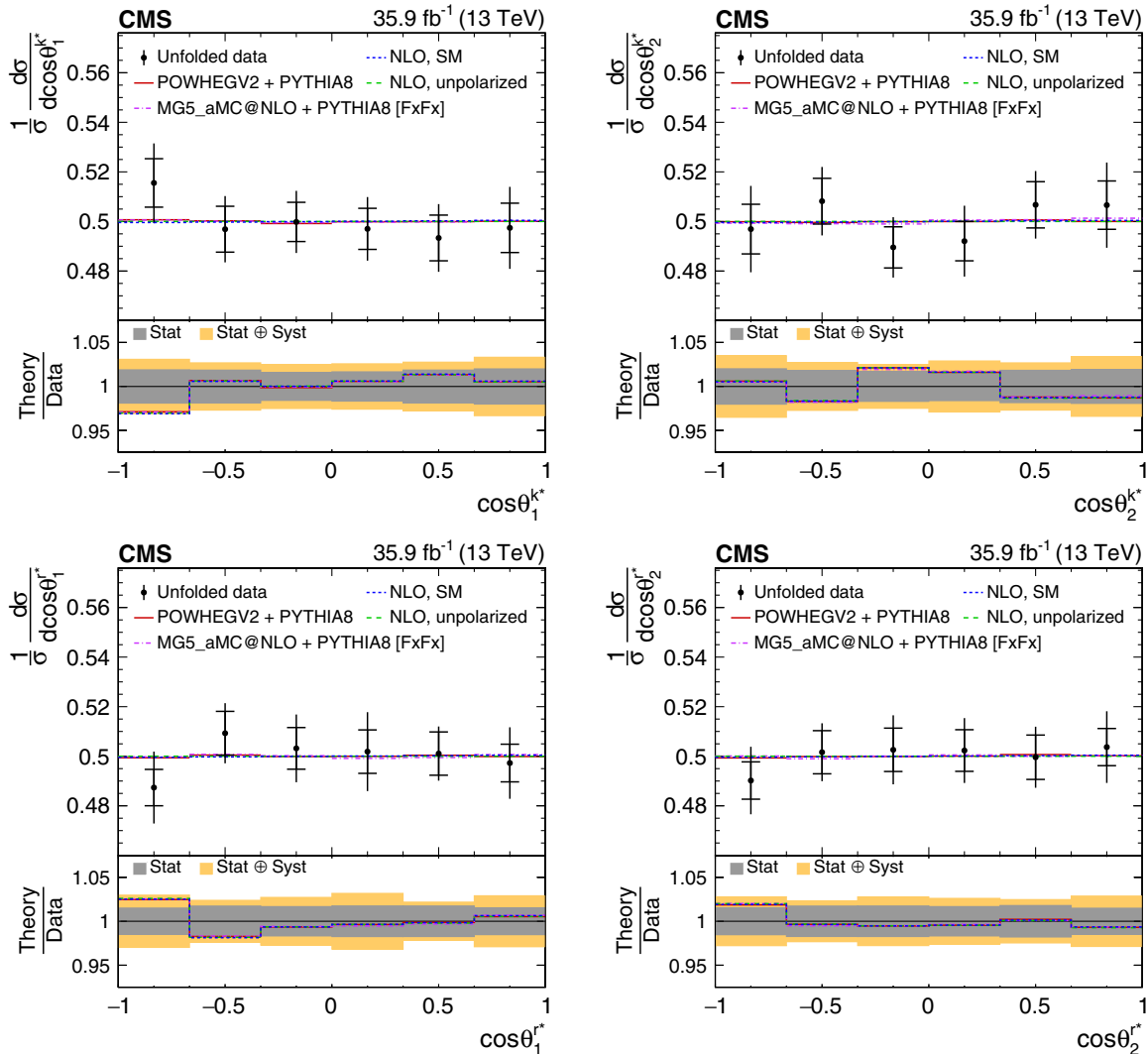
χ^2/d.o.f. of 4.3/5, where d.o.f. is the number of degrees of freedom.

B. Coefficients

From each measured normalized differential cross section, we extract the corresponding coefficient, using the functional forms of Eqs. (8)–(10) and combining the information from the measured bins in a way that minimizes the uncertainty in the coefficient. For the laboratory-frame observables, the shapes of the distributions are instead quantified by the asymmetries defined in Eq. (11). The results for all quantities are shown with their total uncertainties in Table III, where they are compared with predictions from POWHEGv2 and MADGRAPH5_aMC@NLO simulations and the NLO calculations [3,4]. The uncertainties in the NLO

calculations come from varying μ_R and μ_F simultaneously up and down by a factor of 2 from their nominal value of m_t. The NNLO QCD prediction for $A_{|\Delta\phi_{\ell\ell}|}$ is $0.115^{+0.005}_{-0.001}$ [69], where the uncertainties are taken from the largest deviations when varying μ_R and μ_F individually and simultaneously up and down by a factor of 2 from the nominal choice of $(m_T^t + m_T^{\bar{t}})/4$. The results are also shown in Figs. 9–11.

There is good agreement between the measured coefficients and all the SM predictions, while substantial variation is seen in the predicted laboratory-frame asymmetries, which have sizable scale uncertainties. In the fixed-order calculations of Refs. [3,4], the numerator and denominator of the normalized differential cross section are computed at NLO QCD including EW corrections, and then the ratio is consistently expanded to NLO. On the

FIG. 6. Unfolded data (points) and predicted (horizontal lines) normalized differential cross sections for the diagonal spin correlation observables (first two rows) and the laboratory-frame observables (bottom row). The vertical lines on the points represent the total uncertainties, with the statistical components indicated by horizontal bars. The ratios of various predictions to the data are shown in the lower panels.
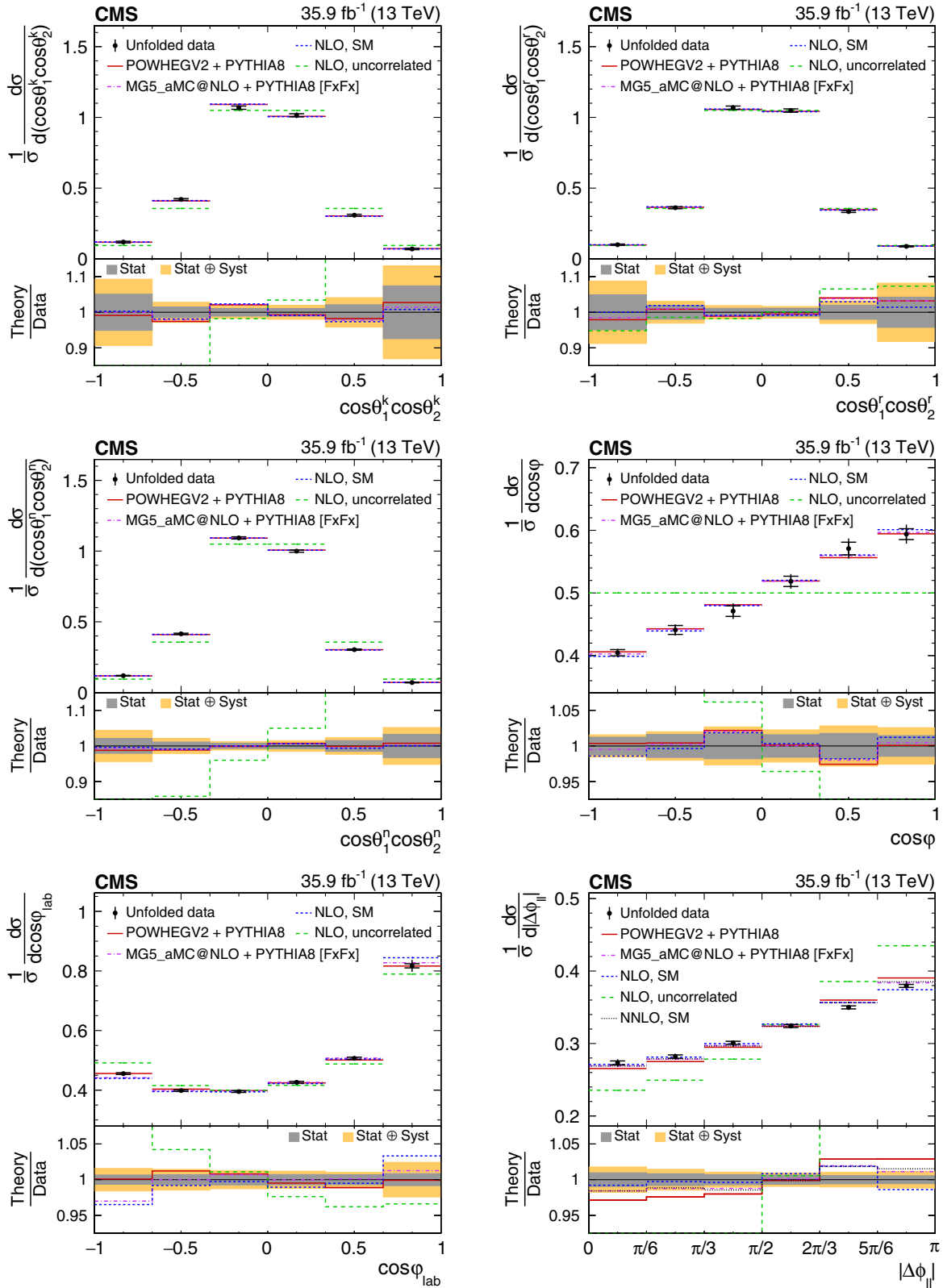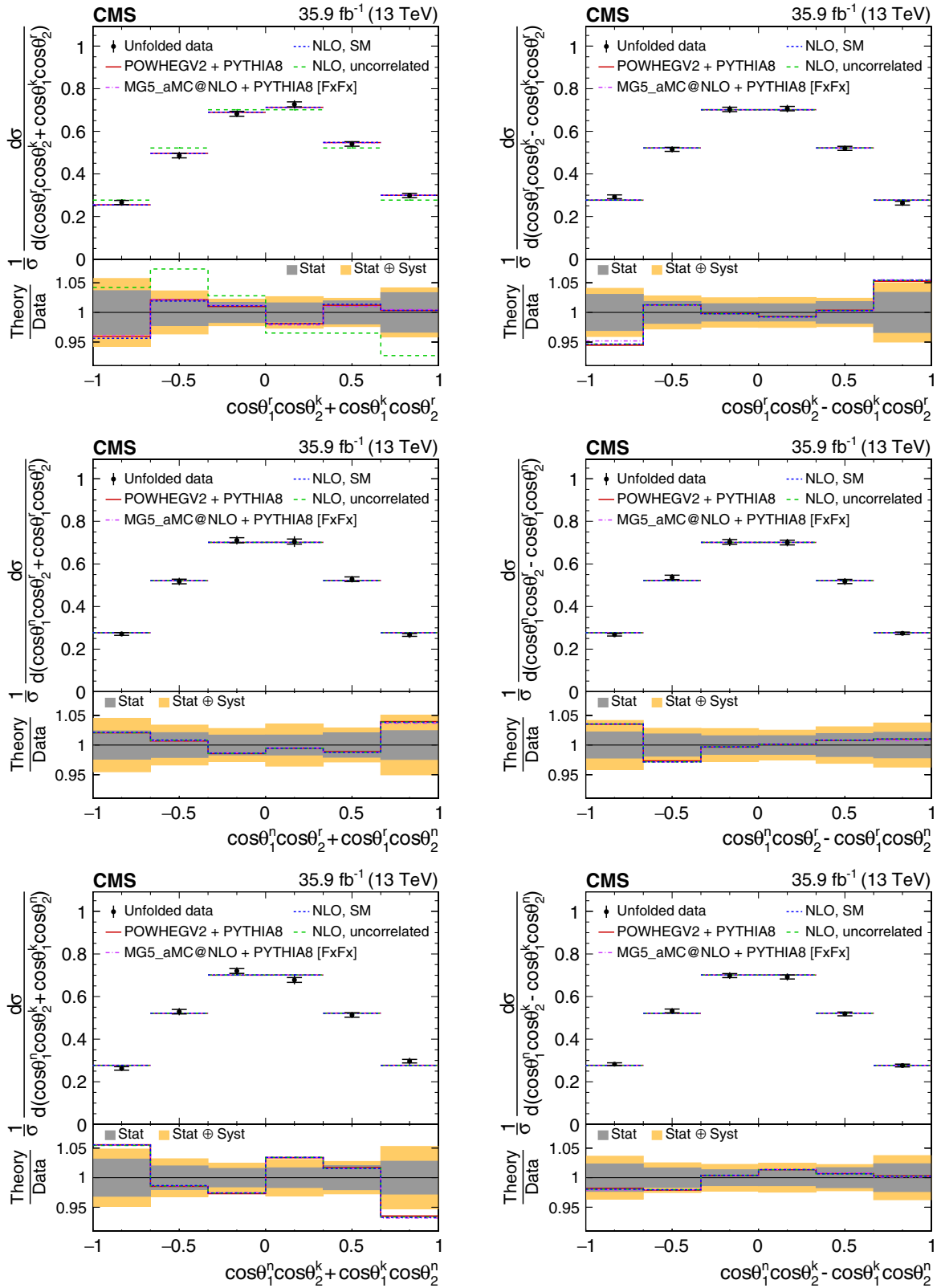
FIG. 7. Unfolded data (points) and predicted (horizontal lines) normalized differential cross sections for the cross spin correlation observables. The vertical lines on the points represent the total uncertainties, with the statistical components indicated by horizontal bars. The ratios of various predictions to the data are shown in the lower panels.
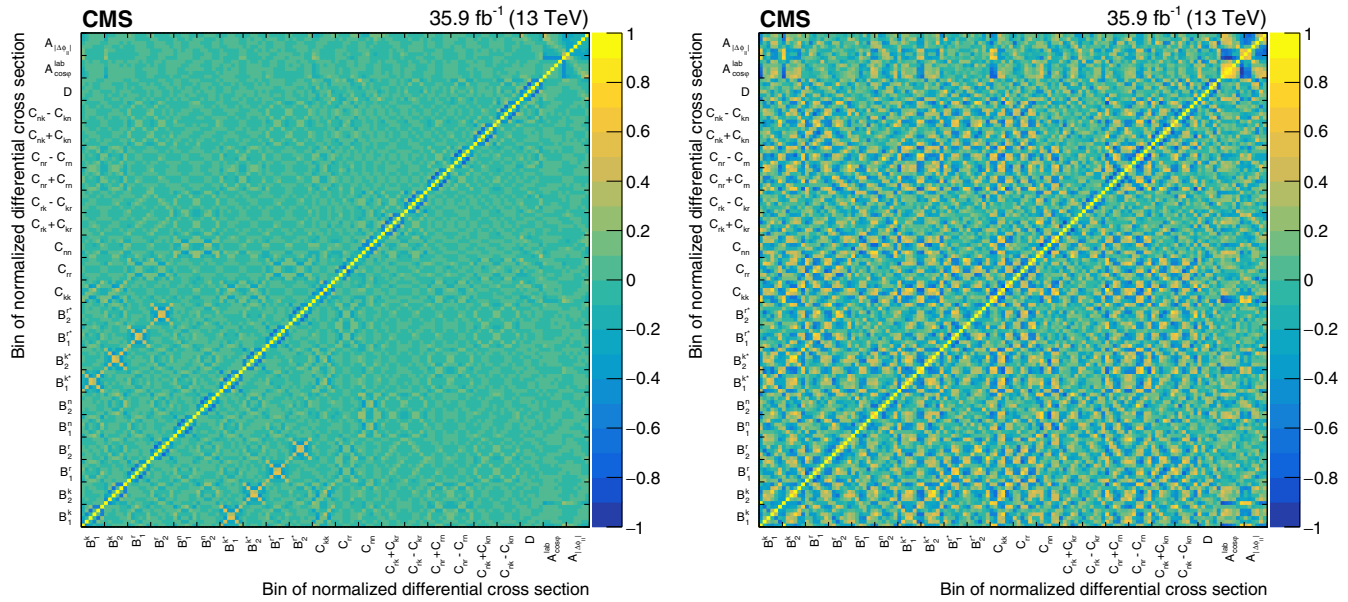
FIG. 8.   Values (gray scale) of the total statistical (left) and systematic (right) correlation matrices for all measured bins of the normalized differential cross sections. Each group of six bins along each axis corresponds to a measured distribution, and for conciseness is labeled by the name of the associated coefficient (as defined in Table I).

TABLE II.   The χ^2 between the data and the predictions for all measured normalized differential cross sections (Figs. 4–7). The last column refers to the prediction in the case of no spin correlation or polarization. The χ^2 values are evaluated using the sum of the measured statistical and systematic covariance matrices. The number of degrees of freedom (d.o.f.) is 5 for all observables. In the last row, the χ^2 values are given for the set of all measured bins.

	χ^2 between data and prediction (d.o.f. = 5)			
Observable	POWHEGv2	MG5_aMC@NLO	NLO calculation	No spin correlation/polarization
$\cos\theta_1^k$	1.1	1.0	1.1	1.1
$\cos\theta_2^k$	5.2	5.0	5.2	5.2
$\cos\theta_1^r$	4.3	4.4	4.2	3.9
$\cos\theta_2^r$	0.7	0.5	0.6	0.5
$\cos\theta_1^n$	1.9	1.8	1.8	1.9
$\cos\theta_2^n$	3.2	3.1	2.1	3.1
$\cos\theta_1^{k*}$	1.3	1.3	1.4	1.3
$\cos\theta_2^{k*}$	1.8	1.6	1.7	1.8
$\cos\theta_1^{r*}$	1.5	1.5	1.6	1.6
$\cos\theta_2^{r*}$	0.5	0.6	0.6	0.6
$\cos\theta_1^k\cos\theta_2^k$	3.1	3.2	3.5	66.7
$\cos\theta_1^r\cos\theta_2^r$	2.0	1.7	1.1	7.4
$\cos\theta_1^n\cos\theta_2^n$	0.6	0.3	0.3	267.0
$\cos\theta_1^r\cos\theta_2^k + \cos\theta_1^k\cos\theta_2^r$	1.5	1.6	1.7	12.3
$\cos\theta_1^r\cos\theta_2^k - \cos\theta_1^k\cos\theta_2^r$	3.6	3.1	3.6	3.6
$\cos\theta_1^n\cos\theta_2^r + \cos\theta_1^r\cos\theta_2^n$	1.7	1.7	1.8	1.8
$\cos\theta_1^n\cos\theta_2^r - \cos\theta_1^r\cos\theta_2^n$	1.8	1.9	1.9	1.9
$\cos\theta_1^n\cos\theta_2^k + \cos\theta_1^k\cos\theta_2^n$	3.8	4.0	4.0	3.9
$\cos\theta_1^n\cos\theta_2^k - \cos\theta_1^k\cos\theta_2^n$	2.3	2.4	2.2	2.2
$\cos\varphi$	1.5	0.7	1.4	496.2
$\cos\varphi_{\text{lab}}$	3.9	7.6	7.0	66.5
$|\Delta\phi_{\ell\ell}|$	10.8	4.0	9.2	190.4
All (d.o.f. = 110)	88.4	89.7	88.6	2119.8

TABLE III. Measured coefficients and asymmetries and their total uncertainties. Predicted values from simulation are quoted with a combination of statistical and scale uncertainties, while the NLO calculated values are quoted with their scale uncertainties [3,4]. The NNLO QCD prediction for $A_{|\Delta\phi_{\ell\ell}|}$, with scale uncertainties, is $0.115^{+0.005}_{-0.001}$ [69].

Coefficient	Measured	POWHEGv2	MG5_aMC@NLO	NLO calculation
B^k_1	0.005 ± 0.023	$0.004^{+0.001}_{-0.001}$	$0.000^{+0.001}_{-0.001}$	$4.0^{+1.7}_{-1.2} \times 10^{-3}$
B^k_2	0.007 ± 0.023	$0.006^{+0.001}_{-0.001}$	$-0.002^{+0.001}_{-0.001}$	$4.0^{+1.7}_{-1.2} \times 10^{-3}$
B^r_1	-0.023 ± 0.017	$0.002^{+0.001}_{-0.001}$	$0.002^{+0.001}_{-0.001}$	$1.6^{+1.2}_{-0.9} \times 10^{-3}$
B^r_2	-0.010 ± 0.020	$0.003^{+0.001}_{-0.001}$	$0.000^{+0.001}_{-0.001}$	$1.6^{+1.2}_{-0.9} \times 10^{-3}$
B^n_1	0.006 ± 0.013	$-0.001^{+0.001}_{-0.001}$	$0.001^{+0.001}_{-0.001}$	$5.7^{+0.5}_{-0.4} \times 10^{-3}$
B^n_2	0.017 ± 0.013	$-0.001^{+0.001}_{-0.001}$	$0.000^{+0.001}_{-0.001}$	$5.7^{+0.5}_{-0.4} \times 10^{-3}$
B^{k*}_1	-0.016 ± 0.018	$-0.001^{+0.001}_{-0.001}$	$0.000^{+0.001}_{-0.001}$	$<10^{-3}$
B^{k*}_2	0.007 ± 0.019	$0.001^{+0.001}_{-0.001}$	$0.003^{+0.002}_{-0.001}$	$<10^{-3}$
B^{r*}_1	0.001 ± 0.017	$0.000^{+0.001}_{-0.001}$	$0.000^{+0.001}_{-0.001}$	$<10^{-3}$
B^{r*}_2	0.010 ± 0.017	$0.001^{+0.001}_{-0.001}$	$0.001^{+0.001}_{-0.001}$	$<10^{-3}$
C_{kk}	0.300 ± 0.038	$0.314^{+0.005}_{-0.004}$	$0.325^{+0.011}_{-0.006}$	$0.331^{+0.002}_{-0.002}$
C_{rr}	0.081 ± 0.032	$0.048^{+0.007}_{-0.006}$	$0.052^{+0.007}_{-0.005}$	$0.071^{+0.008}_{-0.006}$
C_{nn}	0.329 ± 0.020	$0.317^{+0.001}_{-0.001}$	$0.324^{+0.002}_{-0.002}$	$0.326^{+0.002}_{-0.002}$
$C_{rk} + C_{kr}$	-0.193 ± 0.064	$-0.201^{+0.004}_{-0.003}$	$-0.198^{+0.004}_{-0.005}$	$-0.206^{+0.002}_{-0.002}$
$C_{rk} - C_{kr}$	0.057 ± 0.046	$-0.001^{+0.002}_{-0.002}$	$0.004^{+0.002}_{-0.002}$	0
$C_{nr} + C_{rn}$	-0.004 ± 0.037	$-0.003^{+0.002}_{-0.002}$	$0.001^{+0.002}_{-0.002}$	$1.06^{+0.01}_{-0.01} \times 10^{-3}$
$C_{nr} - C_{rn}$	-0.001 ± 0.038	$0.002^{+0.002}_{-0.002}$	$0.001^{+0.003}_{-0.002}$	0
$C_{nk} + C_{kn}$	-0.043 ± 0.041	$-0.002^{+0.002}_{-0.002}$	$0.003^{+0.002}_{-0.002}$	$2.15^{+0.04}_{-0.07} \times 10^{-3}$
$C_{nk} - C_{kn}$	0.040 ± 0.029	$-0.001^{+0.002}_{-0.002}$	$-0.001^{+0.002}_{-0.002}$	0
D	-0.237 ± 0.011	$-0.226^{+0.003}_{-0.004}$	$-0.233^{+0.004}_{-0.006}$	$-0.243^{+0.003}_{-0.003}$
$A^{\text{lab}}_{\cos\varphi}$	0.167 ± 0.010	$0.161^{+0.002}_{-0.002}$	$0.174^{+0.004}_{-0.003}$	$0.181^{+0.004}_{-0.003}$
$A_{|\Delta\phi_{\ell\ell}|}$	0.103 ± 0.008	$0.125^{+0.004}_{-0.005}$	$0.115^{+0.003}_{-0.005}$	$0.108^{+0.009}_{-0.012}$

other hand, in the computations from simulation the ratio is not expanded. This leads to differences that are nominally of order α_S^2, in addition to the EW corrections (which are not included in the simulation). However, for $A_{|\Delta\phi_{\ell\ell}|}$ the EW corrections are found to be only at the level of 2% using the computational setup of Ref. [3]. In the NNLO QCD calculation, the ratio is not expanded [69].

The breakdown of the systematic and statistical uncertainties in the polarization and spin correlation measurements is given in Tables IV and V, respectively. The systematic and statistical uncertainties are of comparable size for most of the measured coefficients. The exception is $B^k_{1,2}$, because the JES and b quark fragmentation uncertainties have a large effect on the reconstructed top quark momentum in the $t\bar{t}$ CM frame. The laboratory-frame asymmetries have statistical uncertainties smaller than their systematic uncertainties. The excellent reconstruction resolution results in little dilution of the statistical precision of the measured asymmetries. There is also a large background uncertainty in $A^{\text{lab}}_{\cos\varphi}$, owing to the large $Z +$ jets

contribution near $\cos\varphi_{\text{lab}} = 1$, and a large top quark p_{T} modeling uncertainty in $A_{|\Delta\phi_{\ell\ell}|}$.

The statistical and systematic correlation matrices for the measured coefficients are shown in Fig. 12. The coefficients are largely statistically uncorrelated, as expected for the measurement of independent quantities. The expected statistical correlations between the related D and diagonal C coefficients are clear, as are the correlations between D and the two related laboratory-frame asymmetries. The systematic correlations are in general much stronger. In particular, strong correlations are evident for the polarization measurements with positively and negatively charged leptons (except for the B^n_i, where the largest sources of systematic uncertainty have a substantial statistical uncertainty from the simulation). The coefficients with significant statistical correlations naturally have significant systematic correlations as well.

The sums and differences of the pairs of B coefficients are of interest, as they correspond to the CP-even and CP-odd components of the polarization. The results obtained using the measured coefficients and their covariance
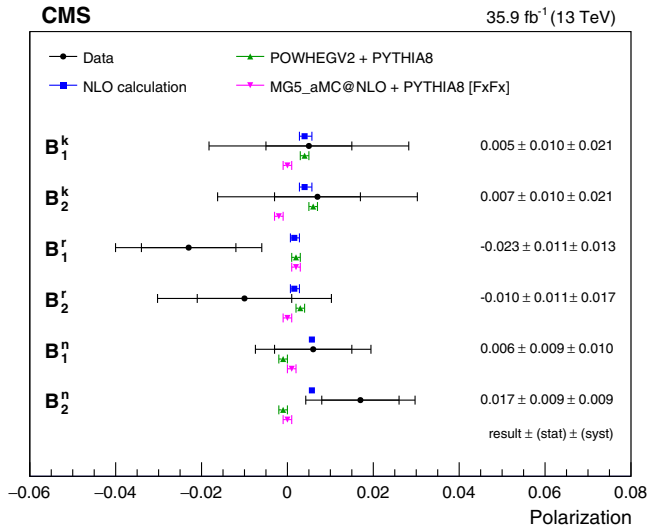
FIG. 9. Measured values of the polarization coefficients (circles) and the predictions from POWHEGv2 (triangles), MADGRAPH5_aMC@NLO (inverted triangles), and the NLO calculation [4] (squares). The inner vertical bars on the circles give the statistical uncertainty in the data and the outer bars give the total uncertainty. The numerical measured values with their statistical and systematic uncertainties are given on the right. The vertical bars on the values from simulation represent the combination of statistical and scale uncertainties, while for the calculated values they represent the scale uncertainties.

FIG. 11. Measured values of the cross spin correlation coefficients (circles) and the predictions from POWHEGv2 (triangles), MADGRAPH5_aMC@NLO (inverted triangles), and the NLO calculation [4] (squares). The inner vertical bars on the circles give the statistical uncertainty in the data and the outer bars give the total uncertainty. The numerical measured values with their statistical and systematic uncertainties are given on the right. The vertical bars on the values from simulation represent the combination of statistical and scale uncertainties, while for the calculated values they represent the scale uncertainties.
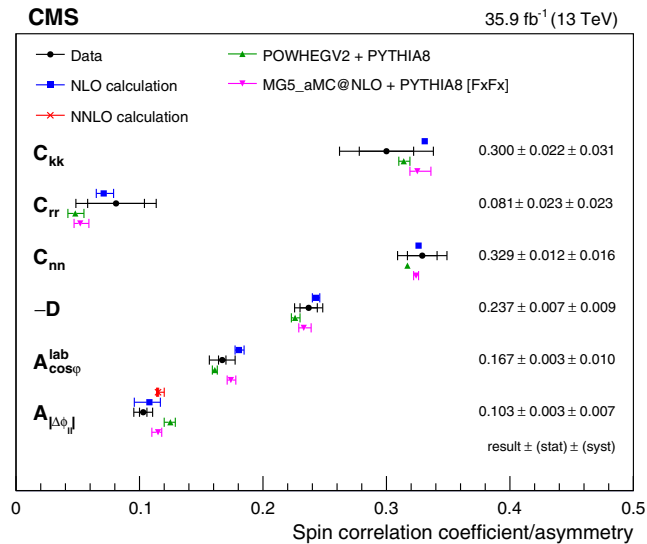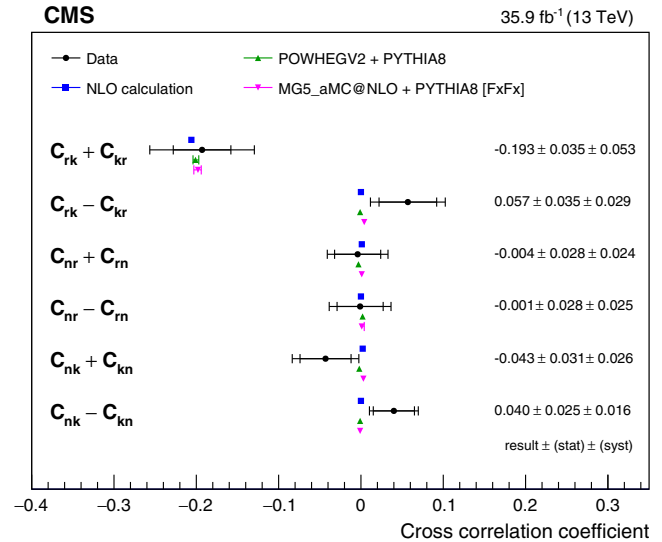

FIG. 10. Measured values of the spin correlation coefficients and asymmetries (circles) and the predictions from POWHEGv2 (triangles), MADGRAPH5_aMC@NLO (inverted triangles), the NLO calculation [3,4] (squares), and the NNLO calculation [69] (cross). The inner vertical bars on the circles give the statistical uncertainty in the data and the outer bars give the total uncertainty. The numerical measured values with their statistical and systematic uncertainties are given on the right. The vertical bars on the values from simulation represent the combination of statistical and scale uncertainties, while for the calculated values they represent the scale uncertainties.

matrices are given in Table VI, and are consistent with the SM predictions.

For the coefficients in Table III sensitive to P- and CP-even spin correlations (which are substantial in the SM), we use the NLO calculations to transform the measurements into determinations of f_{SM}, the strength of the given measure of spin correlations relative to the SM prediction. A linear dependence of f_{SM} on the measured coefficient is defined, where $f_{SM} = 1$ and $f_{SM} = 0$ correspond to measurements in agreement with the NLO calculations in the presence and absence of spin correlations, respectively. The resulting measurements of f_{SM} are shown in Table VII, where the theoretical scale uncertainty from the transformation is shown as a separate uncertainty. There is a potential correlation between the theoretical scale uncertainty and the scale component of the experimental systematic uncertainty. A similar correlation may exist with the top quark p_T systematic uncertainty, owing to its connection to missing higher-order QCD terms. These effects are neglected because their effect on the total uncertainty would be small. The f_{SM} results are also shown in Fig. 13. The results are all consistent with unity, demonstrating the agreement of the measured spin correlation strengths with the SM predictions for all considered combinations of reference axes.

TABLE IV. Summary of the systematic, statistical, and total uncertainties in the extracted top quark polarization coefficients. An ellipsis ($\cdots$) is shown where the values are < 0.0005.

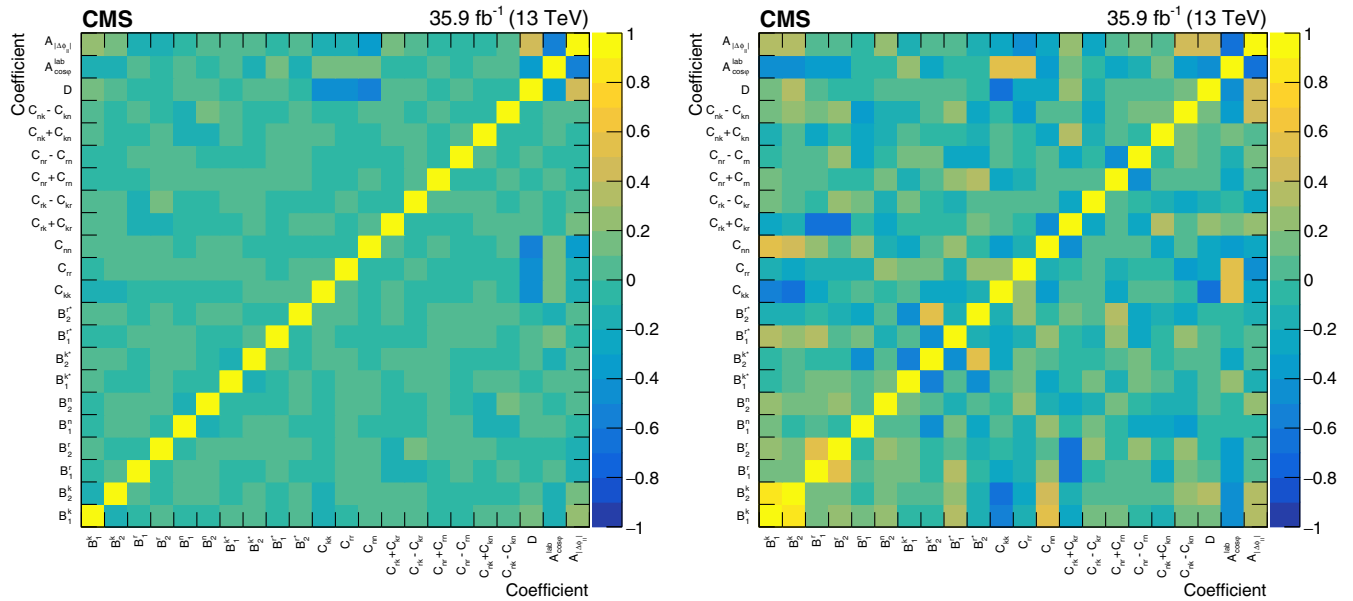|	Uncertainty									
Source	B_1^k	B_2^k	B_1^r	B_2^r	B_1^n	B_2^n	B_1^{k*}	B_2^{k*}	B_1^{r*}	B_2^{r*}
Trigger	0.001	0.001	0.001	0.001	$\cdots$	$\cdots$	0.001	0.001	0.002	0.002
Lepton ident./isolation	0.001	$\cdots$	$\cdots$	$\cdots$	$\cdots$	$\cdots$	$\cdots$	$\cdots$	$\cdots$	$\cdots$
Kinematic reconstruction	$\cdots$	$\cdots$	$\cdots$	$\cdots$	$\cdots$	$\cdots$	$\cdots$	$\cdots$	$\cdots$	$\cdots$
Pileup	$\cdots$	$\cdots$	0.002	0.002	$\cdots$	0.001	0.001	0.001	$\cdots$	$\cdots$
b tagging	0.003	0.004	0.003	0.003	$\cdots$	$\cdots$	0.002	0.002	0.001	0.001
JES	0.011	0.012	0.007	0.009	0.003	0.003	0.009	0.008	0.007	0.007
Unclustered energy	0.001	0.002	0.001	0.001	$\cdots$	0.001	0.001	$\cdots$	0.001	0.002
JER	0.001	0.002	0.001	0.001	0.001	0.001	$\cdots$	0.001	0.001	0.001
Scales	0.005	0.004	0.004	0.009	0.003	0.004	0.003	0.004	0.006	0.005
ME/PS matching	0.006	0.006	0.004	0.001	0.003	0.004	0.003	0.003	0.004	0.004
Color reconnection	0.005	0.003	0.003	0.004	0.008	0.005	0.006	0.008	0.006	0.008
Underlying event	0.001	0.003	0.001	0.003	0.002	0.003	0.003	0.002	0.004	0.004
b quark fragmentation	0.009	0.009	0.004	0.005	$\cdots$	0.001	0.001	0.001	0.001	0.001
b hadron semilept. decays	0.001	0.001	$\cdots$	$\cdots$	$\cdots$	$\cdots$	$\cdots$	$\cdots$	$\cdots$	$\cdots$
PDF	0.001	0.001	$\cdots$	$\cdots$	$\cdots$	$\cdots$	0.001	0.001	0.001	0.001
Top quark mass	0.007	0.007	$\cdots$	0.001	0.001	0.002	0.002	0.001	0.002	0.002
Top quark p_{T}	0.003	0.004	0.001	0.001	$\cdots$	$\cdots$	0.001	0.001	$\cdots$	$\cdots$
Background	0.008	0.008	0.005	0.008	0.001	0.001	0.004	0.005	0.002	0.002
Total systematic	0.021	0.021	0.013	0.017	0.010	0.009	0.013	0.014	0.013	0.013
Data statistical	0.009	0.008	0.009	0.009	0.007	0.008	0.010	0.010	0.010	0.009
Signal simulation statistical	0.003	0.003	0.003	0.003	0.003	0.003	0.004	0.004	0.004	0.003
Background sim. statistical	0.005	0.005	0.005	0.005	0.004	0.004	0.006	0.006	0.005	0.005
Total statistical	0.010	0.010	0.011	0.011	0.009	0.009	0.012	0.012	0.012	0.011
Total	0.023	0.023	0.017	0.020	0.013	0.013	0.018	0.019	0.017	0.017

FIG. 12. Values (gray scale) of the total statistical (left) and systematic (right) correlation matrices for all measured coefficients and laboratory-frame asymmetries.

TABLE V. Summary of the systematic, statistical, and total uncertainties in the extracted $t\bar{t}$ spin correlation coefficients and asymmetries. An ellipsis ($\cdots$) is shown where the values are <0.0005.

Source	Uncertainty												
	C_{kk}	C_{rr}	C_{nn}	$C_{rk}+C_{kr}$	$C_{rk}-C_{kr}$	$C_{nr}+C_{rn}$	$C_{nr}-C_{rn}$	$C_{nk}+C_{kn}$	$C_{nk}-C_{kn}$	D	$A^{\text{lab}}_{\cos\varphi}$	$A_{|\Delta\phi_{\ell\ell}|}$
Trigger	0.001	0.001	$\cdots$	0.002	$\cdots$	$\cdots$	$\cdots$	$\cdots$	$\cdots$	$\cdots$	0.001	$\cdots$
Lepton ident./iso.	0.001	0.001	$\cdots$	0.001	$\cdots$	$\cdots$	$\cdots$	$\cdots$	$\cdots$	$\cdots$	$\cdots$	$\cdots$
Kinematic reco.	$\cdots$	$\cdots$	$\cdots$	$\cdots$	$\cdots$	$\cdots$	$\cdots$	$\cdots$	$\cdots$	$\cdots$	$\cdots$	$\cdots$
Pileup	0.002	$\cdots$	0.001	0.004	0.001	0.001	0.002	0.001	0.001	0.001	$\cdots$	0.001
b tagging	0.004	0.001	0.002	0.005	0.001	0.001	0.001	0.001	0.001	0.001	$\cdots$	$\cdots$
JES	0.012	0.009	0.005	0.022	0.011	0.011	0.009	0.012	0.007	0.002	$\cdots$	0.001
Unclust. energy	0.001	0.001	0.001	0.004	0.001	0.001	0.002	0.001	0.001	$\cdots$	$\cdots$	0.001
JER	0.001	0.002	0.001	0.004	0.002	0.001	0.001	0.003	0.001	$\cdots$	$\cdots$	$\cdots$
Scales	0.012	0.006	0.007	0.026	0.011	0.007	0.014	0.011	0.007	0.003	0.002	0.003
ME/PS matching	0.004	0.003	0.001	0.009	0.016	0.011	0.001	0.012	0.009	0.002	0.002	0.004
Color reconnect.	0.005	0.013	0.006	0.013	0.011	0.014	0.017	0.009	0.008	0.002	0.001	0.001
Underlying event	0.008	0.002	0.002	0.004	0.010	0.007	0.005	0.007	0.002	0.003	0.001	0.001
b quark fragment.	0.014	0.002	0.005	0.017	0.001	0.001	0.001	0.002	0.001	0.003	$\cdots$	0.001
b had. semilep. d.	$\cdots$	0.001	0.001	0.002	$\cdots$	0.001	$\cdots$	$\cdots$	$\cdots$	0.001	$\cdots$	$\cdots$
PDF	0.002	0.002	0.001	0.002	$\cdots$	$\cdots$	$\cdots$	$\cdots$	$\cdots$	0.001	0.003	0.001
Top quark mass	0.001	0.002	0.006	0.006	0.009	0.002	0.002	0.009	0.001	0.002	0.001	$\cdots$
Top quark p_{T}	0.008	0.011	0.005	0.019	$\cdots$	0.001	$\cdots$	0.001	$\cdots$	0.004	0.003	0.005
Background	0.017	0.009	0.008	0.025	0.006	0.004	0.004	0.007	0.003	0.004	0.008	0.002
Total systematic	0.031	0.023	0.016	0.053	0.029	0.024	0.025	0.026	0.016	0.009	0.010	0.007
Data statistical	0.018	0.019	0.010	0.029	0.029	0.024	0.025	0.025	0.020	0.006	0.003	0.003
Signal sim. stat.	0.007	0.007	0.004	0.011	0.011	0.009	0.009	0.010	0.008	0.002	0.001	0.001
Bkg. sim. stat.	0.010	0.010	0.005	0.018	0.017	0.012	0.010	0.015	0.012	0.003	0.002	0.002
Total statistical	0.022	0.023	0.012	0.035	0.035	0.028	0.028	0.031	0.025	0.007	0.003	0.003
Total	0.038	0.032	0.020	0.064	0.046	0.037	0.038	0.041	0.029	0.011	0.010	0.008

IX. LIMITS ON HIGHER-DIMENSIONAL OPERATORS

A. Constraining the top quark CMDM

Analogous to the magnetic dipole moment of an electrically charged particle, the chromomagnetic dipole moment (CMDM) of a color-charged particle in color fields can be defined. In the SM, the intrinsic spin of the top quark and its color charge give it a small CMDM [3,4]. Several BSM models, such as two-Higgs-doublet models (e.g., supersymmetry), technicolor, and top quark compositeness models [71,72], predict an anomalous CMDM, leading to modifications of the $t\bar{t}$ production rate and spin structure. As a consequence, the measurement of the $t\bar{t}$ production spin density matrix represents a powerful probe of the top quark CMDM and can be used to search for BSM phenomena.

As in Ref. [12], the effect of an anomalous CMDM on $t\bar{t}$ production is predicted using an EFT framework in which a fixed set of dimension-six operators is added to the SM Lagrangian [73,74]. The anomalous CMDM of the top quark is a consequence of the O_{tG} operator [71],

$$O_{\text{tG}} = y_t g_S (\bar{Q}\sigma^{\mu\nu}T^a t)\tilde{\phi}G^a_{\mu\nu}, \qquad (12)$$

where y_t denotes the Yukawa coupling of the top quark, g_S is the strong coupling ($g_S = 2\sqrt{\pi\alpha_S}$), Q is the left-handed third-generation quark doublet, $\sigma^{\mu\nu}$ are the Dirac matrices, T^a are the Gell–Mann matrices divided by 2, t is the right-handed top quark singlet, $\tilde{\phi}$ is the charge-conjugated Higgs doublet field, and $G^a_{\mu\nu}$ is the gluon field strength tensor. Besides modifying the $gt\bar{t}$ vertex, O_{tG} also leads to a new $ggt\bar{t}$ vertex. The contribution due to O_{tG} is parametrized by a dimensionless Wilson coefficient divided by the square of the BSM scale (Λ), assumed to be large compared to the scales typically probed at the LHC. The real part of this Wilson coefficient is denoted as C_{tG}. The imaginary part corresponds to a top quark chromoelectric dipole moment (CEDM), and is assumed to be zero in this section. The top quark CEDM is constrained in Sec. IX B.

To produce predictions for the normalized $t\bar{t}$ differential cross section, the model of Ref. [71] is implemented in the MADGRAPH5_aMC@NLO generator at NLO in QCD. The setup is similar to that of the MADGRAPH5_aMC@NLO sample introduced in Sec. IV, but without extra partons at the ME level. The RIVET framework [75] is used to apply the object definitions and calculate the spin density matrix observables.

Four observables are chosen to constrain C_{tG}/Λ^2, corresponding to the four dimensions in Eq. (6), with

TABLE VI. Measured sums and differences of the B coefficients and their statistical and systematic uncertainties. The NLO calculated coefficients are quoted with their scale uncertainties [4].

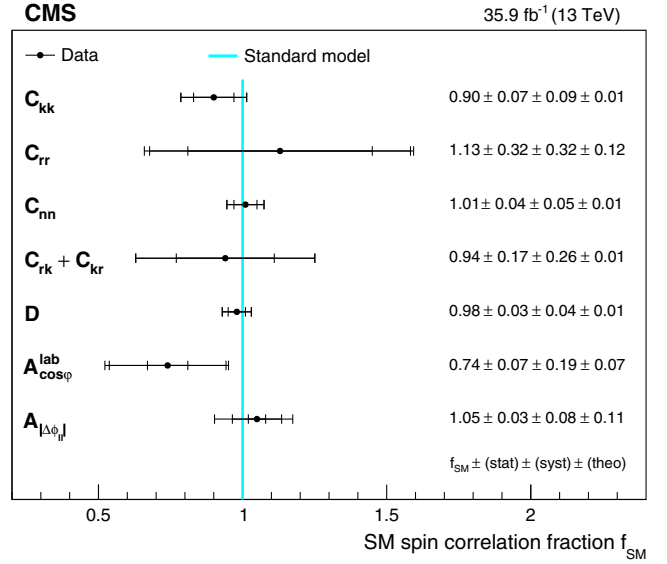| Coefficient	Measured $\pm$ (stat) $\pm$ (syst)	NLO calculation
$B_1^k + B_2^k$	$0.012 \pm 0.013 \pm 0.040$	$8.0^{+3.4}_{-2.4} \times 10^{-3}$
$B_1^k - B_2^k$	$-0.002 \pm 0.015 \pm 0.011$	0
$B_1^r + B_2^r$	$-0.033 \pm 0.015 \pm 0.026$	$3.2^{+2.3}_{-1.7} \times 10^{-3}$
$B_1^r - B_2^r$	$-0.012 \pm 0.016 \pm 0.014$	0
$B_1^n + B_2^n$	$0.024 \pm 0.012 \pm 0.013$	$11.3^{+0.9}_{-0.7} \times 10^{-3}$
$B_1^n - B_2^n$	$-0.011 \pm 0.014 \pm 0.013$	0
$B_1^{k*} + B_2^{k*}$	$-0.010 \pm 0.016 \pm 0.012$	$<10^{-3}$
$B_1^{k*} - B_2^{k*}$	$-0.023 \pm 0.018 \pm 0.024$	0
$B_1^{r*} + B_2^{r*}$	$0.011 \pm 0.016 \pm 0.018$	$<10^{-3}$
$B_1^{r*} - B_2^{r*}$	$-0.008 \pm 0.016 \pm 0.020$	0

FIG. 13. Measured values of f_{SM}, the strength of the measured spin correlations relative to the SM prediction. The inner vertical bars give the statistical uncertainty, the middle bars give the total experimental uncertainty (statistical and systematic), and the outer bars give the total uncertainty. The numerical measured values with their uncertainties are given on the right.

TABLE VII. Values of f_{SM}, the strength of the measured spin correlations relative to the SM prediction, derived from the measurements in Table III. The uncertainties shown are statistical, systematic, and theoretical, respectively. Their sum in quadrature is shown in the last column.

Coefficient	$f_{SM} \pm$ (stat) $\pm$ (syst) $\pm$ (theo)	Total uncertainty
C_{kk}	$0.90 \pm 0.07 \pm 0.09 \pm 0.01$	± 0.11
C_{rr}	$1.13 \pm 0.32 \pm 0.32^{+0.10}_{-0.13}$	$^{+0.46}_{-0.47}$
C_{nn}	$1.01 \pm 0.04 \pm 0.05 \pm 0.01$	± 0.06
$C_{rk} + C_{kr}$	$0.94 \pm 0.17 \pm 0.26 \pm 0.01$	± 0.31
D	$0.98 \pm 0.03 \pm 0.04 \pm 0.01$	± 0.05
$A_{\cos\varphi}^{lab}$	$0.74 \pm 0.07 \pm 0.19^{+0.06}_{-0.08}$	$^{+0.21}_{-0.22}$
$A_{|\Delta\phi_{\ell\ell}|}$	$1.05 \pm 0.03 \pm 0.08^{+0.09}_{-0.12}$	$^{+0.13}_{-0.15}$

the restriction that they are independent from each other. For example, only two of the observables $\cos\theta_1^k$, $\cos\theta_1^r$, and $\cos\theta_1^n$ are independent because they are the direction cosines of the $\{\hat{k}, \hat{r}, \hat{n}\}$ coordinate system. The C_{kk}, C_{nn}, $C_{rk} + C_{kr}$, and D coefficients are all directly sensitive to C_{tG}/Λ^2 [4], and the corresponding four observables (as defined in Table I) are chosen.

A χ^2 minimization technique is used to constrain C_{tG}/Λ^2, with

$$\chi^2(C_{tG}/\Lambda^2) = \sum_{i=1}^{N} \sum_{j=1}^{N} [\text{data}_i - \text{pred}_i(C_{tG}/\Lambda^2)]$$
$$\times [\text{data}_j - \text{pred}_j(C_{tG}/\Lambda^2)]\text{Cov}_{ij}^{-1}, \quad (13)$$

where data_i and $\text{pred}_i(C_{tG}/\Lambda^2)$ are the measured and predicted normalized differential cross sections in the ith of the N bins of the chosen observables, and Cov_{ij}^{-1} is the (ith, jth) element of the inverse of the data covariance

matrix for those N bins. The covariance matrix, corresponding to a subset of the bins illustrated in Fig. 8, accounts for all systematic and statistical uncertainties, as well as the interbin correlations introduced in the unfolding process. In order to break the linear dependencies between the bins of each distribution after normalization to unit area, one bin from each distribution is excluded from the fit, along with the rows and columns associated with it in the covariance matrix. The fit result is independent of the choice of excluded bins.

The χ^2 minimization procedure is performed twice: first including the full contribution from C_{tG}/Λ^2 to the $t\bar{t}$ cross section, and second including only the contribution that is linear in C_{tG}/Λ^2, which describes the interference of the O_{tG} amplitudes with those of the SM. In both cases the best-fit value of C_{tG}/Λ^2 is 0.06 TeV^{-2}, corresponding to a χ^2/d.o.f. of 8/19. The difference between the two results is negligible, indicating that the value of C_{tG}/Λ^2 is small enough to justify the linear approximation.

Assuming Gaussian probability density functions for the uncertainties in the unfolded data, constraints with confidence levels (C.L.) can be estimated from the values of C_{tG}/Λ^2 for which the $\Delta\chi^2$ reaches certain values. The $\Delta\chi^2$ is defined as the change in χ^2 from its minimum value, and is shown as a function of C_{tG}/Λ^2 in Fig. 14. Since the uncertainties in the theoretical predictions do not have a clear frequentist interpretation, they are not included in the confidence intervals. They are estimated separately in Fig. 14 from the maximally positive and negative effects on the best-fit value of C_{tG}/Λ^2 when changing μ_R and μ_F
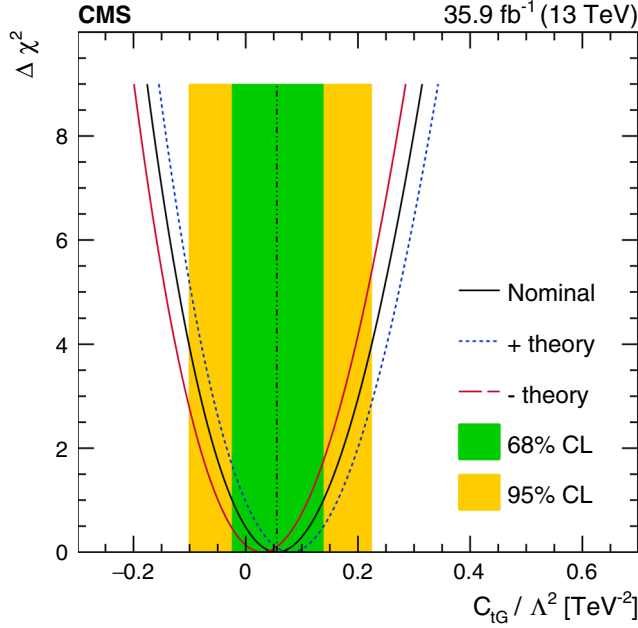
FIG. 14. The $\Delta\chi^2$ values from the fit to the data as a function of C_{tG}/Λ^2. The solid line is the result of the nominal fit, and the dotted and dashed lines show the most-positive and most-negative shifts in the best-fit C_{tG}/Λ^2, respectively, when the theoretical inputs are allowed to vary within their uncertainties. The vertical line denotes the best-fit value from the nominal fit, and the inner and outer areas indicate the 68 and 95% C.L., respectively.

individually and simultaneously up and down by a factor of 2 in the MADGRAPH5_aMC@NLO predictions.

The resulting constraint at the 95% C.L. is $-0.10 < C_{tG}/\Lambda^2 < 0.22$ TeV^{-2}. In Ref. [71], a 95% C.L. constraint of $-0.42 < C_{tG}/\Lambda^2 < 0.30$ TeV^{-2} was derived using NLO predictions for the contributions from O_{tG} to the total $t\bar{t}$ cross section, combined with ATLAS and CMS measurements at $\sqrt{s} = 8$ TeV, as well as $-0.32 < C_{tG}/\Lambda^2 < 0.73$ TeV^{-2}, using Fermilab Tevatron results. From a measurement of the absolute $t\bar{t}$ differential cross section as a function of $|\Delta\phi_{\ell\ell}|$ at the particle level, CMS determined $-0.06 < C_{tG}/\Lambda^2 < 0.41$ TeV^{-2} at the 95% C.L. [12]. The results presented here are consistent with and improve on these previous limits. Compared to Ref. [12], the sensitivity to C_{tG}/Λ^2 in this analysis is improved by 30% and the theoretical uncertainties are substantially smaller.

B. Constraining anomalous couplings

The top quark anomalous CMDM operator is just one of the 11 independent dimension-six operators relevant for hadronic $t\bar{t}$ production [4]. The normalized differential cross sections measured in Sec. VIII A are sensitive to ten of these operators, and each can be constrained using a fit similar to that in Sec. IX A. However, in the absence of a consistent simulation of all these operators compatible with

the NLO QCD predictions in the MADGRAPH5_aMC@NLO generator [71], we instead use the known functional forms of Eqs. (8)–(10) to fit the data. We use the calculations from Ref. [4] to determine the coefficients and their dependence on the contributions from the different operators. The calculations for the NLO SM part are the same as those introduced in Sec. VIII A. For the contributions from the operators, only tree-level interference terms with the QCD amplitudes in the linear approximation are considered [4].

The anomalous couplings associated with the 11 operators are listed in Table VIII, with a brief description of their properties. Unlike the Wilson coefficient C_{tG} considered in Sec. IX A, the anomalous couplings apply to operators in their form after spontaneous symmetry breaking [4]. The couplings $\hat{\mu}_t$ and $\hat{d}_t$ represent the top quark anomalous CMDM and CEDM, respectively, and there are two further CP-odd operators involving two top quarks and up to three gluons (with couplings $\hat{c}_{--}$ and $\hat{c}_{-+}$). The operators associated with the remaining couplings represent CP-even four-quark interactions, with weak isospin quantum numbers either 0 or 1. The operators are described in detail in Ref. [4].

The normalized differential cross sections measured in Sec. VIII A are sensitive to all the anomalous couplings given in Table VIII except $\hat{c}_{AA}$, which is constrained by measurements of the $t\bar{t}$ charge asymmetry [4]. Using the same fitting procedure as in Sec. IX A, we set a limit on each coupling, setting the other couplings to zero. The 95% C.L. limits are given in Table IX, and the measured values and uncertainties are listed and displayed in Fig. 15. Theoretical uncertainties are estimated from the simultaneous variation of μ_R and μ_F up and down by a factor of 2. Limits are given for the combination of couplings $\hat{c}_1 - \hat{c}_2 + \hat{c}_3$ rather than $\hat{c}_2$ alone because this is the combination of couplings to which the measurements are

TABLE VIII. Anomalous couplings associated with the dimension-six operators relevant for hadronic $t\bar{t}$ production, the operator type of the effective interaction vertex they represent, and their P and CP symmetry properties. It is not possible to combine the isospin-1 operators such that they have definite properties with respect to C and P [4].

Coupling	Operator type	Symmetry properties
$\hat{\mu}_t$	2 quarks plus gluon(s)	P-even, CP-even
$\hat{d}_t$	2 quarks plus gluon(s)	P-odd, CP-odd
$\hat{c}_{--}$	2 quarks plus gluon(s)	P-odd, CP-odd
$\hat{c}_{-+}$	2 quarks plus gluon(s)	P-even, CP-odd
$\hat{c}_{VV}$	4 quarks (weak isospin 0)	P-even, CP-even
$\hat{c}_{VA}$	4 quarks (weak isospin 0)	P-odd, CP-even
$\hat{c}_{AV}$	4 quarks (weak isospin 0)	P-odd, CP-even
$\hat{c}_{AA}$	4 quarks (weak isospin 0)	P-even, CP-even
$\hat{c}_1$	4 quarks (weak isospin 1)	CP-even
$\hat{c}_2$	4 quarks (weak isospin 1)	CP-even
$\hat{c}_3$	4 quarks (weak isospin 1)	CP-even

TABLE IX. The 95% C.L. limits on the anomalous couplings listed in Table VIII, derived by fitting the distributions measured in Sec. VIII A and setting the other anomalous couplings to zero. The confidence intervals include only the experimental uncertainties as in Sec. IX A. The theoretical uncertainties, the χ^2 values (d.o.f. = 19), and the distributions used in each fit are given in the last three columns. For conciseness, the distributions are labeled by their associated coefficients (as defined in Table I). An ellipsis ($\cdots$) is shown where the uncertainties are <0.0005.

	95% C.L.	Theoretical unc.	χ^2	Coefficients
$\hat{\mu}_t$	$-0.014 < \hat{\mu}_t < 0.004$	± 0.001	7	$C_{kk}, C_{nn}, C_{rk} + C_{kr}, D$
$\hat{d}_t$	$-0.020 < \hat{d}_t < 0.012$	$\cdots$	9	$B_2^r, B_1^n, C_{nr} - C_{rn}, C_{nk} - C_{kn}$
$\hat{c}_{--}$	$-0.040 < \hat{c}_{--} < 0.006$	± 0.001	7	$B_2^r, B_1^n, C_{nr} - C_{rn}, C_{nk} - C_{kn}$
$\hat{c}_{-+}$	$-0.009 < \hat{c}_{-+} < 0.005$	$\cdots$	11	$B_1^n, B_2^n, B_1^{r*}, C_{nk} + C_{kn}$
$\hat{c}_{VV}$	$-0.011 < \hat{c}_{VV} < 0.042$	± 0.004	7	$C_{kk}, C_{nn}, C_{rk} + C_{kr}, D$
$\hat{c}_{VA}$	$-0.044 < \hat{c}_{VA} < 0.027$	± 0.003	9	$B_2^k, B_2^r, C_{kk}, C_{nr} + C_{rn}$
$\hat{c}_{AV}$	$-0.035 < \hat{c}_{AV} < 0.032$	± 0.001	6	$B_1^{k*}, B_2^{k*}, B_1^{r*}, B_2^{r*}$
$\hat{c}_1$	$-0.09 < \hat{c}_1 < 0.34$	± 0.04	7	$C_{kk}, C_{nn}, C_{rk} + C_{kr}, D$
$\hat{c}_3$	$-0.35 < \hat{c}_3 < 0.21$	± 0.02	9	$B_2^k, B_2^r, C_{kk}, C_{nr} + C_{rn}$
$\hat{c}_1 - \hat{c}_2 + \hat{c}_3$	$-0.17 < \hat{c}_1 - \hat{c}_2 + \hat{c}_3 < 0.15$	± 0.01	6	$B_1^{k*}, B_2^{k*}, B_1^{r*}, B_2^{r*}$

directly sensitive [4]. The strongest constraints are found for the operators probed in the gg initial state. The four-quark operators with isospin 0 are more constrained than those with isospin 1, where contributions from the up and down quark $q\bar{q}$ initial states have opposite signs and similar magnitudes [4,16].

We also consider the simultaneous fitting of multiple couplings. We find that the pairs of four-quark couplings $(\hat{c}_{VV}, \hat{c}_1)$, $(\hat{c}_{VA}, \hat{c}_3)$, and $(\hat{c}_{AV}, \hat{c}_1 - \hat{c}_2 + \hat{c}_3)$ cannot be simultaneously constrained because their predicted effects on the measured distributions can approximately cancel
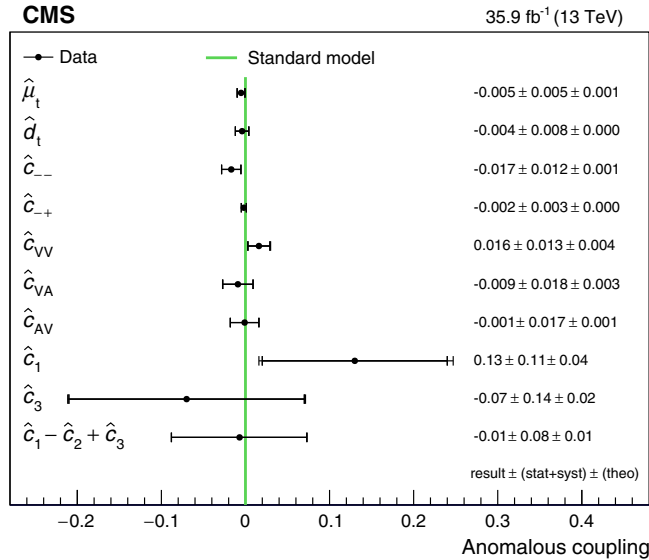

FIG. 15. Measured values of and uncertainties in the fitted anomalous couplings, assuming other anomalous couplings to be zero. The first and second quoted uncertainties are from experimental (statistical and systematic, at the 68% C.L.) and theoretical sources, respectively, and are shown by the inner and outer vertical bars on the points. The expected SM value is shown by the vertical line.
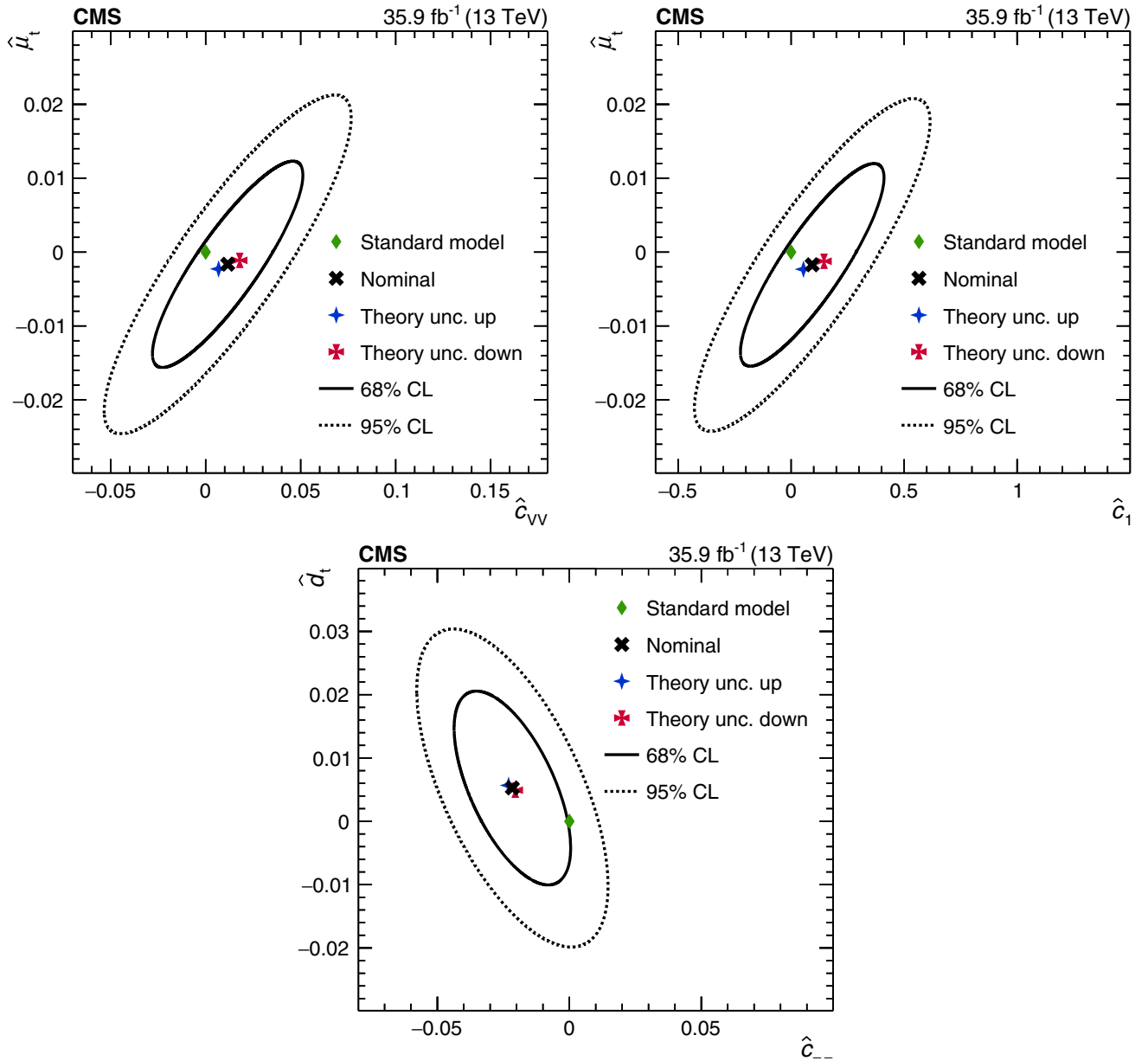
each other. The constraints on the other couplings are found to be independent, and therefore sufficiently characterized by the results of Table IX, with the exception of three combinations of couplings for which we derive two-dimensional 68 and 95% C.L. limits, shown in Fig. 16.

For a direct comparison with the top quark CMDM results of Sec. IX A, we use the relationship $C_{tG}/\Lambda^2 = \hat{\mu}_t/(2m_t^2)$. Taking the result for $\hat{\mu}_t$ from Table IX, we find a central value of $C_{tG}/\Lambda^2 = -0.09$ TeV^{-2}, with $-0.24 < C_{tG}/\Lambda^2 < 0.07$ TeV^{-2} at the 95% C.L. The sensitivity to C_{tG}/Λ^2 (determined from the width of the confidence interval) is the same as that found in Sec. IX A, which suggests that the tree-level calculation of the interference terms, using the linear approximation, is adequate for C_{tG}/Λ^2. The difference in central value is attributable to the difference in the SM predictions for the coefficients in the NLO calculations and the MADGRAPH5_aMC@NLO simulation. Since the SM prediction is of greater accuracy in the NLO calculations (which include EW corrections), we quote the C_{tG}/Λ^2 result of this section as the nominal result of the analysis.

In a similar way, $\hat{d}_t$ is related to the imaginary part of the Wilson coefficient of the O_{tG} operator C_{tG}^I, and we find a constraint at the 95% C.L. of $-0.33 < C_{tG}^I/\Lambda^2 < 0.20$ TeV^{-2}, with a central value of $C_{tG}^I/\Lambda^2 = -0.07$ TeV^{-2}. This represents a substantial improvement over existing direct constraints on the top quark CEDM [76,77], but it is still significantly weaker than the indirect constraint of $|C_{tG}^I/\Lambda^2| < 0.007$ TeV^{-2} [78] derived from the experimental limit on the neutron electric dipole moment [79,80].

Analogous to the magnetic and electric dipole moments, $\hat{\mu}_t$ and $\hat{d}_t$ can be expressed in terms of the dimensionful parameters C_5 and D_5, which are related to the former by a factor of $1/m_t$ [81]. In this parametrization, we find constraints at the 95% C.L. of $(-1.6 < C_5 < 0.5) \times 10^{-18} g_S$ cm and $(-2.3 < D_5 < 1.4) \times 10^{-18} g_S$ cm.

FIG. 16. The two-dimensional 68% (solid curve) and 95% (dotted curve) C.L. limits on (upper left) $\hat{\mu}_t$ vs. $\hat{c}_{VV}$, (upper right) $\hat{\mu}_t$ vs. $\hat{c}_1$, and (lower) $\hat{d}_t$ vs. $\hat{c}_{--}$. The central value from the nominal fit is shown by the cross and the SM prediction is shown by the diamond. "Theory unc. up" refers to the fit value when μ_R and μ_F are simultaneously increased by a factor of 2, and "theory unc. down" when they are decreased by the same factor.

X. SUMMARY

Measurements of the top quark polarization and $t\bar{t}$ spin correlations have been presented, probing all of the independent coefficients of the top quark spin-dependent parts of the $t\bar{t}$ production density matrix for the first time in proton-proton collisions at $\sqrt{s} = 13$ TeV. Each coefficient was extracted from a normalized differential cross section, unfolded to the parton level and extrapolated to the full phase space. The measurements were made using a data sample of events containing two oppositely charged leptons

(e^+e^-, $e^\pm\mu^\mp$, or $\mu^+\mu^-$) and two or more jets, of which at least one was identified as coming from the hadronization of a bottom quark. The data were recorded by the CMS experiment in 2016 and correspond to an integrated luminosity of 35.9 fb^{-1}.

The measured normalized differential cross sections and coefficients were compared with standard model predictions from simulations with NLO accuracy in QCD and from NLO QCD calculations including electroweak corrections. The measured distribution of $|\Delta\phi_{\ell\ell}|$, the absolute value of the difference in azimuthal angle between the two

leptons in the laboratory frame, was additionally compared with a NNLO QCD prediction. All of the measurements were found to be consistent with the expectations of the standard model. The distribution of $\cos\varphi$, equivalent to the dot product of the two lepton directions measured in their parent top quark and antiquark rest frames, is most sensitive to the presence of spin correlations, with a relative uncertainty below 5%.

Statistical and systematic covariance matrices were provided for the set of all measured bins, and were used in simultaneous fits to constrain the contributions from ten dimension-six effective operators. Two of these operators represent the anomalous chromomagnetic and chromo-electric dipole moments of the top quark, and constraints on their Wilson coefficients of $-0.24 < C_{tG}/\Lambda^2 < 0.07\,\mathrm{TeV}^{-2}$ and $-0.33 < C_{tG}^I/\Lambda^2 < 0.20\,\mathrm{TeV}^{-2}$, respectively, were obtained at the 95% confidence level. This constitutes a substantial improvement over previous direct constraints.

ACKNOWLEDGMENTS

[1] Particle Data Group, Review of particle physics, Phys. Rev. D **98**, 030001 (2018).

[2] G. Mahlon and S. J. Parke, Spin correlation effects in top quark pair production at the LHC, Phys. Rev. D **81**, 074024 (2010).

[3] W. Bernreuther and Z.-G. Si, Top quark spin correlations and polarization at the LHC: Standard model predictions and effects of anomalous top chromo moments, Phys. Lett. B **725**, 115 (2013).

[4] W. Bernreuther, D. Heisler, and Z.-G. Si, A set of top quark spin correlation and polarization observables for the LHC: Standard model predictions and new physics contributions, J. High Energy Phys. 12 (2015) 026.

[5] CMS Collaboration, CMS luminosity measurements for the 2016 data taking period, CMS Physics Analysis Summary Report No. CMS-PAS-LUM-17-001 (2017).

[6] ATLAS Collaboration, Measurements of top quark spin observables in $t\bar{t}$ events using dilepton final states in $\sqrt{s} = 8$ TeV pp collisions with the ATLAS detector, J. High Energy Phys. 03 (2017) 113.

[7] CMS Collaboration, Measurements of $t\bar{t}$ Spin Correlations and Top-Quark Polarization using Dilepton Final States in pp Collisions at $\sqrt{s} = 7$ TeV, Phys. Rev. Lett. **112**, 182001 (2014).

[8] ATLAS Collaboration, Measurements of spin correlation in top-antitop quark events from proton-proton collisions at $\sqrt{s} = 7$ TeV using the ATLAS detector, Phys. Rev. D **90**, 112016 (2014).

[9] ATLAS Collaboration, Measurement of the correlation between the polar angles of leptons from top quark decays in the helicity basis at $\sqrt{s} = 7$ TeV using the ATLAS detector, Phys. Rev. D **93**, 012002 (2016).

[10] CMS Collaboration, Measurements of $t\bar{t}$ spin correlations and top quark polarization using dilepton final states in pp collisions at $\sqrt{s} = 8$ TeV, Phys. Rev. D **93**, 052007 (2016).

[11] ATLAS Collaboration, Measurements of top-quark pair spin correlations in the e μ channel at $\sqrt{s} = 13$ TeV using pp collisions in the ATLAS detector, arXiv:1903.07570 [Eur. Phys. J. C (to be published)].

[12] CMS Collaboration, Measurements of $t\bar{t}$ differential cross sections in proton-proton collisions at $\sqrt{s} = 13$ TeV using events containing two leptons, J. High Energy Phys. 02 (2019) 149.

[13] M. Baumgart and B. Tweedie, A new twist on top quark spin correlations, J. High Energy Phys. 03 (2013) 117.

[14] M. Fabbrichesi, M. Pinamonti, and A. Tonero, Limits on anomalous top quark gauge couplings from Tevatron and LHC data, Eur. Phys. J. C **74**, 3193 (2014).

[15] Q.-H. Cao, B. Yan, J.-H. Yu, and C. Zhang, A general analysis of Wtb anomalous couplings, Chin. Phys. C **41**, 063101 (2017).

[16] C. Degrande, J.-M. Gérard, C. Grojean, F. Maltoni, and G. Servant, Non-resonant new physics in top pair production at hadron colliders, J. High Energy Phys. 03 (2011) 125.

[17] A. Brandenburg, Z.-G. Si, and P. Uwer, QCD-corrected spin analysing power of jets in decays of polarized top quarks, Phys. Lett. B **539**, 235 (2002).

[18] CMS Collaboration, The CMS trigger system, J. Instrum. **12**, P01020 (2017).

[19] CMS Collaboration, The CMS experiment at the CERN LHC, J. Instrum. **3**, S08004 (2008).

[20] S. Frixione, P. Nason, and G. Ridolfi, A positive-weight next-to-leading-order Monte Carlo for heavy flavour hadroproduction, J. High Energy Phys. 09 (2007) 126.

[21] P. Nason, A new method for combining NLO QCD with shower Monte Carlo algorithms, J. High Energy Phys. 11 (2004) 040.

[22] S. Frixione, P. Nason, and C. Oleari, Matching NLO QCD computations with parton shower simulations: The POWHEG method, J. High Energy Phys. 11 (2007) 070.

[23] S. Alioli, P. Nason, C. Oleari, and E. Re, A general framework for implementing NLO calculations in shower Monte Carlo programs: The POWHEG BOX, J. High Energy Phys. 06 (2010) 043.

[24] CMS Collaboration, Investigations of the impact of the parton shower tuning in PYTHIA 8 in the modelling of $t\bar{t}$ at $\sqrt{s} = 8$ and 13 TeV, CMS Physics Analysis Summary CMS-PAS-TOP-16-021 (2016).

[25] T. Sjöstrand, S. Ask, J. R. Christiansen, R. Corke, N. Desai, P. Ilten, S. Mrenna, S. Prestel, C. O. Rasmussen, and P. Z. Skands, An introduction to PYTHIA 8.2, Comput. Phys. Commun. **191**, 159 (2015).

[26] CMS Collaboration, Event generator tunes obtained from underlying event and multiparton scattering measurements, Eur. Phys. J. C **76**, 155 (2016).

[27] P. Skands, S. Carrazza, and J. Rojo, Tuning PYTHIA 8.1: The Monash 2013 tune, Eur. Phys. J. C **74**, 3024 (2014).

[28] J. Alwall, R. Frederix, S. Frixione, V. Hirschi, F. Maltoni, O. Mattelaer, H. S. Shao, T. Stelzer, P. Torrielli, and M. Zaro, The automated computation of tree-level and next-to-leading order differential cross sections, and their matching to parton shower simulations, J. High Energy Phys. 07 (2014) 079.

[29] P. Artoisenet, R. Frederix, O. Mattelaer, and R. Rietkerk, Automatic spin-entangled decays of heavy resonances in Monte Carlo simulations, J. High Energy Phys. 03 (2013) 015.

[30] R. Frederix and S. Frixione, Merging meets matching in MC@NLO, J. High Energy Phys. 12 (2012) 061.

[31] J. Alwall, S. Höche, F. Krauss, N. Lavesson, L. Lönnblad, F. Maltoni, M. L. Mangano, M. Moretti, C. G. Papadopoulos, F. Piccinini, S. Schumann, M. Treccani, J. Winter, and M. Worek, Comparative study of various algorithms for the merging of parton showers and matrix elements in hadronic collisions, Eur. Phys. J. C **53**, 473 (2008).

[32] S. Alioli, P. Nason, C. Oleari, and E. Re, NLO single-top production matched with shower in POWHEG: s- and t-channel contributions, J. High Energy Phys. 09 (2009) 111.

[33] E. Re, Single-top Wt-channel production matched with parton showers using the POWHEG method, Eur. Phys. J. C **71**, 1547 (2011).

[34] R. D. Ball, V. Bertone, F. Cerutti, L. Del Debbio, S. Forte, A. Guffanti, J. I. Latorre, J. Rojo, and M. Ubiali (NNPDF Collaboration), Unbiased global determination of parton distributions and their uncertainties at NNLO and LO, Nucl. Phys. **B855**, 153 (2012).

[35] R. D. Ball, V. Bertone, S. Carrazza, C. S. Deans, L. Del Debbio, S. Forte, A. Guffanti, N. P. Hartland, J. I. Latorre, J. Rojo, and M. Ubiali (NNPDF Collaboration),

Parton distributions for the LHC Run II, J. High Energy Phys. 04 (2015) 040.

[36] Y. Li and F. Petriello, Combining QCD and electroweak corrections to dilepton production in FEWZ, Phys. Rev. D **86,** 094034 (2012).

[37] N. Kidonakis, Two-loop soft anomalous dimensions for single top quark associated production with W^- or H^-, Phys. Rev. D **82,** 054018 (2010).

[38] J. M. Campbell, R. K. Ellis, and C. Williams, Vector boson pair production at the LHC, J. High Energy Phys. 07 (2011) 018.

[39] F. Maltoni, D. Pagani, and I. Tsinikos, Associated production of a top-quark pair with vector bosons at NLO in QCD: Impact on $t\bar{t}H$ searches at the LHC, J. High Energy Phys. 02 (2016) 113.

[40] M. Czakon and A. Mitov, TOP++: A program for the calculation of the top-pair cross-section at hadron colliders, Comput. Phys. Commun. **185,** 2930 (2014).

[41] S. Agostinelli et al. (GEANT4 Collaboration), GEANT4—A simulation toolkit, Nucl. Instrum. Methods Phys. Res., Sect. A **506,** 250 (2003).

[42] CMS Collaboration, Particle-flow reconstruction and global event description with the CMS detector, J. Instrum. **12,** P10003 (2017).

[43] CMS Collaboration, Performance of electron reconstruction and selection with the CMS detector in proton-proton collisions at $\sqrt{s} = 8$ TeV, J. Instrum. **10,** P06005 (2015).

[44] CMS Collaboration, Performance of the CMS muon detector and muon reconstruction with proton-proton collisions at $\sqrt{s} = 13$ TeV, J. Instrum. **13,** P06015 (2018).

[45] M. Cacciari, G. P. Salam, and G. Soyez, The anti-k_T jet clustering algorithm, J. High Energy Phys. 04 (2008) 063.

[46] M. Cacciari, G. P. Salam, and G. Soyez, FastJet user manual, Eur. Phys. J. C **72,** 1896 (2012).

[47] CMS Collaboration, Identification and filtering of uncharacteristic noise in the CMS hadron calorimeter, J. Instrum. **5,** T03014 (2010).

[48] CMS Collaboration, Identification of heavy-flavour jets with the CMS detector in pp collisions at 13 TeV, J. Instrum. **13,** P05011 (2018).

[49] CMS Collaboration, Measurement of the differential cross section for top quark pair production in pp collisions at $\sqrt{s} = 8$ TeV, Eur. Phys. J. C **75,** 542 (2015).

[50] CMS Collaboration, Measurement of the Top Quark Pair Production Cross Section in Proton-Proton Collisions at $\sqrt{s} = 13$ TeV with the CMS Detector, Phys. Rev. Lett. **116,** 052002 (2016).

[51] S. Schmitt, TUnfold, an algorithm for correcting migration effects in high energy physics, J. Instrum. **7,** T10003 (2012).

[52] CMS Collaboration, Measurement of the $t\bar{t}$ production cross section, the top quark mass, and the strong coupling constant using dilepton events in pp collisions at $\sqrt{s} = 13$ TeV, Eur. Phys. J. C **79,** 368 (2019).

[53] CMS Collaboration, Measurement of the Drell-Yan cross sections in pp collisions at $\sqrt{s} = 7$ TeV with the CMS experiment, J. High Energy Phys. 10 (2011) 007.

[54] ATLAS Collaboration, Measurement of the Inelastic Proton-Proton Cross Section at $\sqrt{s} = 13$ TeV with the ATLAS Detector at the LHC, Phys. Rev. Lett. **117,** 182002 (2016).

[55] CMS Collaboration, Jet energy scale and resolution in the CMS experiment in pp collisions at 8 TeV, J. Instrum. **12,** P02014 (2017).

[56] S. Argyropoulos and T. Sjöstrand, Effects of color reconnection on $t\bar{t}$ final states at the LHC, J. High Energy Phys. 11 (2014) 043.

[57] J. R. Christiansen and P. Z. Skands, String formation beyond leading colour, J. High Energy Phys. 08 (2015) 003.

[58] M. G. Bowler, e^+e^- production of heavy quarks in the string model, Z. Phys. C **11,** 169 (1981).

[59] C. Peterson, D. Schlatter, I. Schmitt, and P. M. Zerwas, Scaling violations in inclusive e^+e^- annihilation spectra, Phys. Rev. D **27,** 105 (1983).

[60] J. Butterworth et al., PDF4LHC recommendations for LHC Run II, J. Phys. G **43,** 023001 (2016).

[61] CMS Collaboration, Measurement of differential top-quark pair production cross sections in pp collisions at $\sqrt{s} = 7$ TeV, Eur. Phys. J. C **73,** 2339 (2013).

[62] CMS Collaboration, Measurement of the $t\bar{t}$ production cross section in the all-jets final state in pp collisions at $\sqrt{s} = 8$ TeV, Eur. Phys. J. C **76,** 128 (2016).

[63] CMS Collaboration, Measurement of differential cross sections for top quark pair production using the lepton + jets final state in proton-proton collisions at 13 TeV, Phys. Rev. D **95,** 092001 (2017).

[64] M. Guzzi, K. Lipka, and S.-O. Moch, Top-quark pair production at hadron colliders: Differential cross section and phenomenological applications with DiffTop, J. High Energy Phys. 01 (2015) 082.

[65] N. Kidonakis, NNNLO soft-gluon corrections for the top-quark p_T and rapidity distributions, Phys. Rev. D **91,** 031501(R) (2015).

[66] M. Czakon, D. Heymes, A. Mitov, D. Pagani, I. Tsinikos, and M. Zaro, Top-pair production at the LHC through NNLO QCD and NLO EW, J. High Energy Phys. 10 (2017) 186.

[67] M. Czakon, A. Ferroglia, D. Heymes, A. Mitov, B. D. Pecjak, D. J. Scott, X. Wang, and L. L. Yang, Resummation for (boosted) top-quark pair production at NNLO + NNLL′ in QCD, J. High Energy Phys. 05 (2018) 149.

[68] W. Bernreuther and Z.-G. Si, Distributions and correlations for top quark pair production and decay at the Tevatron and LHC, Nucl. Phys. **B837,** 90 (2010).

[69] A. Behring, M. Czakon, A. Mitov, A. S. Papanastasiou, and R. Poncelet, Higher Order Corrections to Spin Correlations in Top Quark Pair Production at the LHC, Phys. Rev. Lett. **123,** 082001 (2019).

[70] B. Efron, Bootstrap methods: Another look at the jackknife, Ann. Stat. **7,** 1 (1979).

[71] D. B. Franzosi and C. Zhang, Probing the top-quark chromomagnetic dipole moment at next-to-leading order in QCD, Phys. Rev. D **91,** 114010 (2015).

[72] R. Martinez, M. A. Perez, and N. Poveda, Chromomagnetic dipole moment of the top quark revisited, Eur. Phys. J. C **53,** 221 (2008).

[73] W. Buchmüller and D. Wyler, Effective Lagrangian analysis of new interactions and flavor conservation, Nucl. Phys. **B268,** 621 (1986).

[74] B. Grzadkowski, M. Iskrzynski, M. Misiak, and J. Rosiek, Dimension-six terms in the standard model Lagrangian, J. High Energy Phys. 10 (**2010**) 085.

[75] A. Buckley, J. Butterworth, L. Lonnblad, D. Grellscheid, H. Hoeth, J. Monk, H. Schulz, and F. Siegert, Rivet user manual, Comput. Phys. Commun. **184**, 2803 (2013).

[76] Z. Hioki and K. Ohkuma, Latest constraint on nonstandard top-gluon couplings at hadron colliders and its future prospect, Phys. Rev. D **88**, 017503 (2013).

[77] J. A. Aguilar-Saavedra, B. Fuks, and M. L. Mangano, Pinning down top dipole moments with ultra-boosted tops, Phys. Rev. D **91**, 094021 (2015).

[78] D. Barducci *et al.*, Interpreting top-quark LHC measurements in the standard-model effective field theory, arXiv:1802.07237.

[79] C. A. Baker, D. D. Doyle, P. Geltenbort, K. Green, M. G. D. van der Grinten, P. G. Harris, P. Iaydjiev, S. N. Ivanov, D. J. R. May, J. M. Pendlebury, J. D. Richardson, D. Shiers, and K. F. Smith, An Improved Experimental Limit on the Electric Dipole Moment of the Neutron, Phys. Rev. Lett. **97**, 131801 (2006).

[80] J. M. Pendlebury *et al.*, Revised experimental upper limit on the electric dipole moment of the neutron, Phys. Rev. D **92**, 092003 (2015).

[81] J. Sjölin, LHC experimental sensitivity to CP violating $gt\bar{t}$ couplings, J. Phys. G **29**, 543 (2003).

A. M. Sirunyan,[1] A. Tumasyan,[1] W. Adam,[2] F. Ambrogi,[2] E. Asilar,[2] T. Bergauer,[2] J. Brandstetter,[2] M. Dragicevic,[2] J. Erö,[2] A. Escalante Del Valle,[2] M. Flechl,[2] R. Frühwirth,[2,b] V. M. Ghete,[2] J. Hrubec,[2] M. Jeitler,[2,b] N. Krammer,[2] I. Krätschmer,[2] D. Liko,[2] T. Madlener,[2] I. Mikulec,[2] N. Rad,[2] H. Rohringer,[2] J. Schieck,[2,b] R. Schöfbeck,[2] M. Spanring,[2] D. Spitzbart,[2] W. Waltenberger,[2] J. Wittmann,[2] C.-E. Wulz,[2,b] M. Zarucki,[2] V. Chekhovsky,[3] V. Mossolov,[3] J. Suarez Gonzalez,[3] E. A. De Wolf,[4] D. Di Croce,[4] X. Janssen,[4] J. Lauwers,[4] A. Lelek,[4] M. Pieters,[4] H. Van Haevermaet,[4] P. Van Mechelen,[4] N. Van Remortel,[4] F. Blekman,[5] J. D'Hondt,[5] J. De Clercq,[5] K. Deroover,[5] G. Flouris,[5] D. Lontkovskyi,[5] S. Lowette,[5] I. Marchesini,[5] S. Moortgat,[5] L. Moreels,[5] Q. Python,[5] K. Skovpen,[5] S. Tavernier,[5] W. Van Doninck,[5] P. Van Mulders,[5] I. Van Parijs,[5] D. Beghin,[6] B. Bilin,[6] H. Brun,[6] B. Clerbaux,[6] G. De Lentdecker,[6] H. Delannoy,[6] B. Dorney,[6] L. Favart,[6] A. Grebenyuk,[6] A. K. Kalsi,[6] J. Luetic,[6] A. Popov,[6,c] N. Postiau,[6] E. Starling,[6] L. Thomas,[6] C. Vander Velde,[6] P. Vanlaer,[6] D. Vannerom,[6] Q. Wang,[6] T. Cornelis,[7] D. Dobur,[7] A. Fagot,[7] M. Gul,[7] I. Khvastunov,[7,d] C. Roskas,[7] D. Trocino,[7] M. Tytgat,[7] W. Verbeke,[7] B. Vermassen,[7] M. Vit,[7] N. Zaganidis,[7] O. Bondu,[8] G. Bruno,[8] C. Caputo,[8] P. David,[8] C. Delaere,[8] M. Delcourt,[8] A. Giammanco,[8] G. Krintiras,[8] V. Lemaitre,[8] A. Magitteri,[8] K. Piotrzkowski,[8] A. Saggio,[8] M. Vidal Marono,[8] P. Vischia,[8] J. Zobec,[8] F. L. Alves,[9] G. A. Alves,[9] G. Correia Silva,[9] C. Hensel,[9] A. Moraes,[9] M. E. Pol,[9] P. Rebello Teles,[9] E. Belchior Batista Das Chagas,[10] W. Carvalho,[10] J. Chinellato,[10,e] E. Coelho,[10] E. M. Da Costa,[10] G. G. Da Silveira,[10,f] D. De Jesus Damiao,[10] C. De Oliveira Martins,[10] S. Fonseca De Souza,[10] L. M. Huertas Guativa,[10] H. Malbouisson,[10] D. Matos Figueiredo,[10] M. Melo De Almeida,[10] C. Mora Herrera,[10] L. Mundim,[10] H. Nogima,[10] W. L. Prado Da Silva,[10] L. J. Sanchez Rosas,[10] A. Santoro,[10] A. Sznajder,[10] M. Thiel,[10] E. J. Tonelli Manganote,[10,e] F. Torres Da Silva De Araujo,[10] A. Vilela Pereira,[10] S. Ahuja,[11a] C. A. Bernardes,[11a] L. Calligaris,[11a] T. R. Fernandez Perez Tomei,[11a] E. M. Gregores,[11a,11b] P. G. Mercadante,[11a,11b] S. F. Novaes,[11a] Sandra S. Padula,[11a] A. Aleksandrov,[12] R. Hadjiiska,[12] P. Iaydjiev,[12] A. Marinov,[12] M. Misheva,[12] M. Rodozov,[12] M. Shopova,[12] G. Sultanov,[12] A. Dimitrov,[13] L. Litov,[13] B. Pavlov,[13] P. Petkov,[13] W. Fang,[14,g] X. Gao,[14,g] L. Yuan,[14] M. Ahmad,[15] J. G. Bian,[15] G. M. Chen,[15] H. S. Chen,[15] M. Chen,[15] Y. Chen,[15] C. H. Jiang,[15] D. Leggat,[15] H. Liao,[15] Z. Liu,[15] S. M. Shaheen,[15,h] A. Spiezia,[15] J. Tao,[15] E. Yazgan,[15] H. Zhang,[15] S. Zhang,[15,h] J. Zhao,[15] Y. Ban,[16] G. Chen,[16] A. Levin,[16] J. Li,[16] L. Li,[16] Q. Li,[16] Y. Mao,[16] S. J. Qian,[16] D. Wang,[16] Y. Wang,[17] C. Avila,[18] A. Cabrera,[18] C. A. Carrillo Montoya,[18] L. F. Chaparro Sierra,[18] C. Florez,[18] C. F. González Hernández,[18] M. A. Segura Delgado,[18] J. D. Ruiz Alvarez,[19] N. Godinovic,[20] D. Lelas,[20] I. Puljak,[20] T. Sculac,[20] Z. Antunovic,[21] M. Kovac,[21] V. Brigljevic,[22] D. Ferencek,[22] K. Kadija,[22] B. Mesic,[22] M. Roguljic,[22] A. Starodumov,[22,i] T. Susa,[22] M. W. Ather,[23] A. Attikis,[23] E. Erodotou,[23] M. Kolosova,[23] S. Konstantinou,[23] G. Mavromanolakis,[23] J. Mousa,[23] C. Nicolaou,[23] F. Ptochos,[23] P. A. Razis,[23] H. Rykaczewski,[23] M. Finger,[24,j] M. Finger Jr.,[24,j] E. Ayala,[25] E. Carrera Jarrin,[26] H. Abdalla,[27,k] A. A. Abdelalim,[27,l,m] S. Elgammal,[27,n] S. Bhowmik,[28] A. Carvalho Antunes De Oliveira,[28] R. K. Dewanjee,[28] K. Ehataht,[28] M. Kadastik,[28] M. Raidal,[28] C. Veelken,[28] P. Eerola,[29] H. Kirschenmann,[29] J. Pekkanen,[29] M. Voutilainen,[29] J. Havukainen,[30] J. K. Heikkilä,[30] T. Järvinen,[30] V. Karimäki,[30] R. Kinnunen,[30] T. Lampén,[30] K. Lassila-Perini,[30] S. Laurila,[30] S. Lehti,[30] T. Lindén,[30] P. Luukka,[30] T. Mäenpää,[30] H. Siikonen,[30] E. Tuominen,[30] J. Tuominiemi,[30] T. Tuuva,[31] M. Besancon,[32] F. Couderc,[32] M. Dejardin,[32] D. Denegri,[32] J. L. Faure,[32] F. Ferri,[32] S. Ganjour,[32] A. Givernaud,[32] P. Gras,[32] G. Hamel de Monchenault,[32] P. Jarry,[32] C. Leloup,[32] E. Locci,[32] J. Malcles,[32] J. Rander,[32] A. Rosowsky,[32] M. Ö. Sahin,[32] A. Savoy-Navarro,[32,o] M. Titov,[32] C. Amendola,[33] F. Beaudette,[33] P. Busson,[33] C. Charlot,[33] B. Diab,[33] R. Granier de Cassagnac,[33] I. Kucher,[33] A. Lobanov,[33] J. Martin Blanco,[33] C. Martin Perez,[33] M. Nguyen,[33] C. Ochando,[33] G. Ortona,[33] P. Paganini,[33] J. Rembser,[33] R. Salerno,[33] J. B. Sauvan,[33] Y. Sirois,[33] A. Zabi,[33]

A. Zghiche,[33] J.-L. Agram,[34,p] J. Andrea,[34] D. Bloch,[34] G. Bourgatte,[34] J.-M. Brom,[34] E. C. Chabert,[34] C. Collard,[34] E. Conte,[34,p] J.-C. Fontaine,[34,p] D. Gelé,[34] U. Goerlach,[34] M. Jansová,[34] A.-C. Le Bihan,[34] N. Tonon,[34] P. Van Hove,[34] S. Gadrat,[35] S. Beauceron,[36] C. Bernet,[36] G. Boudoul,[36] N. Chanon,[36] R. Chierici,[36] D. Contardo,[36] P. Depasse,[36] H. El Mamouni,[36] J. Fay,[36] S. Gascon,[36] M. Gouzevitch,[36] G. Grenier,[36] B. Ille,[36] F. Lagarde,[36] I. B. Laktineh,[36] H. Lattaud,[36] M. Lethuillier,[36] L. Mirabito,[36] S. Perries,[36] V. Sordini,[36] G. Touquet,[36] M. Vander Donckt,[36] S. Viret,[36] T. Toriashvili,[37,q] D. Lomidze,[38] C. Autermann,[39] L. Feld,[39] M. K. Kiesel,[39] K. Klein,[39] M. Lipinski,[39] D. Meuser,[39] A. Pauls,[39] M. Preuten,[39] M. P. Rauch,[39] C. Schomakers,[39] J. Schulz,[39] M. Teroerde,[39] B. Wittmer,[39] A. Albert,[40] M. Erdmann,[40] S. Erdweg,[40] T. Esch,[40] R. Fischer,[40] S. Ghosh,[40] T. Hebbeker,[40] C. Heidemann,[40] K. Hoepfner,[40] H. Keller,[40] L. Mastrolorenzo,[40] M. Merschmeyer,[40] A. Meyer,[40] P. Millet,[40] S. Mukherjee,[40] A. Novak,[40] T. Pook,[40] A. Pozdnyakov,[40] M. Radziej,[40] H. Reithler,[40] M. Rieger,[40] A. Schmidt,[40] A. Sharma,[40] D. Teyssier,[40] S. Thüer,[40] G. Flügge,[41] O. Hlushchenko,[41] T. Kress,[41] T. Müller,[41] A. Nehrkorn,[41] A. Nowack,[41] C. Pistone,[41] O. Pooth,[41] D. Roy,[41] H. Sert,[41] A. Stahl,[41,r] M. Aldaya Martin,[42] T. Arndt,[42] C. Asawatangtrakuldee,[42] I. Babounikau,[42] H. Bakhshiansohi,[42] K. Beernaert,[42] O. Behnke,[42] U. Behrens,[42] A. Bermúdez Martínez,[42] D. Bertsche,[42] A. A. Bin Anuar,[42] K. Borras,[42,s] V. Botta,[42] A. Campbell,[42] P. Connor,[42] C. Contreras-Campana,[42] V. Danilov,[42] A. De Wit,[42] M. M. Defranchis,[42] C. Diez Pardos,[42] D. Domínguez Damiani,[42] G. Eckerlin,[42] T. Eichhorn,[42] A. Elwood,[42] E. Eren,[42] E. Gallo,[42,t] A. Geiser,[42] J. M. Grados Luyando,[42] A. Grohsjean,[42] M. Guthoff,[42] M. Haranko,[42] A. Harb,[42] N. Z. Jomhari,[42] H. Jung,[42] M. Kasemann,[42] J. Keaveney,[42] C. Kleinwort,[42] J. Knolle,[42] D. Krücker,[42] W. Lange,[42] T. Lenz,[42] J. Leonard,[42] K. Lipka,[42] W. Lohmann,[42,u] R. Mankel,[42] I.-A. Melzer-Pellmann,[42] A. B. Meyer,[42] M. Meyer,[42] M. Missiroli,[42] G. Mittag,[42] J. Mnich,[42] V. Myronenko,[42] S. K. Pflitsch,[42] D. Pitzl,[42] A. Raspereza,[42] A. Saibel,[42] M. Savitskyi,[42] P. Saxena,[42] V. Scheurer,[42] P. Schütze,[42] C. Schwanenberger,[42] R. Shevchenko,[42] A. Singh,[42] H. Tholen,[42] O. Turkot,[42] A. Vagnerini,[42] M. Van De Klundert,[42] G. P. Van Onsem,[42] R. Walsh,[42] Y. Wen,[42] K. Wichmann,[42] C. Wissing,[42] O. Zenaiev,[42] R. Aggleton,[43] S. Bein,[43] L. Benato,[43] A. Benecke,[43] V. Blobel,[43] T. Dreyer,[43] A. Ebrahimi,[43] E. Garutti,[43] D. Gonzalez,[43] P. Gunnellini,[43] J. Haller,[43] A. Hinzmann,[43] A. Karavdina,[43] G. Kasieczka,[43] R. Klanner,[43] R. Kogler,[43] N. Kovalchuk,[43] S. Kurz,[43] V. Kutzner,[43] J. Lange,[43] D. Marconi,[43] J. Multhaup,[43] M. Niedziela,[43] C. E. N. Niemeyer,[43] D. Nowatschin,[43] A. Perieanu,[43] A. Reimers,[43] O. Rieger,[43] C. Scharf,[43] P. Schleper,[43] S. Schumann,[43] J. Schwandt,[43] J. Sonneveld,[43] H. Stadie,[43] G. Steinbrück,[43] F. M. Stober,[43] M. Stöver,[43] B. Vormwald,[43] I. Zoi,[43] M. Akbiyik,[44] C. Barth,[44] M. Baselga,[44] S. Baur,[44] T. Berger,[44] E. Butz,[44] R. Caspart,[44] T. Chwalek,[44] W. De Boer,[44] A. Dierlamm,[44] K. El Morabit,[44] N. Faltermann,[44] M. Giffels,[44] M. A. Harrendorf,[44] F. Hartmann,[44,r] U. Husemann,[44] I. Katkov,[44,c] S. Kudella,[44] S. Mitra,[44] M. U. Mozer,[44] Th. Müller,[44] M. Musich,[44] G. Quast,[44] K. Rabbertz,[44] M. Schröder,[44] I. Shvetsov,[44] H. J. Simonis,[44] R. Ulrich,[44] M. Weber,[44] C. Wöhrmann,[44] R. Wolf,[44] G. Anagnostou,[45] G. Daskalakis,[45] T. Geralis,[45] A. Kyriakis,[45] D. Loukas,[45] G. Paspalaki,[45] A. Agapitos,[46] G. Karathanasis,[46] P. Kontaxakis,[46] A. Panagiotou,[46] I. Papavergou,[46] N. Saoulidou,[46] K. Vellidis,[46] G. Bakas,[47] K. Kousouris,[47] I. Papakrivopoulos,[47] G. Tsipolitis,[47] I. Evangelou,[48] C. Foudas,[48] P. Gianneios,[48] P. Katsoulis,[48] P. Kokkas,[48] S. Mallios,[48] K. Manitara,[48] N. Manthos,[48] I. Papadopoulos,[48] E. Paradas,[48] J. Strologas,[48] F. A. Triantis,[48] D. Tsitsonis,[48] M. Bartók,[49,v] M. Csanad,[49] N. Filipovic,[49] P. Major,[49] K. Mandal,[49] A. Mehta,[49] M. I. Nagy,[49] G. Pasztor,[49] O. Surányi,[49] G. I. Veres,[49] G. Bencze,[50] C. Hajdu,[50] D. Horvath,[50,w] Á. Hunyadi,[50] F. Sikler,[50] T. Á. Vámi,[50] V. Veszpremi,[50] G. Vesztergombi,[50,a,x] N. Beni,[51] S. Czellar,[51] J. Karancsi,[51,v] A. Makovec,[51] J. Molnar,[51] Z. Szillasi,[51] P. Raics,[52] Z. L. Trocsanyi,[52] B. Ujvari,[52] S. Choudhury,[53] J. R. Komaragiri,[53] P. C. Tiwari,[53] S. Bahinipati,[54,y] C. Kar,[54] P. Mal,[54] A. Nayak,[54,z] S. Roy Chowdhury,[54] D. K. Sahoo,[54,y] S. K. Swain,[54] S. Bansal,[55] S. B. Beri,[55] V. Bhatnagar,[55] S. Chauhan,[55] R. Chawla,[55] N. Dhingra,[55] R. Gupta,[55] A. Kaur,[55] M. Kaur,[55] S. Kaur,[55] P. Kumari,[55] M. Lohan,[55] M. Meena,[55] K. Sandeep,[55] S. Sharma,[55] J. B. Singh,[55] A. K. Virdi,[55] G. Walia,[55] A. Bhardwaj,[56] B. C. Choudhary,[56] R. B. Garg,[56] M. Gola,[56] S. Keshri,[56] Ashok Kumar,[56] S. Malhotra,[56] M. Naimuddin,[56] P. Priyanka,[56] K. Ranjan,[56] Aashaq Shah,[56] R. Sharma,[56] R. Bhardwaj,[57,aa] M. Bharti,[57,aa] R. Bhattacharya,[57] S. Bhattacharya,[57] U. Bhawandeep,[57,aa] D. Bhowmik,[57] S. Dey,[57] S. Dutt,[57,aa] S. Dutta,[57] S. Ghosh,[57] M. Maity,[57,bb] K. Mondal,[57] S. Nandan,[57] A. Purohit,[57] P. K. Rout,[57] A. Roy,[57] G. Saha,[57] S. Sarkar,[57] T. Sarkar,[57,bb] M. Sharan,[57] B. Singh,[57,aa] S. Thakur,[57,aa] P. K. Behera,[58] A. Muhammad,[58] R. Chudasama,[59] D. Dutta,[59] V. Jha,[59] V. Kumar,[59] D. K. Mishra,[59] P. K. Netrakanti,[59] L. M. Pant,[59] P. Shukla,[59] P. Suggisetti,[59] T. Aziz,[60] M. A. Bhat,[60] S. Dugad,[60] G. B. Mohanty,[60] N. Sur,[60] Ravindra Kumar Verma,[60] S. Banerjee,[61] S. Bhattacharya,[61] S. Chatterjee,[61] P. Das,[61] M. Guchait,[61] Sa. Jain,[61] S. Karmakar,[61] S. Kumar,[61] G. Majumder,[61] K. Mazumdar,[61] N. Sahoo,[61] S. Sawant,[61] S. Chauhan,[62] S. Dube,[62] V. Hegde,[62] A. Kapoor,[62] K. Kothekar,[62] S. Pandey,[62] A. Rane,[62] A. Rastogi,[62] S. Sharma,[62] S. Chenarani,[63,cc] E. Eskandari Tadavani,[63]

S. M. Etesami,[63,cc] M. Khakzad,[63] M. Mohammadi Najafabadi,[63] M. Naseri,[63] F. Rezaei Hosseinabadi,[63] B. Safarzadeh,[63,dd] M. Zeinali,[63] M. Felcini,[64] M. Grunewald,[64] M. Abbrescia,[65a,65b] C. Calabria,[65a,65b] A. Colaleo,[65a] D. Creanza,[65a,65c] L. Cristella,[65a,65b] N. De Filippis,[65a,65c] M. De Palma,[65a,65b] A. Di Florio,[65a,65b] F. Errico,[65a,65b] L. Fiore,[65a] A. Gelmi,[65a,65b] G. Iaselli,[65a,65c] M. Ince,[65a,65b] S. Lezki,[65a,65b] G. Maggi,[65a,65c] M. Maggi,[65a] G. Miniello,[65a,65b] S. My,[65a,65b] S. Nuzzo,[65a,65b] A. Pompili,[65a,65b] G. Pugliese,[65a,65c] R. Radogna,[65a] A. Ranieri,[65a] G. Selvaggi,[65a,65b] L. Silvestris,[65a] R. Venditti,[65a] P. Verwilligen,[65a] G. Abbiendi,[66a] C. Battilana,[66a,66b] D. Bonacorsi,[66a,66b] L. Borgonovi,[66a,66b] S. Braibant-Giacomelli,[66a,66b] R. Campanini,[66a,66b] P. Capiluppi,[66a,66b] A. Castro,[66a,66b] F. R. Cavallo,[66a] S. S. Chhibra,[66a,66b] G. Codispoti,[66a,66b] M. Cuffiani,[66a,66b] G. M. Dallavalle,[66a] F. Fabbri,[66a] A. Fanfani,[66a,66b] E. Fontanesi,[66a] P. Giacomelli,[66a] C. Grandi,[66a] L. Guiducci,[66a,66b] F. Iemmi,[66a,66b] S. Lo Meo,[66a,ee] S. Marcellini,[66a] G. Masetti,[66a] A. Montanari,[66a] F. L. Navarria,[66a,66b] A. Perrotta,[66a] F. Primavera,[66a,66b] A. M. Rossi,[66a,66b] T. Rovelli,[66a,66b] G. P. Siroli,[66a,66b] N. Tosi,[66a] S. Albergo,[67a,67b,ff] A. Di Mattia,[67a] R. Potenza,[67a,67b] A. Tricomi,[67a,67b,ff] C. Tuve,[67a,67b] G. Barbagli,[68a] K. Chatterjee,[68a,68b] V. Ciulli,[68a,68b] C. Civinini,[68a] R. D'Alessandro,[68a,68b] E. Focardi,[68a,68b] G. Latino,[68a] P. Lenzi,[68a,68b] M. Meschini,[68a] S. Paoletti,[68a] L. Russo,[68a,gg] G. Sguazzoni,[68a] D. Strom,[68a] L. Viliani,[68a] L. Benussi,[69] S. Bianco,[69] F. Fabbri,[69] D. Piccolo,[69] F. Ferro,[70a] R. Mulargia,[70a,70b] E. Robutti,[70a] S. Tosi,[70a,70b] A. Benaglia,[71a] A. Beschi,[71a,71b] F. Brivio,[71a,71b] V. Ciriolo,[71a,71b,r] S. Di Guida,[71a,71b,r] M. E. Dinardo,[71a,71b] S. Fiorendi,[71a,71b] S. Gennai,[71a] A. Ghezzi,[71a,71b] P. Govoni,[71a,71b] M. Malberti,[71a,71b] S. Malvezzi,[71a] D. Menasce,[71a] F. Monti,[71a] L. Moroni,[71a] M. Paganoni,[71a,71b] D. Pedrini,[71a] S. Ragazzi,[71a,71b] T. Tabarelli de Fatis,[71a,71b] D. Zuolo,[71a,71b] S. Buontempo,[72a] N. Cavallo,[72a,72c] A. De Iorio,[72a,72b] A. Di Crescenzo,[72a,72b] F. Fabozzi,[72a,72c] F. Fienga,[72a] G. Galati,[72a] A. O. M. Iorio,[72a,72b] L. Lista,[72a,72b] S. Meola,[72a,72d,r] P. Paolucci,[72a,r] C. Sciacca,[72a,72b] E. Voevodina,[72a,72b] P. Azzi,[73a] N. Bacchetta,[73a] A. Boletti,[73a,73b] A. Bragagnolo,[73a] R. Carlin,[73a,73b] P. Checchia,[73a] M. Dall'Osso,[73a,73b] P. De Castro Manzano,[73a] T. Dorigo,[73a] U. Dosselli,[73a] F. Gasparini,[73a,73b] U. Gasparini,[73a,73b] A. Gozzelino,[73a] S. Y. Hoh,[73a] S. Lacaprara,[73a] P. Lujan,[73a] M. Margoni,[73a,73b] A. T. Meneguzzo,[73a,73b] J. Pazzini,[73a,73b] N. Pozzobon,[73a,73b] M. Presilla,[73a,73b] P. Ronchese,[73a,73b] R. Rossin,[73a,73b] F. Simonetto,[73a,73b] A. Tiko,[73a] E. Torassa,[73a] M. Tosi,[73a,73b] M. Zanetti,[73a,73b] P. Zotto,[73a,73b] G. Zumerle,[73a,73b] A. Braghieri,[74a] A. Magnani,[74a] P. Montagna,[74a,74b] S. P. Ratti,[74a,74b] V. Re,[74a] M. Ressegotti,[74a,74b] C. Riccardi,[74a,74b] P. Salvini,[74a] I. Vai,[74a,74b] P. Vitulo,[74a,74b] M. Biasini,[75a,75b] G. M. Bilei,[75a] C. Cecchi,[75a,75b] D. Ciangottini,[75a,75b] L. Fanò,[75a,75b] P. Lariccia,[75a,75b] R. Leonardi,[75a,75b] E. Manoni,[75a] G. Mantovani,[75a,75b] V. Mariani,[75a,75b] M. Menichelli,[75a] A. Rossi,[75a,75b] A. Santocchia,[75a,75b] D. Spiga,[75a] K. Androsov,[76a] P. Azzurri,[76a] G. Bagliesi,[76a] L. Bianchini,[76a] T. Boccali,[76a] L. Borrello,[76a] R. Castaldi,[76a] M. A. Ciocci,[76a,76b] R. Dell'Orso,[76a] G. Fedi,[76a] F. Fiori,[76a,76c] L. Giannini,[76a,76c] A. Giassi,[76a] M. T. Grippo,[76a] F. Ligabue,[76a,76c] E. Manca,[76a,76c] G. Mandorli,[76a,76c] A. Messineo,[76a,76b] F. Palla,[76a] A. Rizzi,[76a,76b] G. Rolandi,[76a,hh] A. Scribano,[76a] P. Spagnolo,[76a] R. Tenchini,[76a] G. Tonelli,[76a,76b] A. Venturi,[76a] P. G. Verdini,[76a] L. Barone,[77a,77b] F. Cavallari,[77a] M. Cipriani,[77a,77b] D. Del Re,[77a,77b] E. Di Marco,[77a,77b] M. Diemoz,[77a] S. Gelli,[77a,77b] E. Longo,[77a,77b] B. Marzocchi,[77a,77b] P. Meridiani,[77a] G. Organtini,[77a,77b] F. Pandolfi,[77a] R. Paramatti,[77a,77b] F. Preiato,[77a,77b] C. Quaranta,[77a,77b] S. Rahatlou,[77a,77b] C. Rovelli,[77a] F. Santanastasio,[77a,77b] N. Amapane,[78a,78b] R. Arcidiacono,[78a,78c] S. Argiro,[78a,78b] M. Arneodo,[78a,78c] N. Bartosik,[78a] R. Bellan,[78a,78b] C. Biino,[78a] A. Cappati,[78a,78b] N. Cartiglia,[78a] F. Cenna,[78a,78b] S. Cometti,[78a] M. Costa,[78a,78b] R. Covarelli,[78a,78b] N. Demaria,[78a] B. Kiani,[78a,78b] C. Mariotti,[78a] S. Maselli,[78a] E. Migliore,[78a,78b] V. Monaco,[78a,78b] E. Monteil,[78a,78b] M. Monteno,[78a] M. M. Obertino,[78a,78b] L. Pacher,[78a,78b] N. Pastrone,[78a] M. Pelliccioni,[78a] G. L. Pinna Angioni,[78a,78b] A. Romero,[78a,78b] M. Ruspa,[78a,78c] R. Sacchi,[78a,78b] R. Salvatico,[78a,78b] K. Shchelina,[78a,78b] V. Sola,[78a] A. Solano,[78a,78b] D. Soldi,[78a,78b] A. Staiano,[78a] S. Belforte,[79a] V. Candelise,[79a,79b] M. Casarsa,[79a] F. Cossutti,[79a] A. Da Rold,[79a,79b] G. Della Ricca,[79a,79b] F. Vazzoler,[79a,79b] A. Zanetti,[79a] D. H. Kim,[80] G. N. Kim,[80] M. S. Kim,[80] J. Lee,[80] S. W. Lee,[80] C. S. Moon,[80] Y. D. Oh,[80] S. I. Pak,[80] S. Sekmen,[80] D. C. Son,[80] Y. C. Yang,[80] H. Kim,[81] D. H. Moon,[81] G. Oh,[81] B. Francois,[82] J. Goh,[82,ii] T. J. Kim,[82] S. Cho,[83] S. Choi,[83] Y. Go,[83] D. Gyun,[83] S. Ha,[83] B. Hong,[83] Y. Jo,[83] K. Lee,[83] K. S. Lee,[83] S. Lee,[83] J. Lim,[83] S. K. Park,[83] Y. Roh,[83] H. S. Kim,[84] J. Almond,[85] J. Kim,[85] J. S. Kim,[85] H. Lee,[85] K. Lee,[85] S. Lee,[85] K. Nam,[85] S. B. Oh,[85] B. C. Radburn-Smith,[85] S. h. Seo,[85] U. K. Yang,[85] H. D. Yoo,[85] G. B. Yu,[85] D. Jeon,[86] H. Kim,[86] J. H. Kim,[86] J. S. H. Lee,[86] I. C. Park,[86] Y. Choi,[87] C. Hwang,[87] J. Lee,[87] I. Yu,[87] V. Veckalns,[88,jj] V. Dudenas,[89] A. Juodagalvis,[89] J. Vaitkus,[89] Z. A. Ibrahim,[90] M. A. B. Md Ali,[90,kk] F. Mohamad Idris,[90,ll] W. A. T. Wan Abdullah,[90] M. N. Yusli,[90] Z. Zolkapli,[90] J. F. Benitez,[91] A. Castaneda Hernandez,[91] J. A. Murillo Quijada,[91] H. Castilla-Valdez,[92] E. De La Cruz-Burelo,[92] M. C. Duran-Osuna,[92] I. Heredia-De La Cruz,[92,mm] R. Lopez-Fernandez,[92] R. I. Rabadan-Trejo,[92] G. Ramirez-Sanchez,[92] R. Reyes-Almanza,[92] A. Sanchez-Hernandez,[92] S. Carrillo Moreno,[93] C. Oropeza Barrera,[93] M. Ramirez-Garcia,[93] F. Vazquez Valencia,[93] J. Eysermans,[94] I. Pedraza,[94] H. A. Salazar Ibarguen,[94] C. Uribe Estrada,[94]

A. Morelos Pineda,[95] N. Raicevic,[96] D. Krofcheck,[97] S. Bheesette,[98] P. H. Butler,[98] A. Ahmad,[99] M. Ahmad,[99] M. I. Asghar,[99] Q. Hassan,[99] H. R. Hoorani,[99] W. A. Khan,[99] M. A. Shah,[99] M. Shoaib,[99] M. Waqas,[99] H. Bialkowska,[100] M. Bluj,[100] B. Boimska,[100] T. Frueboes,[100] M. Górski,[100] M. Kazana,[100] M. Szleper,[100] P. Traczyk,[100] P. Zalewski,[100] K. Bunkowski,[101] A. Byszuk,[101,nn] K. Doroba,[101] A. Kalinowski,[101] M. Konecki,[101] J. Krolikowski,[101] M. Misiura,[101] M. Olszewski,[101] A. Pyskir,[101] M. Walczak,[101] M. Araujo,[102] P. Bargassa,[102] D. Bastos,[102] C. Beirão Da Cruz E Silva,[102] A. Di Francesco,[102] P. Faccioli,[102] B. Galinhas,[102] M. Gallinaro,[102] J. Hollar,[102] N. Leonardo,[102] J. Seixas,[102] G. Strong,[102] O. Toldaiev,[102] J. Varela,[102] S. Afanasiev,[103] P. Bunin,[103] M. Gavrilenko,[103] I. Golutvin,[103] I. Gorbunov,[103] A. Kamenev,[103] V. Karjavine,[103] A. Lanev,[103] A. Malakhov,[103] V. Matveev,[103,oo,pp] P. Moisenz,[103] V. Palichik,[103] V. Perelygin,[103] S. Shmatov,[103] S. Shulha,[103] N. Skatchkov,[103] V. Smirnov,[103] N. Voytishin,[103] A. Zarubin,[103] V. Golovtsov,[104] Y. Ivanov,[104] V. Kim,[104,qq] E. Kuznetsova,[104,rr] P. Levchenko,[104] V. Murzin,[104] V. Oreshkin,[104] I. Smirnov,[104] D. Sosnov,[104] V. Sulimov,[104] L. Uvarov,[104] S. Vavilov,[104] A. Vorobyev,[104] Yu. Andreev,[105] A. Dermenev,[105] S. Gninenko,[105] N. Golubev,[105] A. Karneyeu,[105] M. Kirsanov,[105] N. Krasnikov,[105] A. Pashenkov,[105] A. Shabanov,[105] D. Tlisov,[105] A. Toropin,[105] V. Epshteyn,[106] V. Gavrilov,[106] N. Lychkovskaya,[106] V. Popov,[106] I. Pozdnyakov,[106] G. Safronov,[106] A. Spiridonov,[106] A. Stepennov,[106] V. Stolin,[106] M. Toms,[106] E. Vlasov,[106] A. Zhokin,[106] T. Aushev,[107] R. Chistov,[108,ss] M. Danilov,[108,ss] P. Parygin,[108] E. Tarkovskii,[108] V. Andreev,[109] M. Azarkin,[109] I. Dremin,[109,pp] M. Kirakosyan,[109] A. Terkulov,[109] A. Baskakov,[110] A. Belyaev,[110] E. Boos,[110] V. Bunichev,[110] M. Dubinin,[110,tt] L. Dudko,[110] V. Klyukhin,[110] N. Korneeva,[110] I. Lokhtin,[110] S. Obraztsov,[110] M. Perfilov,[110] V. Savrin,[110] P. Volkov,[110] A. Barnyakov,[111,uu] V. Blinov,[111,uu] T. Dimova,[111,uu] L. Kardapoltsev,[111,uu] Y. Skovpen,[111,uu] I. Azhgirey,[112] I. Bayshev,[112] S. Bitioukov,[112] V. Kachanov,[112] A. Kalinin,[112] D. Konstantinov,[112] P. Mandrik,[112] V. Petrov,[112] R. Ryutin,[112] S. Slabospitskii,[112] A. Sobol,[112] S. Troshin,[112] N. Tyurin,[112] A. Uzunian,[112] A. Volkov,[112] A. Babaev,[113] S. Baidali,[113] A. Iuzhakov,[113] V. Okhotnikov,[113] P. Adzic,[114,vv] P. Cirkovic,[114] D. Devetak,[114] M. Dordevic,[114] P. Milenovic,[114,ww] J. Milosevic,[114] J. Alcaraz Maestre,[115] A. Álvarez Fernández,[115] I. Bachiller,[115] M. Barrio Luna,[115] J. A. Brochero Cifuentes,[115] M. Cerrada,[115] N. Colino,[115] B. De La Cruz,[115] A. Delgado Peris,[115] C. Fernandez Bedoya,[115] J. P. Fernández Ramos,[115] J. Flix,[115] M. C. Fouz,[115] O. Gonzalez Lopez,[115] S. Goy Lopez,[115] J. M. Hernandez,[115] M. I. Josa,[115] D. Moran,[115] A. Pérez-Calero Yzquierdo,[115] J. Puerta Pelayo,[115] I. Redondo,[115] L. Romero,[115] S. Sánchez Navas,[115] M. S. Soares,[115] A. Triossi,[115] C. Albajar,[116] J. F. de Trocóniz,[116] J. Cuevas,[117] C. Erice,[117] J. Fernandez Menendez,[117] S. Folgueras,[117] I. Gonzalez Caballero,[117] J. R. González Fernández,[117] E. Palencia Cortezon,[117] V. Rodríguez Bouza,[117] S. Sanchez Cruz,[117] J. M. Vizan Garcia,[117] I. J. Cabrillo,[118] A. Calderon,[118] B. Chazin Quero,[118] J. Duarte Campderros,[118] M. Fernandez,[118] P. J. Fernández Manteca,[118] A. García Alonso,[118] G. Gomez,[118] A. Lopez Virto,[118] C. Martinez Rivero,[118] P. Martinez Ruiz del Arbol,[118] F. Matorras,[118] J. Piedra Gomez,[118] C. Prieels,[118] T. Rodrigo,[118] A. Ruiz-Jimeno,[118] L. Scodellaro,[118] N. Trevisani,[118] I. Vila,[118] N. Wickramage,[119] D. Abbaneo,[120] B. Akgun,[120] E. Auffray,[120] G. Auzinger,[120] P. Baillon,[120,a] A. H. Ball,[120] D. Barney,[120] J. Bendavid,[120] M. Bianco,[120] A. Bocci,[120] C. Botta,[120] E. Brondolin,[120] T. Camporesi,[120] M. Cepeda,[120] G. Cerminara,[120] E. Chapon,[120] Y. Chen,[120] G. Cucciati,[120] D. d'Enterria,[120] A. Dabrowski,[120] N. Daci,[120] V. Daponte,[120] A. David,[120] A. De Roeck,[120] N. Deelen,[120] M. Dobson,[120] M. Dünser,[120] N. Dupont,[120] A. Elliott-Peisert,[120] F. Fallavollita,[120,xx] D. Fasanella,[120] G. Franzoni,[120] J. Fulcher,[120] W. Funk,[120] D. Gigi,[120] A. Gilbert,[120] K. Gill,[120] F. Glege,[120] M. Gruchala,[120] M. Guilbaud,[120] D. Gulhan,[120] J. Hegeman,[120] C. Heidegger,[120] Y. Iiyama,[120] V. Innocente,[120] G. M. Innocenti,[120] A. Jafari,[120] P. Janot,[120] O. Karacheban,[120,u] J. Kieseler,[120] A. Kornmayer,[120] M. Krammer,[120,b] C. Lange,[120] P. Lecoq,[120] C. Lourenço,[120] L. Malgeri,[120] M. Mannelli,[120] A. Massironi,[120] F. Meijers,[120] J. A. Merlin,[120] S. Mersi,[120] E. Meschi,[120] F. Moortgat,[120] M. Mulders,[120] J. Ngadiuba,[120] S. Nourbakhsh,[120] S. Orfanelli,[120] L. Orsini,[120] F. Pantaleo,[120,r] L. Pape,[120] E. Perez,[120] M. Peruzzi,[120] A. Petrilli,[120] G. Petrucciani,[120] A. Pfeiffer,[120] M. Pierini,[120] F. M. Pitters,[120] D. Rabady,[120] A. Racz,[120] M. Rovere,[120] H. Sakulin,[120] C. Schäfer,[120] C. Schwick,[120] M. Selvaggi,[120] A. Sharma,[120] P. Silva,[120] P. Sphicas,[120,yy] A. Stakia,[120] J. Steggemann,[120] V. R. Tavolaro,[120] D. Treille,[120] A. Tsirou,[120] A. Vartak,[120] M. Verzetti,[120] W. D. Zeuner,[120] L. Caminada,[121,zz] K. Deiters,[121] W. Erdmann,[121] R. Horisberger,[121] Q. Ingram,[121] H. C. Kaestli,[121] D. Kotlinski,[121] U. Langenegger,[121] T. Rohe,[121] S. A. Wiederkehr,[121] M. Backhaus,[122] P. Berger,[122] N. Chernyavskaya,[122] G. Dissertori,[122] M. Dittmar,[122] M. Donegà,[122] C. Dorfer,[122] T. A. Gómez Espinosa,[122] C. Grab,[122] D. Hits,[122] T. Klijnsma,[122] W. Lustermann,[122] R. A. Manzoni,[122] M. Marionneau,[122] M. T. Meinhard,[122] F. Micheli,[122] P. Musella,[122] F. Nessi-Tedaldi,[122] F. Pauss,[122] G. Perrin,[122] L. Perrozzi,[122] S. Pigazzini,[122] M. Reichmann,[122] C. Reissel,[122] T. Reitenspiess,[122] D. Ruini,[122] D. A. Sanz Becerra,[122] M. Schönenberger,[122] L. Shchutska,[122] K. Theofilatos,[122] M. L. Vesterbacka Olsson,[122] R. Wallny,[122] D. H. Zhu,[122] T. K. Aarrestad,[123] C. Amsler,[123,aaa] D. Brzhechko,[123]

M. F. Canelli,[123] A. De Cosa,[123] R. Del Burgo,[123] S. Donato,[123] C. Galloni,[123] T. Hreus,[123] B. Kilminster,[123] S. Leontsinis,[123] V. M. Mikuni,[123] I. Neutelings,[123] G. Rauco,[123] P. Robmann,[123] D. Salerno,[123] K. Schweiger,[123] C. Seitz,[123] Y. Takahashi,[123] S. Wertz,[123] A. Zucchetta,[123] T. H. Doan,[124] C. M. Kuo,[124] W. Lin,[124] S. S. Yu,[124] P. Chang,[125] Y. Chao,[125] K. F. Chen,[125] P. H. Chen,[125] W.-S. Hou,[125] Y. F. Liu,[125] R.-S. Lu,[125] E. Paganis,[125] A. Psallidas,[125] A. Steen,[125] B. Asavapibhop,[126] N. Srimanobhas,[126] N. Suwonjandee,[126] A. Bat,[127] F. Boran,[127] S. Cerci,[127,bbb] S. Damarseckin,[127,ccc] Z. S. Demiroglu,[127] F. Dolek,[127] C. Dozen,[127] I. Dumanoglu,[127] G. Gokbulut,[127] Emine Gurpinar Guler,[127,ddd] Y. Guler,[127] I. Hos,[127,eee] C. Isik,[127] E. E. Kangal,[127,fff] O. Kara,[127] A. Kayis Topaksu,[127] U. Kiminsu,[127] M. Oglakci,[127] G. Onengut,[127] K. Ozdemir,[127,ggg] S. Ozturk,[127,hhh] D. Sunar Cerci,[127,bbb] B. Tali,[127,bbb] U. G. Tok,[127] S. Turkcapar,[127] I. S. Zorbakir,[127] C. Zorbilmez,[127] B. Isildak,[128,iii] G. Karapinar,[128,jjj] M. Yalvac,[128] M. Zeyrek,[128] I. O. Atakisi,[129] E. Gülmez,[129] M. Kaya,[129,kkk] O. Kaya,[129,lll] B. Kaynak,[129] Ö. Özçelik,[129] S. Ozkorucuklu,[129,mmm] S. Tekten,[129] E. A. Yetkin,[129,nnn] A. Cakir,[130] K. Cankocak,[130] Y. Komurcu,[130] S. Sen,[130,ooo] B. Grynyov,[131] L. Levchuk,[132] F. Ball,[133] J. J. Brooke,[133] D. Burns,[133] E. Clement,[133] D. Cussans,[133] O. Davignon,[133] H. Flacher,[133] J. Goldstein,[133] G. P. Heath,[133] H. F. Heath,[133] L. Kreczko,[133] D. M. Newbold,[133,ppp] S. Paramesvaran,[133] B. Penning,[133] T. Sakuma,[133] D. Smith,[133] V. J. Smith,[133] J. Taylor,[133] A. Titterton,[133] K. W. Bell,[134] A. Belyaev,[134,qqq] C. Brew,[134] R. M. Brown,[134] D. Cieri,[134] D. J. A. Cockerill,[134] J. A. Coughlan,[134] K. Harder,[134] S. Harper,[134] J. Linacre,[134] K. Manolopoulos,[134] E. Olaiya,[134] D. Petyt,[134] T. Reis,[134] T. Schuh,[134] C. H. Shepherd-Themistocleous,[134] A. Thea,[134] I. R. Tomalin,[134] T. Williams,[134] W. J. Womersley,[134] R. Bainbridge,[135] P. Bloch,[135] J. Borg,[135] S. Breeze,[135] O. Buchmuller,[135] A. Bundock,[135] Gurpreet Singh CHAHAL,[135,rrr] D. Colling,[135] P. Dauncey,[135] G. Davies,[135] M. Della Negra,[135] R. Di Maria,[135] P. Everaerts,[135] G. Hall,[135] G. Iles,[135] T. James,[135] M. Komm,[135] C. Laner,[135] L. Lyons,[135] A.-M. Magnan,[135] S. Malik,[135] A. Martelli,[135] V. Milosevic,[135] J. Nash,[135,sss] A. Nikitenko,[135,i] V. Palladino,[135] M. Pesaresi,[135] D. M. Raymond,[135] A. Richards,[135] A. Rose,[135] E. Scott,[135] C. Seez,[135] A. Shtipliyski,[135] M. Stoye,[135] T. Strebler,[135] S. Summers,[135] A. Tapper,[135] K. Uchida,[135] T. Virdee,[135,r] N. Wardle,[135] D. Winterbottom,[135] J. Wright,[135] S. C. Zenz,[135] J. E. Cole,[136] P. R. Hobson,[136] A. Khan,[136] P. Kyberd,[136] C. K. Mackay,[136] A. Morton,[136] I. D. Reid,[136] L. Teodorescu,[136] S. Zahid,[136] K. Call,[137] J. Dittmann,[137] K. Hatakeyama,[137] C. Madrid,[137] B. McMaster,[137] N. Pastika,[137] C. Smith,[137] R. Bartek,[138] A. Dominguez,[138] A. Buccilli,[139] O. Charaf,[139] S. I. Cooper,[139] C. Henderson,[139] P. Rumerio,[139] C. West,[139] D. Arcaro,[140] T. Bose,[140] Z. Demiragli,[140] D. Gastler,[140] S. Girgis,[140] D. Pinna,[140] C. Richardson,[140] J. Rohlf,[140] D. Sperka,[140] I. Suarez,[140] L. Sulak,[140] D. Zou,[140] G. Benelli,[141] B. Burkle,[141] X. Coubez,[141] D. Cutts,[141] M. Hadley,[141] J. Hakala,[141] U. Heintz,[141] J. M. Hogan,[141,ttt] K. H. M. Kwok,[141] E. Laird,[141] G. Landsberg,[141] J. Lee,[141] Z. Mao,[141] M. Narain,[141] S. Sagir,[141,uuu] R. Syarif,[141] E. Usai,[141] D. Yu,[141] R. Band,[142] C. Brainerd,[142] R. Breedon,[142] D. Burns,[142] M. Calderon De La Barca Sanchez,[142] M. Chertok,[142] J. Conway,[142] R. Conway,[142] P. T. Cox,[142] R. Erbacher,[142] C. Flores,[142] G. Funk,[142] W. Ko,[142] O. Kukral,[142] R. Lander,[142] M. Mulhearn,[142] D. Pellett,[142] J. Pilot,[142] M. Shi,[142] D. Stolp,[142] D. Taylor,[142] K. Tos,[142] M. Tripathi,[142] Z. Wang,[142] F. Zhang,[142] M. Bachtis,[143] C. Bravo,[143] R. Cousins,[143] A. Dasgupta,[143] A. Florent,[143] J. Hauser,[143] M. Ignatenko,[143] N. Mccoll,[143] S. Regnard,[143] D. Saltzberg,[143] C. Schnaible,[143] V. Valuev,[143] K. Burt,[144] R. Clare,[144] J. W. Gary,[144] S. M. A. Ghiasi Shirazi,[144] G. Hanson,[144] G. Karapostoli,[144] E. Kennedy,[144] O. R. Long,[144] M. Olmedo Negrete,[144] M. I. Paneva,[144] W. Si,[144] L. Wang,[144] H. Wei,[144] S. Wimpenny,[144] B. R. Yates,[144] J. G. Branson,[145] P. Chang,[145] S. Cittolin,[145] M. Derdzinski,[145] R. Gerosa,[145] D. Gilbert,[145] B. Hashemi,[145] A. Holzner,[145] D. Klein,[145] G. Kole,[145] V. Krutelyov,[145] J. Letts,[145] M. Masciovecchio,[145] S. May,[145] D. Olivito,[145] S. Padhi,[145] M. Pieri,[145] V. Sharma,[145] M. Tadel,[145] J. Wood,[145] F. Würthwein,[145] A. Yagil,[145] G. Zevi Della Porta,[145] N. Amin,[146] R. Bhandari,[146] C. Campagnari,[146] M. Citron,[146] V. Dutta,[146] M. Franco Sevilla,[146] L. Gouskos,[146] J. Incandela,[146] B. Marsh,[146] H. Mei,[146] A. Ovcharova,[146] H. Qu,[146] J. Richman,[146] U. Sarica,[146] D. Stuart,[146] S. Wang,[146] J. Yoo,[146] D. Anderson,[147] A. Bornheim,[147] J. M. Lawhorn,[147] N. Lu,[147] H. B. Newman,[147] T. Q. Nguyen,[147] J. Pata,[147] M. Spiropulu,[147] J. R. Vlimant,[147] R. Wilkinson,[147] S. Xie,[147] Z. Zhang,[147] R. Y. Zhu,[147] M. B. Andrews,[148] T. Ferguson,[148] T. Mudholkar,[148] M. Paulini,[148] M. Sun,[148] I. Vorobiev,[148] M. Weinberg,[148] J. P. Cumalat,[149] W. T. Ford,[149] F. Jensen,[149] A. Johnson,[149] E. MacDonald,[149] T. Mulholland,[149] R. Patel,[149] A. Perloff,[149] K. Stenson,[149] K. A. Ulmer,[149] S. R. Wagner,[149] J. Alexander,[150] J. Chaves,[150] Y. Cheng,[150] J. Chu,[150] A. Datta,[150] A. Frankenthal,[150] K. Mcdermott,[150] N. Mirman,[150] J. Monroy,[150] J. R. Patterson,[150] D. Quach,[150] A. Rinkevicius,[150] A. Ryd,[150] L. Skinnari,[150] L. Soffi,[150] S. M. Tan,[150] Z. Tao,[150] J. Thom,[150] J. Tucker,[150] P. Wittich,[150] M. Zientek,[150] S. Abdullin,[151] M. Albrow,[151] M. Alyari,[151] G. Apollinari,[151] A. Apresyan,[151] A. Apyan,[151] S. Banerjee,[151] L. A. T. Bauerdick,[151] A. Beretvas,[151] J. Berryhill,[151] P. C. Bhat,[151] K. Burkett,[151] J. N. Butler,[151] A. Canepa,[151] G. B. Cerati,[151] H. W. K. Cheung,[151] F. Chlebana,[151] M. Cremonesi,[151] J. Duarte,[151] V. D. Elvira,[151]

J. Freeman,[151] Z. Gecse,[151] E. Gottschalk,[151] L. Gray,[151] D. Green,[151] S. Grünendahl,[151] O. Gutsche,[151] J. Hanlon,[151] R. M. Harris,[151] S. Hasegawa,[151] R. Heller,[151] J. Hirschauer,[151] Z. Hu,[151] B. Jayatilaka,[151] S. Jindariani,[151] M. Johnson,[151] U. Joshi,[151] B. Klima,[151] M. J. Kortelainen,[151] B. Kreis,[151] S. Lammel,[151] D. Lincoln,[151] R. Lipton,[151] M. Liu,[151] T. Liu,[151] J. Lykken,[151] K. Maeshima,[151] J. M. Marraffino,[151] D. Mason,[151] P. McBride,[151] P. Merkel,[151] S. Mrenna,[151] S. Nahn,[151] V. O'Dell,[151] K. Pedro,[151] C. Pena,[151] O. Prokofyev,[151] G. Rakness,[151] F. Ravera,[151] A. Reinsvold,[151] L. Ristori,[151] B. Schneider,[151] E. Sexton-Kennedy,[151] N. Smith,[151] A. Soha,[151] W. J. Spalding,[151] L. Spiegel,[151] S. Stoynev,[151] J. Strait,[151] N. Strobbe,[151] L. Taylor,[151] S. Tkaczyk,[151] N. V. Tran,[151] L. Uplegger,[151] E. W. Vaandering,[151] C. Vernieri,[151] M. Verzocchi,[151] R. Vidal,[151] M. Wang,[151] H. A. Weber,[151] D. Acosta,[152] P. Avery,[152] P. Bortignon,[152] D. Bourilkov,[152] A. Brinkerhoff,[152] L. Cadamuro,[152] A. Carnes,[152] V. Cherepanov,[152] D. Curry,[152] R. D. Field,[152] S. V. Gleyzer,[152] B. M. Joshi,[152] M. Kim,[152] J. Konigsberg,[152] A. Korytov,[152] K. H. Lo,[152] P. Ma,[152] K. Matchev,[152] N. Menendez,[152] G. Mitselmakher,[152] D. Rosenzweig,[152] K. Shi,[152] J. Wang,[152] S. Wang,[152] X. Zuo,[152] Y. R. Joshi,[153] S. Linn,[153] T. Adams,[154] A. Askew,[154] S. Hagopian,[154] V. Hagopian,[154] K. F. Johnson,[154] R. Khurana,[154] T. Kolberg,[154] G. Martinez,[154] T. Perry,[154] H. Prosper,[154] A. Saha,[154] C. Schiber,[154] R. Yohay,[154] M. M. Baarmand,[155] V. Bhopatkar,[155] S. Colafranceschi,[155] M. Hohlmann,[155] D. Noonan,[155] M. Rahmani,[155] T. Roy,[155] M. Saunders,[155] F. Yumiceva,[155] M. R. Adams,[156] L. Apanasevich,[156] D. Berry,[156] R. R. Betts,[156] R. Cavanaugh,[156] X. Chen,[156] S. Dittmer,[156] O. Evdokimov,[156] C. E. Gerber,[156] D. A. Hangal,[156] D. J. Hofman,[156] K. Jung,[156] C. Mills,[156] M. B. Tonjes,[156] N. Varelas,[156] H. Wang,[156] X. Wang,[156] Z. Wu,[156] J. Zhang,[156] M. Alhusseini,[157] B. Bilki,[157,ddd] W. Clarida,[157] K. Dilsiz,[157,vvv] S. Durgut,[157] R. P. Gandrajula,[157] M. Haytmyradov,[157] V. Khristenko,[157] O. K. Köseyan,[157] J.-P. Merlo,[157] A. Mestvirishvili,[157] A. Moeller,[157] J. Nachtman,[157] H. Ogul,[157,www] Y. Onel,[157] F. Ozok,[157,xxx] A. Penzo,[157] C. Snyder,[157] E. Tiras,[157] J. Wetzel,[157] B. Blumenfeld,[158] A. Cocoros,[158] N. Eminizer,[158] D. Fehling,[158] L. Feng,[158] A. V. Gritsan,[158] W. T. Hung,[158] P. Maksimovic,[158] J. Roskes,[158] M. Swartz,[158] M. Xiao,[158] A. Al-bataineh,[159] P. Baringer,[159] A. Bean,[159] S. Boren,[159] J. Bowen,[159] A. Bylinkin,[159] J. Castle,[159] S. Khalil,[159] A. Kropivnitskaya,[159] D. Majumder,[159] W. Mcbrayer,[159] M. Murray,[159] C. Rogan,[159] S. Sanders,[159] E. Schmitz,[159] J. D. Tapia Takaki,[159] Q. Wang,[159] S. Duric,[160] A. Ivanov,[160] K. Kaadze,[160] D. Kim,[160] Y. Maravin,[160] D. R. Mendis,[160] T. Mitchell,[160] A. Modak,[160] A. Mohammadi,[160] F. Rebassoo,[161] D. Wright,[161] A. Baden,[162] O. Baron,[162] A. Belloni,[162] S. C. Eno,[162] Y. Feng,[162] C. Ferraioli,[162] N. J. Hadley,[162] S. Jabeen,[162] G. Y. Jeng,[162] R. G. Kellogg,[162] J. Kunkle,[162] A. C. Mignerey,[162] S. Nabili,[162] F. Ricci-Tam,[162] M. Seidel,[162] Y. H. Shin,[162] A. Skuja,[162] S. C. Tonwar,[162] K. Wong,[162] D. Abercrombie,[163] B. Allen,[163] V. Azzolini,[163] A. Baty,[163] R. Bi,[163] S. Brandt,[163] W. Busza,[163] I. A. Cali,[163] M. D'Alfonso,[163] G. Gomez Ceballos,[163] M. Goncharov,[163] P. Harris,[163] D. Hsu,[163] M. Hu,[163] M. Klute,[163] D. Kovalskyi,[163] Y.-J. Lee,[163] P. D. Luckey,[163] B. Maier,[163] A. C. Marini,[163] C. Mcginn,[163] C. Mironov,[163] S. Narayanan,[163] X. Niu,[163] C. Paus,[163] D. Rankin,[163] C. Roland,[163] G. Roland,[163] Z. Shi,[163] G. S. F. Stephans,[163] K. Sumorok,[163] K. Tatar,[163] D. Velicanu,[163] J. Wang,[163] T. W. Wang,[163] B. Wyslouch,[163] A. C. Benvenuti,[164,a] R. M. Chatterjee,[164] A. Evans,[164] P. Hansen,[164] J. Hiltbrand,[164] Sh. Jain,[164] S. Kalafut,[164] M. Krohn,[164] Y. Kubota,[164] Z. Lesko,[164] J. Mans,[164] R. Rusack,[164] M. A. Wadud,[164] J. G. Acosta,[165] S. Oliveros,[165] E. Avdeeva,[166] K. Bloom,[166] D. R. Claes,[166] C. Fangmeier,[166] L. Finco,[166] F. Golf,[166] R. Gonzalez Suarez,[166] R. Kamalieddin,[166] I. Kravchenko,[166] J. E. Siado,[166] G. R. Snow,[166] B. Stieger,[166] A. Godshalk,[167] C. Harrington,[167] I. Iashvili,[167] A. Kharchilava,[167] C. Mclean,[167] D. Nguyen,[167] A. Parker,[167] S. Rappoccio,[167] B. Roozbahani,[167] G. Alverson,[168] E. Barberis,[168] C. Freer,[168] Y. Haddad,[168] A. Hortiangtham,[168] G. Madigan,[168] D. M. Morse,[168] T. Orimoto,[168] A. Tishelman-Charny,[168] T. Wamorkar,[168] B. Wang,[168] A. Wisecarver,[168] D. Wood,[168] S. Bhattacharya,[169] J. Bueghly,[169] T. Gunter,[169] K. A. Hahn,[169] N. Odell,[169] M. H. Schmitt,[169] K. Sung,[169] M. Trovato,[169] M. Velasco,[169] R. Bucci,[170] N. Dev,[170] R. Goldouzian,[170] M. Hildreth,[170] K. Hurtado Anampa,[170] C. Jessop,[170] D. J. Karmgard,[170] K. Lannon,[170] W. Li,[170] N. Loukas,[170] N. Marinelli,[170] F. Meng,[170] C. Mueller,[170] Y. Musienko,[170,oo] M. Planer,[170] R. Ruchti,[170] P. Siddireddy,[170] G. Smith,[170] S. Taroni,[170] M. Wayne,[170] A. Wightman,[170] M. Wolf,[170] A. Woodard,[170] J. Alimena,[171] L. Antonelli,[171] B. Bylsma,[171] L. S. Durkin,[171] S. Flowers,[171] B. Francis,[171] C. Hill,[171] W. Ji,[171] A. Lefeld,[171] T. Y. Ling,[171] W. Luo,[171] B. L. Winer,[171] S. Cooperstein,[172] G. Dezoort,[172] P. Elmer,[172] J. Hardenbrook,[172] N. Haubrich,[172] S. Higginbotham,[172] A. Kalogeropoulos,[172] S. Kwan,[172] D. Lange,[172] M. T. Lucchini,[172] J. Luo,[172] D. Marlow,[172] K. Mei,[172] I. Ojalvo,[172] J. Olsen,[172] C. Palmer,[172] P. Piroué,[172] J. Salfeld-Nebgen,[172] D. Stickland,[172] C. Tully,[172] Z. Wang,[172] S. Malik,[173] S. Norberg,[173] A. Barker,[174] V. E. Barnes,[174] S. Das,[174] L. Gutay,[174] M. Jones,[174] A. W. Jung,[174] A. Khatiwada,[174] B. Mahakud,[174] D. H. Miller,[174] G. Negro,[174] N. Neumeister,[174] C. C. Peng,[174] S. Piperov,[174] H. Qiu,[174] J. F. Schulte,[174] J. Sun,[174] F. Wang,[174] R. Xiao,[174] W. Xie,[174] T. Cheng,[175] J. Dolen,[175]

N. Parashar,[175] Z. Chen,[176] K. M. Ecklund,[176] S. Freed,[176] F. J. M. Geurts,[176] M. Kilpatrick,[176] Arun Kumar,[176] W. Li,[176] B. P. Padley,[176] J. Roberts,[176] J. Rorie,[176] W. Shi,[176] A. G. Stahl Leiton,[176] Z. Tu,[176] A. Zhang,[176] A. Bodek,[177] P. de Barbaro,[177] R. Demina,[177] Y. t. Duh,[177] J. L. Dulemba,[177] C. Fallon,[177] T. Ferbel,[177] M. Galanti,[177] A. Garcia-Bellido,[177] J. Han,[177] O. Hindrichs,[177] A. Khukhunaishvili,[177] E. Ranken,[177] P. Tan,[177] R. Taus,[177] B. Chiarito,[178] J. P. Chou,[178] Y. Gershtein,[178] E. Halkiadakis,[178] A. Hart,[178] M. Heindl,[178] E. Hughes,[178] S. Kaplan,[178] S. Kyriacou,[178] I. Laflotte,[178] A. Lath,[178] R. Montalvo,[178] K. Nash,[178] M. Osherson,[178] H. Saka,[178] S. Salur,[178] S. Schnetzer,[178] D. Sheffield,[178] S. Somalwar,[178] R. Stone,[178] S. Thomas,[178] P. Thomassen,[178] H. Acharya,[179] A. G. Delannoy,[179] J. Heideman,[179] G. Riley,[179] S. Spanier,[179] O. Bouhali,[180,yyy] A. Celik,[180] M. Dalchenko,[180] M. De Mattia,[180] A. Delgado,[180] S. Dildick,[180] R. Eusebi,[180] J. Gilmore,[180] T. Huang,[180] T. Kamon,[180,zzz] S. Luo,[180] D. Marley,[180] R. Mueller,[180] D. Overton,[180] L. Perniè,[180] D. Rathjens,[180] A. Safonov,[180] N. Akchurin,[181] J. Damgov,[181] F. De Guio,[181] P. R. Dudero,[181] S. Kunori,[181] K. Lamichhane,[181] S. W. Lee,[181] T. Mengke,[181] S. Muthumuni,[181] T. Peltola,[181] S. Undleeb,[181] I. Volobouev,[181] Z. Wang,[181] A. Whitbeck,[181] S. Greene,[182] A. Gurrola,[182] R. Janjam,[182] W. Johns,[182] C. Maguire,[182] A. Melo,[182] H. Ni,[182] K. Padeken,[182] F. Romeo,[182] P. Sheldon,[182] S. Tuo,[182] J. Velkovska,[182] M. Verweij,[182] Q. Xu,[182] M. W. Arenton,[183] P. Barria,[183] B. Cox,[183] R. Hirosky,[183] M. Joyce,[183] A. Ledovskoy,[183] H. Li,[183] C. Neu,[183] Y. Wang,[183] E. Wolfe,[183] F. Xia,[183] R. Harr,[184] P. E. Karchin,[184] N. Poudyal,[184] J. Sturdy,[184] P. Thapa,[184] S. Zaleski,[184] J. Buchanan,[185] C. Caillol,[185] D. Carlsmith,[185] S. Dasu,[185] I. De Bruyn,[185] L. Dodd,[185] B. Gomber,[185,aaaa] M. Grothe,[185] M. Herndon,[185] A. Hervé,[185] U. Hussain,[185] P. Klabbers,[185] A. Lanaro,[185] K. Long,[185] R. Loveless,[185] T. Ruggles,[185] A. Savin,[185] V. Sharma,[185] W. H. Smith,[185] and N. Woods[185]

(CMS Collaboration)

[1]*Yerevan Physics Institute, Yerevan, Armenia*
[2]*Institut für Hochenergiephysik, Wien, Austria*
[3]*Institute for Nuclear Problems, Minsk, Belarus*
[4]*Universiteit Antwerpen, Antwerpen, Belgium*
[5]*Vrije Universiteit Brussel, Brussel, Belgium*
[6]*Université Libre de Bruxelles, Bruxelles, Belgium*
[7]*Ghent University, Ghent, Belgium*
[8]*Université Catholique de Louvain, Louvain-la-Neuve, Belgium*
[9]*Centro Brasileiro de Pesquisas Fisicas, Rio de Janeiro, Brazil*
[10]*Universidade do Estado do Rio de Janeiro, Rio de Janeiro, Brazil*
[11a]*Universidade Estadual Paulista, Universidade Federal do ABC, São Paulo, Brazil*
[11b]*Universidade Federal do ABC, Universidade Federal do ABC, São Paulo, Brazil*
[12]*Institute for Nuclear Research and Nuclear Energy, Bulgarian Academy of Sciences, Sofia, Bulgaria*
[13]*University of Sofia, Sofia, Bulgaria*
[14]*Beihang University, Beijing, China*
[15]*Institute of High Energy Physics, Beijing, China*
[16]*State Key Laboratory of Nuclear Physics and Technology, Peking University, Beijing, China*
[17]*Tsinghua University, Beijing, China*
[18]*Universidad de Los Andes, Bogota, Colombia*
[19]*Universidad de Antioquia, Medellin, Colombia*
[20]*University of Split, Faculty of Electrical Engineering, Mechanical Engineering and Naval Architecture, Split, Croatia*
[21]*University of Split, Faculty of Science, Split, Croatia*
[22]*Institute Rudjer Boskovic, Zagreb, Croatia*
[23]*University of Cyprus, Nicosia, Cyprus*
[24]*Charles University, Prague, Czech Republic*
[25]*Escuela Politecnica Nacional, Quito, Ecuador*
[26]*Universidad San Francisco de Quito, Quito, Ecuador*
[27]*Academy of Scientific Research and Technology of the Arab Republic of Egypt, Egyptian Network of High Energy Physics, Cairo, Egypt*
[28]*National Institute of Chemical Physics and Biophysics, Tallinn, Estonia*
[29]*Department of Physics, University of Helsinki, Helsinki, Finland*
[30]*Helsinki Institute of Physics, Helsinki, Finland*
[31]*Lappeenranta University of Technology, Lappeenranta, Finland*

[32]IRFU, CEA, Université Paris-Saclay, Gif-sur-Yvette, France

[33]Laboratoire Leprince-Ringuet, Ecole polytechnique, CNRS/IN2P3,
Université Paris-Saclay, Palaiseau, France

[34]Université de Strasbourg, CNRS, IPHC UMR 7178, Strasbourg, France

[35]Centre de Calcul de l'Institut National de Physique Nucleaire et de Physique des Particules,
CNRS/IN2P3, Villeurbanne, France

[36]Université de Lyon, Université Claude Bernard Lyon 1, CNRS-IN2P3,
Institut de Physique Nucléaire de Lyon, Villeurbanne, France

[37]Georgian Technical University, Tbilisi, Georgia

[38]Tbilisi State University, Tbilisi, Georgia

[39]RWTH Aachen University, I. Physikalisches Institut, Aachen, Germany

[40]RWTH Aachen University, III. Physikalisches Institut A, Aachen, Germany

[41]RWTH Aachen University, III. Physikalisches Institut B, Aachen, Germany

[42]Deutsches Elektronen-Synchrotron, Hamburg, Germany

[43]University of Hamburg, Hamburg, Germany

[44]Karlsruher Institut fuer Technologie, Karlsruhe, Germany

[45]Institute of Nuclear and Particle Physics (INPP), NCSR Demokritos, Aghia Paraskevi, Greece

[46]National and Kapodistrian University of Athens, Athens, Greece

[47]National Technical University of Athens, Athens, Greece

[48]University of Ioánnina, Ioánnina, Greece

[49]MTA-ELTE Lendület CMS Particle and Nuclear Physics Group, Eötvös Loránd University,
Budapest, Hungary

[50]Wigner Research Centre for Physics, Budapest, Hungary

[51]Institute of Nuclear Research ATOMKI, Debrecen, Hungary

[52]Institute of Physics, University of Debrecen, Debrecen, Hungary

[53]Indian Institute of Science (IISc), Bangalore, India

[54]National Institute of Science Education and Research, HBNI, Bhubaneswar, India

[55]Panjab University, Chandigarh, India

[56]University of Delhi, Delhi, India

[57]Saha Institute of Nuclear Physics, HBNI, Kolkata,India

[58]Indian Institute of Technology Madras, Madras, India

[59]Bhabha Atomic Research Centre, Mumbai, India

[60]Tata Institute of Fundamental Research-A, Mumbai, India

[61]Tata Institute of Fundamental Research-B, Mumbai, India

[62]Indian Institute of Science Education and Research (IISER), Pune, India

[63]Institute for Research in Fundamental Sciences (IPM), Tehran, Iran

[64]University College Dublin, Dublin, Ireland

[65a]INFN Sezione di Bari, Politecnico di Bari, Bari, Italy

[65b]Università di Bari, Politecnico di Bari, Bari, Italy

[65c]Politecnico di Bari, Politecnico di Bari, Bari, Italy

[66a]INFN Sezione di Bologna, Bologna, Italy

[66b]Università di Bologna, Bologna, Italy

[67a]INFN Sezione di Catania, Catania, Italy

[67b]Università di Catania, Catania, Italy

[68a]INFN Sezione di Firenze, Firenze, Italy

[68b]Università di Firenze, Firenze, Italy

[69]INFN Laboratori Nazionali di Frascati, Frascati, Italy

[70a]INFN Sezione di Genova, Genova, Italy

[70b]Università di Genova, Genova, Italy

[71a]INFN Sezione di Milano-Bicocca, Milano, Italy

[71b]Università di Milano-Bicocca, Milano, Italy

[72a]INFN Sezione di Napoli, Napoli, Italy

[72b]Università di Napoli 'Federico II', Napoli, Italy

[72c]Università della Basilicata, Potenza, Italy

[72d]Università G. Marconi, Roma, Italy

[73a]INFN Sezione di Padova, Padova, Italy

[73b]Università di Padova, Padova, Italy

[73c]Università di Trento, Trento, Italy

[74a]INFN Sezione di Pavia

[74b]Università di Pavia

[75a]*INFN Sezione di Perugia, Perugia, Italy*
[75b]*Università di Perugia, Perugia, Italy*
[76a]*INFN Sezione di Pisa, Scuola Normale Superiore di Pisa, Pisa, Italy*
[76b]*Università di Pisa, Scuola Normale Superiore di Pisa, Pisa, Italy*
[76c]*Scuola Normale Superiore di Pisa, Scuola Normale Superiore di Pisa, Pisa, Italy*
[77a]*INFN Sezione di Roma, Rome, Italy*
[77b]*Sapienza Università di Roma, Rome, Italy*
[78a]*INFN Sezione di Torino, Torino, Italy*
[78b]*Università di Torino, Torino, Italy*
[78c]*Università del Piemonte Orientale, Torino, Italy*
[79a]*INFN Sezione di Trieste, Trieste, Italy*
[79b]*Università di Trieste, Trieste, Italy*
[80]*Kyungpook National University, Daegu, Korea*
[81]*Chonnam National University, Institute for Universe and Elementary Particles, Kwangju, Korea*
[82]*Hanyang University, Seoul, Korea*
[83]*Korea University, Seoul, Korea*
[84]*Sejong University, Seoul, Korea*
[85]*Seoul National University, Seoul, Korea*
[86]*University of Seoul, Seoul, Korea*
[87]*Sungkyunkwan University, Suwon, Korea*
[88]*Riga Technical University, Riga, Latvia*
[89]*Vilnius University, Vilnius, Lithuania*
[90]*National Centre for Particle Physics, Universiti Malaya, Kuala Lumpur, Malaysia*
[91]*Universidad de Sonora (UNISON), Hermosillo, Mexico*
[92]*Centro de Investigacion y de Estudios Avanzados del IPN, Mexico City, Mexico*
[93]*Universidad Iberoamericana, Mexico City, Mexico*
[94]*Benemerita Universidad Autonoma de Puebla, Puebla, Mexico*
[95]*Universidad Autónoma de San Luis Potosí, San Luis Potosí, Mexico*
[96]*University of Montenegro, Podgorica, Montenegro*
[97]*University of Auckland, Auckland, New Zealand*
[98]*University of Canterbury, Christchurch, New Zealand*
[99]*National Centre for Physics, Quaid-I-Azam University, Islamabad, Pakistan*
[100]*National Centre for Nuclear Research, Swierk, Poland*
[101]*Institute of Experimental Physics, Faculty of Physics, University of Warsaw, Warsaw, Poland*
[102]*Laboratório de Instrumentação e Física Experimental de Partículas, Lisboa, Portugal*
[103]*Joint Institute for Nuclear Research, Dubna, Russia*
[104]*Petersburg Nuclear Physics Institute, Gatchina (St. Petersburg), Russia*
[105]*Institute for Nuclear Research, Moscow, Russia*
[106]*Institute for Theoretical and Experimental Physics named by A.I. Alikhanov of NRC*
'Kurchatov Institute', Moscow, Russia
[107]*Moscow Institute of Physics and Technology, Moscow, Russia*
[108]*National Research Nuclear University 'Moscow Engineering Physics Institute' (MEPhI),*
Moscow, Russia
[109]*P.N. Lebedev Physical Institute, Moscow, Russia*
[110]*Skobeltsyn Institute of Nuclear Physics, Lomonosov Moscow State University, Moscow, Russia*
[111]*Novosibirsk State University (NSU), Novosibirsk, Russia*
[112]*Institute for High Energy Physics of National Research Centre 'Kurchatov Institute', Protvino, Russia*
[113]*National Research Tomsk Polytechnic University, Tomsk, Russia*
[114]*University of Belgrade: Faculty of Physics and VINCA Institute of Nuclear Sciences*
[115]*Centro de Investigaciones Energéticas Medioambientales y Tecnológicas (CIEMAT), Madrid, Spain*
[116]*Universidad Autónoma de Madrid, Madrid, Spain*
[117]*Universidad de Oviedo, Oviedo, Spain*
[118]*Instituto de Física de Cantabria (IFCA), CSIC-Universidad de Cantabria, Santander, Spain*
[119]*University of Ruhuna, Department of Physics, Matara, Sri Lanka*
[120]*CERN, European Organization for Nuclear Research, Geneva, Switzerland*
[121]*Paul Scherrer Institut, Villigen, Switzerland*
[122]*ETH Zurich - Institute for Particle Physics and Astrophysics (IPA), Zurich, Switzerland*
[123]*Universität Zürich, Zurich, Switzerland*
[124]*National Central University, Chung-Li, Taiwan*
[125]*National Taiwan University (NTU), Taipei, Taiwan*

[126]Chulalongkorn University, Faculty of Science, Department of Physics, Bangkok, Thailand

[127]Çukurova University, Physics Department, Science and Art Faculty, Adana, Turkey

[128]Middle East Technical University, Physics Department, Ankara, Turkey

[129]Bogazici University, Istanbul, Turkey

[130]Istanbul Technical University, Istanbul, Turkey

[131]Institute for Scintillation Materials of National Academy of Science of Ukraine, Kharkov, Ukraine

[132]National Scientific Center, Kharkov Institute of Physics and Technology, Kharkov, Ukraine

[133]University of Bristol, Bristol, United Kingdom

[134]Rutherford Appleton Laboratory, Didcot, United Kingdom

[135]Imperial College, London, United Kingdom

[136]Brunel University, Uxbridge, United Kingdom

[137]Baylor University, Waco, Texas, USA

[138]Catholic University of America, Washington, DC, USA

[139]The University of Alabama, Tuscaloosa, Alabama, USA

[140]Boston University, Boston, Massachusetts, USA

[141]Brown University, Providence, Rhode Island, USA

[142]University of California, Davis, Davis, California, USA

[143]University of California, Los Angeles, California, USA

[144]University of California, Riverside, Riverside, California, USA

[145]University of California, San Diego, La Jolla, California, USA

[146]University of California, Santa Barbara - Department of Physics, Santa Barbara, California, USA

[147]California Institute of Technology, Pasadena, California, USA

[148]Carnegie Mellon University, Pittsburgh, Pennsylvania, USA

[149]University of Colorado Boulder, Boulder, Colorado, USA

[150]Cornell University, Ithaca, New York, USA

[151]Fermi National Accelerator Laboratory, Batavia, Illinois, USA

[152]University of Florida, Gainesville, Florida, USA

[153]Florida International University, Miami, Florida, USA

[154]Florida State University, Tallahassee, Florida, USA

[155]Florida Institute of Technology, Melbourne, Florida, USA

[156]University of Illinois at Chicago (UIC), Chicago, Illinois, USA

[157]The University of Iowa, Iowa City, Iowa, USA

[158]Johns Hopkins University, Baltimore, Maryland, USA

[159]The University of Kansas, Lawrence, Kansas, USA

[160]Kansas State University, Manhattan, Kansas, USA

[161]Lawrence Livermore National Laboratory, Livermore, California, USA

[162]University of Maryland, College Park, Maryland, USA

[163]Massachusetts Institute of Technology, Cambridge, Massachusetts, USA

[164]University of Minnesota, Minneapolis, Minnesota, USA

[165]University of Mississippi, Oxford, Mississippi, USA

[166]University of Nebraska-Lincoln, Lincoln, Nebraska, USA

[167]State University of New York at Buffalo, Buffalo, New York, USA

[168]Northeastern University, Boston, Massachusetts, USA

[169]Northwestern University, Evanston, Illinois, USA

[170]University of Notre Dame, Notre Dame, Indiana, USA

[171]The Ohio State University, Columbus, Ohio, USA

[172]Princeton University, Princeton, New Jersey, USA

[173]University of Puerto Rico, Mayaguez, Puerto Rico

[174]Purdue University, West Lafayette, Indiana, USA

[175]Purdue University Northwest, Hammond, Indiana, USA

[176]Rice University, Houston, Texas, USA

[177]University of Rochester, Rochester, New York, USA

[178]Rutgers, The State University of New Jersey, Piscataway, New Jersey, USA

[179]University of Tennessee, Knoxville, Tennessee, USA

[180]Texas A&M University, College Station, Texas, USA

[181]Texas Tech University, Lubbock, Texas, USA

[182]Vanderbilt University, Nashville, Tennessee, USA

[183]University of Virginia, Charlottesville, Virginia, USA

[184]Wayne State University, Detroit, Michigan, USA

[185]University of Wisconsin - Madison, Madison, Wisconsin, USA

[a]Deceased.

[b]Also at Vienna University of Technology, Vienna, Austria.

[c]Also at Skobeltsyn Institute of Nuclear Physics, Lomonosov Moscow State University, Moscow, Russia.

[d]Also at IRFU, CEA, Université Paris-Saclay, Gif-sur-Yvette, France.

[e]Also at Universidade Estadual de Campinas, Campinas, Brazil.

[f]Also at Federal University of Rio Grande do Sul, Porto Alegre, Brazil.

[g]Also at Université Libre de Bruxelles, Bruxelles, Belgium.

[h]Also at University of Chinese Academy of Sciences.

[i]Also at Institute for Theoretical and Experimental Physics named by A.I. Alikhanov of NRC 'Kurchatov Institute', Moscow, Russia.

[j]Also at Joint Institute for Nuclear Research, Dubna, Russia.

[k]Also at Cairo University, Cairo, Egypt.

[l]Also at Helwan University, Cairo, Egypt.

[m]Also at Zewail City of Science and Technology, Zewail, Egypt.

[n]Also at British University in Egypt, Cairo, Egypt.

[o]Also at Purdue University, West Lafayette, Indiana, USA.

[p]Also at Université de Haute Alsace, Mulhouse, France.

[q]Also at Tbilisi State University, Tbilisi, Georgia.

[r]Also at CERN, European Organization for Nuclear Research, Geneva, Switzerland.

[s]Also at RWTH Aachen University, III. Physikalisches Institut A, Aachen, Germany.

[t]Also at University of Hamburg, Hamburg, Germany.

[u]Also at Brandenburg University of Technology, Cottbus, Germany.

[v]Also at Institute of Physics, University of Debrecen, Debrecen, Hungary.

[w]Also at Institute of Nuclear Research ATOMKI, Debrecen, Hungary.

[x]Also at MTA-ELTE Lendület CMS Particle and Nuclear Physics Group, Eötvös Loránd University, Budapest, Hungary.

[y]Also at IIT Bhubaneswar, Bhubaneswar, India.

[z]Also at Institute of Physics, Bhubaneswar, India.

[aa]Also at Shoolini University, Solan, India.

[bb]Also at University of Visva-Bharati, Santiniketan, India.

[cc]Also at Isfahan University of Technology, Isfahan, Iran.

[dd]Also at Plasma Physics Research Center, Science and Research Branch, Islamic Azad University, Tehran, Iran.

[ee]Also at Italian National Agency for New Technologies, Energy and Sustainable Economic Development.

[ff]Also at Centro Siciliano di Fisica Nucleare e di Struttura Della Materia.

[gg]Also at Università degli Studi di Siena, Siena, Italy.

[hh]Also at Scuola Normale e Sezione dell'INFN, Pisa, Italy.

[ii]Also at Kyung Hee University, Department of Physics.

[jj]Also at Riga Technical University, Riga, Latvia.

[kk]Also at International Islamic University of Malaysia, Kuala Lumpur, Malaysia.

[ll]Also at Malaysian Nuclear Agency, MOSTI, Kajang, Malaysia.

[mm]Also at Consejo Nacional de Ciencia y Tecnología, Mexico City, Mexico.

[nn]Also at Warsaw University of Technology, Institute of Electronic Systems, Warsaw, Poland.

[oo]Also at Institute for Nuclear Research, Moscow, Russia.

[pp]Also at National Research Nuclear University 'Moscow Engineering Physics Institute' (MEPhI), Moscow, Russia.

[qq]Also at St. Petersburg State Polytechnical University, St. Petersburg, Russia.

[rr]Also at University of Florida, Gainesville, Florida, USA.

[ss]Also at P.N. Lebedev Physical Institute, Moscow, Russia.

[tt]Also at California Institute of Technology, Pasadena, California, USA.

[uu]Also at Budker Institute of Nuclear Physics, Novosibirsk, Russia.

[vv]Also at Faculty of Physics, University of Belgrade, Belgrade, Serbia.

[ww]Also at University of Belgrade: Faculty of Physics and VINCA Institute of Nuclear Sciences.

[xx]Also at INFN Sezione di Pavia, Università di Pavia, Pavia, Italy.

[yy]Also at National and Kapodistrian University of Athens, Athens, Greece.

[zz]Also at Universität Zürich, Zurich, Switzerland.

[aaa]Also at Stefan Meyer Institute for Subatomic Physics, Vienna, Austria

[bbb]Also at Adiyaman University, Adiyaman, Turkey.

[ccc]Also at Sirnak University.

[ddd]Also at Beykent University, Istanbul, Turkey.

[eee]Also at Istanbul Aydin University, Istanbul, Turkey.

[fff]Also at Mersin University, Mersin, Turkey.

[ggg]Also at Piri Reis University, Istanbul, Turkey.

[hhh] Also at Gaziosmanpasa University, Tokat, Turkey.

[iii] Also at Ozyegin University, Istanbul, Turkey.

[jjj] Also at Izmir Institute of Technology, Izmir, Turkey.

[kkk] Also at Marmara University, Istanbul, Turkey.

[lll] Also at Kafkas University, Kars, Turkey.

[mmm] Also at Istanbul University, Istanbul, Turkey.

[nnn] Also at Istanbul Bilgi University, Istanbul, Turkey.

[ooo] Also at Hacettepe University, Ankara, Turkey.

[ppp] Also at Rutherford Appleton Laboratory, Didcot, United Kingdom.

[qqq] Also at School of Physics and Astronomy, University of Southampton, Southampton, United Kingdom.

[rrr] Also at IPPP Durham University.

[sss] Also at Monash University, Faculty of Science, Clayton, Australia.

[ttt] Also at Bethel University, St. Paul, Minneapolis, USA.

[uuu] Also at Karamanoğlu Mehmetbey University, Karaman, Turkey.

[vvv] Also at Bingol University, Bingol, Turkey.

[www] Also at Sinop University, Sinop, Turkey.

[xxx] Also at Mimar Sinan University, Istanbul, Istanbul, Turkey.

[yyy] Also at Texas A&M University at Qatar, Doha, Qatar.

[zzz] Also at Kyungpook National University, Daegu, Korea.

[aaaa] Also at University of Hyderabad, Hyderabad, India.